TECHNISCHE UNIVERSITÄT MÜNCHEN
TUM SCHOOL OF ENGINEERING AND DESIGN

Development of the high temperature superconducting REBCO coated conductor magnet system for ultra-high-field thermonuclear fusion power plants

Xiaodong Li

Vollständiger Abdruck der von der TUM School of Engineering and Design

der Technischen Universität München

zur Erlangung eines

Doktors der Ingenieurswissenschaften (Dr.-Ing.)

genehmigten Dissertation.

Vorsitz: Prof. Dr. rer. nat. Thomas Hamacher

Prüfer*innen der Dissertation:
1. Prof. Rafael Macián-Juan, Ph.D.
2. Assoc. Prof. Dr. Wenjiang Yang
3. Dr. Mark Ainslie

Die Dissertation wurde am 25.04.2023 bei der Technischen Universität München eingereicht und durch die TUM School of Engineering and Design am 01.10.2023 angenommen.

Acknowledgements

I wish to express my great thanks to Prof. Rafael Macián-Juan, who is my supervisor, mentor, and role model. He regularly discussed my research during my Ph.D. studies with me. He stands by me when I encounter setbacks and stands behind me with applause when I succeed. His encouragement and support have greatly motivated me to persevere in my research. His patience, kindness, and attitude towards academics would profoundly impact me.

I appreciate many for Prof. Wenjiang Yang. He was my supervisor during my master's degree at Beihang University, and my mentor during my Ph.D. studies at Technische Universität München. He is also my enlightenment teacher on the road of scientific research. Without him, I might not have had the opportunity to enjoy my research and work in superconductivity. He supported many of my work during my master's and Ph.D. studies.

I owe a debt of gratitude to Prof. Antonino Cardella. His nuclear fusion courses profoundly influenced me, providing a deep foundation for my research in this field. He offered me many valuable suggestions for my magnet design and helped me many at the beginning of my doctoral career; his kindness and sincerity impressed me greatly in my pursuit of truth.

I want to thank Dr. Veit Große and Dr. Anis Samara for their full support in my doing the experimental tests of critical current density in REBCO coated conductors. The experience of cooperation with them in Theva Dünnschichttechnik GmbH is a valuable treasure to me.

I want to thank Ms. Petra Popp-Münich, the secretary in our research group. Her attitude towards work is rigorous. In addition, she is optimistic about life. She treats us in the Chair like her family members. I learned a lot from her and appreciate her support.

I thank many of my friends: Yangmeihui Song, Xiangyu Gao, Long Tang, Hao Long, Jing Shi, Shuqi Xie, Yanzhu Hu, Ran Niu, Chi Zhang, Ye Su, Jie Liu, Xiaolie Wang, Qi Wang, Soobeen Yum, Yuanwei Cao, and Chunyu Liu for their love and support, which bring me too much sweet memories in Munich.

Last but not least, I wish to thank my parents. Their family education has allowed me to establish a correct concept of learning since I was a child. Their attitude towards work and life inspired me a lot, and their harmonious family atmosphere was the source of my happiness. I could not go so far on the academic road without their support.

Abstract

An ultra-high-field path toward large-scale fusion could accelerate our exploration and realization of fusion energy, as fusion power from the thermonuclear reactor is proportional to the fourth power of the toroidal field. The maximum toroidal field of the International Thermonuclear Experimental Reactor (ITER) project can achieve 11.8 Tesla using the low-temperature superconducting (LTS) Nb_3Sn conductors, which was discovered in 1954, and the critical magnetic field of the conductor can reach 25 Tesla at liquid helium environment. However, the discovery of high-temperature superconductivity in rare-earth barium copper oxide (REBCO) materials with ultra-high critical magnetic fields of more than 100 Tesla in 1986, and the commercialization of REBCO coated conductors with extremely high engineering critical current density in 2006 brought an ultra-high-field path towards large-scale fusion. The current challenge focuses on developing a feasible REBCO cabling method to increase inductance balance and decrease magnetic diffusion while having an ultra-high current-carrying capacity. The REBCO coated conductor is a ceramic superconductor whose mechanical behavior is relatively weak and very different from the metallic Nb_3Sn superconductor. In addition, the REBCO coated conductor's cross-section is rectangular, which differs from the circular section of Nb_3Sn conductors. The screening current might quickly affect the REBCO coated conductor, and the cable-in-conduit conductor (CICC) method developed for Nb_3Sn conductors might not be feasible for the REBCO coated conductors. To achieve an ultra-high field of more than 20 Tesla using REBCO coated conductors for large-scale fusion, a suitable cabling method for REBCO coated conductors is crucial.

In 2021, MIT Plasma Science and Fusion Center successfully used REBCO coated conductors to achieve 20 Tesla for the SPARC toroidal field coil module using a racetrack coil. The charging lasts 50 hours, and the current ramping rate is around 0.28 mT/s, a breakthrough for REBCO coated conductor to achieve ultra-high fields of more than 20 Tesla. However, the limitation is that the racetrack coil has no function for REBCO coated conductors to achieve inductance balance that results in a very-low current ramping and can only be feasible for ultra-high stable toroidal field coils used in compact fusion reactors. In addition, the racetrack coil can only use REBCO coated conductors to achieve a racetrack shape and is not a cabling method that can be used for any ultra-high-field applications with enough flexibility. Furthermore, the central solenoid coils used for plasma charging in the thermonuclear reactor require an ultra-high current ramping rate of 4.0 T/s. The research and development of REBCO cabling methods to meet these ultra-high-field requirements for ultra-high-field large-scale fusion reactors are still essential and remain to be solved.

This article developed a non-twisted cabling method with outstanding current-carrying capacity that can be used for the toroidal field coils of compact and large-scale fusion reactors. Meanwhile, a star-link cabling method with high-level inductance balance for the central solenoid coils of ultra-high-field compact and large-scale fusion reactors is also developed. The feasibility analysis of these cabling

methods is based on the critical current experiments of REBCO coated conductors carried out in Theva Dünnschichttechnik GmbH and the construction of the benchmark model by using **H**-formulation, **T**-**A** formulation, and **A**-**V** formulation-based finite element methods. The study demonstrates that the non-twisted REBCO cabling method is feasible for the stable toroidal field coils, and the star-link cabling method is applicable for the central solenoid coils of ultra-high-field large-scale thermonuclear fusion reactors. The research is significant in using REBCO coated conductors to develop ultra-high-field magnet systems for compact and large-scale thermonuclear fusion reactors.

Zusammenfassung

Die Fusionsleistung des thermonuklearen Reaktors ist proportional zur vierten Potenz des Torusfeldes. Ein Ultrahochfeld-Weg zu einer Fusion im großen Maßstab könnte unsere Erforschung und Realisierung von Fusionsenergie definitiv beschleunigen. Das maximale toroidale Feld des International Thermonuclear Experimental Reactor (ITER)-Projekts kann 11.8 Tesla erreichen, wenn die 1954 entdeckten niedertemperatursupraleitenden (LTS) Nb_3Sn-Leiter verwendet werden, und das kritische Magnetfeld des Leiters kann bei flüssigem Helium 25 Tesla erreichen Umgebung. Die Entdeckung der Hochtemperatur-Supraleitung in Seltenerd-Barium-Kupferoxid (REBCO)-Materialien mit ultrahohen kritischen Magnetfeldern von mehr als 100 Tesla im Jahr 1986 und die Kommerzialisierung von REBCO-beschichteten Leitern mit extrem hoher technischer kritischer Stromdichte im Jahr 2006 bringen ein Ultrahochfeld-Weg zur Fusion im großen Maßstab. Die aktuelle Herausforderung konzentriert sich auf die Entwicklung einer praktikablen REBCO-Verkabelungsmethode, die das Induktivitätsgleichgewicht erhöhen und die magnetische Diffusion verringern kann und gleichzeitig eine ultrahohe Strombelastbarkeit aufweist. Der REBCO-beschichtete Leiter ist ein keramischer Supraleiter, dessen mechanisches Verhalten ziemlich schwach ist und sich stark von dem metallischen Nb3Sn-Supraleiter unterscheidet. Außerdem hat der Querschnitt des mit REBCO beschichteten Leiters eine rechteckige Form, die sich von den Nb_3Sn-Leitern mit kreisförmigem Querschnitt unterscheidet. Dies bedeutet, dass der ummantelte REBCO-Leiter leicht durch den Abschirmstrom beeinflusst werden kann und der für Nb_3Sn-Leiter entwickelte Cable-in-Conduit-Leiter (CICC)-Verfahren für die ummantelten REBCO-Leiter möglicherweise nicht durchführbar ist. Um Ultrahochfelder von mehr als 20 Tesla mit REBCO-Mantelleitern für die großflächige Fusion zu erreichen, ist eine geeignete Verkabelungsmethode für REBCO-Mantelleiter entscheidend.

Im Jahr 2021 hat das MIT Plasma Science and Fusion Center erfolgreich REBCO-beschichtete Leiter eingesetzt, um 20 Tesla für das SPARC-Toroidfeldspulenmodul unter Verwendung einer Racetrack-Spule zu erreichen. Die Stromladung dauert 50 Stunden und die Stromrampenrate beträgt etwa 0.28 mT/s, was ein Durchbruch für REBCO-beschichtete Leiter ist, um ein Ultrahochfeld von mehr als 20 Tesla zu erreichen. Die Einschränkung besteht jedoch darin, dass die Racetrack-Spule keine Funktion für REBCO-beschichtete Leiter hat, um einen Induktivitätsausgleich zu erreichen, der zu einem sehr geringen Stromanstieg führt und nur für ultrahochstabile Ringfeldspulen in kompakten Fusionsreaktoren machbar ist. Außerdem kann die Racetrack-Spule nur REBCO-beschichtete Leiter verwenden, um eine Racetrack-Form zu erreichen, und ist eigentlich keine Verkabelungsmethode, die für alle Ultrahochfeldanwendungen mit ausreichender Flexibilität verwendet werden kann. Darüber hinaus erfordern die zentralen Solenoidspulen, die zur Plasmaaufladung im thermonuklearen Reaktor verwendet werden, eine ultrahohe Stromrampenrate von 4.0 T/s. Die Erforschung und Entwicklung von REBCO-Verkabelungsmethoden zur Erfüllung dieser Ultrahochfeld-Anforderungen für

großmaßstäbliche Ultrahochfeld-Fusionsreaktoren sind nach wie vor unerlässlich und müssen noch gelöst werden.

In diesem Artikel wurde eine nicht verdrillte Verkabelungsmethode mit hervorragender Strombelastbarkeit entwickelt, die für die toroidalen Feldspulen und poloidalen Feldspulen von kompakten und großen Fusionsreaktoren verwendet werden kann. Inzwischen wird auch ein Sternverbindungs-Verkabelungsverfahren mit hohem Induktivitätsausgleich für die zentralen Solenoidspulen von kompakten und großen Ultrahochfeld-Fusionsreaktoren entwickelt. Die Machbarkeitsanalyse dieser Verkabelungsmethoden basiert auf den in der Theva Dünnschichttechnik GmbH durchgeführten kritischen Stromversuchen an REBCO-beschichteten Leitern und dem Aufbau des Benchmark-Modells unter Verwendung von H-Formulierung, T-A-Formulierung und A-V-Formulierung basierend auf Finite-Elemente-Methoden. Die Studie zeigt, dass die unverdrillte REBCO-Verkabelungsmethode für stabile Ringfeldspulen und die Sternverbindungsverkabelungsmethode für die zentralen Solenoidspulen von großen thermonuklearen Ultrahochfeld-Fusionsreaktoren anwendbar ist. Die Forschung ist von großer Bedeutung bei der Verwendung von REBCO-beschichteten Leitern zur Entwicklung von Ultrahochfeld-Magnetsystemen für kompakte und große thermonukleare Fusionsreaktoren.

Publication List

This dissertation is a publication-based thesis. A publication list with the Ph.D. candidate as the first author and the corresponding author during his Ph.D. studies has been presented as follows. It means that the Ph.D. candidate has been significantly involved in these publications and has taken on a leading function that these publications would not have come about without this involvement. The articles listed below are all peer-reviewed papers published or under review in international journals following the TUM Doctoral Regulations of the Publication-based doctorates at the TUM School of Engineering and Design.

[1]. **Xiaodong Li**, Chunyu Liu, Xiaolie Wang, Wenjiang Yang and Rafael Macián-Juan. (2021). An idea of employing a superconducting cylindrical linear induction pump for the nuclear power system. *Nuclear Engineering and Design*, 380, 111300.

[2]. **Xiaodong Li**, Wenjiang Yang, Huiming Zhang and Rafael Macián-Juan. (2021). Numerical study of AC loss characteristics in a three-phase superconducting induction pump. *IEEE Transactions on Applied Superconductivity*, 31(5), 1-5.

[3]. **Xiaodong Li**, Yue Wu, Wenjiang Yang and Rafael Macián-Juan. (2022). Magneto-hydrodynamic Characteristics of Molten Salts in a Model-based High Temperature Superconducting Conduction Pump. *Physica C: Superconductivity and its Applications*, 1354061.

[4]. **Xiaodong Li**, Dongbin Song, Yue Wu, Yingzhen Liu, Wenjiang Yang and Rafael Macián-Juan, "Current-Carrying Capability and Magnetic Behavior of the HTS Twisted Stacked-Tape Conductor Cable for the Compact Fusion Reactor," in *IEEE Transactions on Applied Superconductivity*, vol. 32, no. 4, pp. 1-5, June 2022, Art no. 4200205.

[5]. **Xiaodong Li**, Veit Große, Dongbin Song, Wenjiang Yang and Rafael Macián-Juan, Electromechanical behavior of REBCO coated conductor based toroidal field coils for magnetic confinement plasma devices, *Journal of Physics D: Applied Physics* 56.4 (2022): 045001.

[6]. **Xiaodong Li**, Mark Ainslie, Dongbin Song, Wenjiang Yang, and Rafael Macián-Juan,"AC losses reduction in REBCO coated conductors using the hexagonal arrangement cabling method", *IEEE Transactions on Applied Superconductivity*, vol. 34, no. 5, pp. 1-5, Aug. 2024, Art no. 5901505.

[7]. **Xiaodong Li**, Mark Ainslie, Dongbin Song, Wenjiang Yang and Rafael Macián-Juan, "REBCO coated conductors for high-field fusion: state-of-the-art, challenges and perspectives", *Superconductor Science and Technology*, Under Review.

[8]. **Xiaodong Li**, Mark Ainslie, Dongbin Song, Yingzhen Liu, Wenjiang Yang, and Rafael Macián-Juan, " Electro-thermal-mechanical behaviour of HTS REBCO coated conductor central solenoid coils for ultra-high-field thermonuclear fusion reactors", *Journal of Physics D: Applied Physics*, Under Review.

Contents

1 Introduction

The discovery of the zero-resistance phenomenon in mercury wires at 4.16 K by Heike Kamerlingh Onnes at the physics laboratory of the University of Leiden in 1911 unlocked the door to the world of superconductivity [1]. The step means possible breakthroughs in ultra-high-field applications and long-distance loss-free power transmission might be achieved. In 1913, Kamerlingh Onnes was awarded the Nobel Prize in Physics. Later, in 1933, Walther Meissner discovered the expulsion of magnetic fields by superconductors [2]. It was known as the Meissner effect, the theory for superconducting levitation. These are the main discoveries of superconductivity in the last century.

After these discoveries, a series of superconducting theories for explaining superconductivity emerged. In 1935, Fritz and Heinz London developed the London equations, which can be used to explain the Meissner effect and estimate the magnetic field penetration depth, also called the London penetration depth, into a superconductor [3]. In 1950, Landau and Ginzburg developed the Ginzburg-Landau theory that can be used to explain the macroscopic properties of type-I superconductors [4], which are generally metal superconductors and only have one critical magnetic field H_c. These superconductors will be quenched when the external magnetic fields exceed H_c. In 1957, Abrikosov further developed the Ginzburg-Landau theory to the type-II superconductors [5], which are typically metal-alloy superconductors or complex oxide ceramic superconductors that have two critical magnetic fields H_{c1} and H_{c2}. When the external magnetic fields exceed the critical magnetic field H_{c1}, the type-II superconductors maintain a superconducting state but into a flux pinning state, where the type-II superconductors can be suspended over a magnet. The thinner the superconducting layer, the stronger the flux pinning occurs. Generally, the H_{c2} of type-II superconductors can be extremely high up to more than 100 Tesla [6]. This makes them perfect candidates for ultra-high-field applications. Landau won the Nobel Prize in Physics for his contributions to the super-fluidity dynamics in low-temperature environment in 1968. Ginzburg and Abrikosov received the Nobel Prize in Physics in 2003 for their work in the Ginzburg-Landau theory. London equations and Ginzburg-Landau theory can explain the phenomenon of superconductivity in a macroscopic way. A complete microscopic theory of superconductivity that is known as the BCS theory was proposed by Bardeen, Cooper, and Schrieffer in 1957 [7]. The BCS theory believes that a pair of electrons in a superconducting material can interact with each other through the exchange of phonons, and their connection becomes the Cooper pair. The super-fluidity of Copper pairs in the superconductor can form into superconducting currents with zero resistance. Bardeen, Cooper, and Schrieffer received the Nobel Prize in Physics in 1972 for their contributions to the BCS theory. Based on the theory, in 1962, Josephson proposed a theoretical prediction that a supercurrent can flow between two pieces of superconductors, which are separated by a thin-layer insulator, which is the Josephson Effect [8]. This effect has been widely used for superconducting quantum interference devices, which can measure magnetic fluxes as low as 5×10^{-14} T

[9]. Josephson received the Nobel Prize in Physics in 1973 for his work on the Josephson Effect. In 2020, it was discovered that there is a smooth transition between the Bose-Einstein condensation and the BCS theory [10]. However, the BCS theory can explain well many of the type-I superconductors. The extension of the theory to unconventional superconductors, such as type-II superconductors and graphene, is still controversial. In 2022, experiments showed that the copper-oxide high-temperature superconductivity mechanism might be related to the super-exchange of electrons [11]. Exploring theories for superconductivity, especially for type-II superconductors, is still in progress. It is one of the major unsolved issues for the theoretical physics community this century.

1.1 Superconductivity in rare-earth barium copper oxide materials

The discovery of superconductivity in rare-earth barium copper oxide (REBCO) materials by Georg Bednorz and K. Alex Müller in 1986 opened the world of high-temperature superconductivity [12]. Bednorz and Müller were awarded the Nobel Prize in Physics in 1987 for their contributions to the discovery. In 1987, yttrium barium copper oxide (YBCO) materials were demonstrated to have an ultra-high critical temperature of more than 90 K [13], which allows the cryogenic environment for superconductivity to achieve the high-temperature liquid nitrogen environment; this is the meaning of high-temperature superconductivity. In addition to having a very high critical temperature, REBCO materials also have an incredibly high critical current and a critical magnetic field. However, the relationship between critical temperature, critical current, and critical magnetic field in superconductivity is always mutually restrictive. This means that the lower the operating temperature, the higher the critical current and the critical magnetic field. The relationship between the critical current density of superconductivity and external magnetic field at low operating temperature environments can be seen in Fig.1 [14]. It shows the superiority of REBCO materials in achieving outstanding current-carrying capacity compared with other superconductors. Therefore, to achieve an ultra-high-field performance for REBCO materials, the operating temperature should be as low as possible.

In achieving ultra-high fields for large-scale applications of fusion reactors, the superiority of superconductivity is mainly related to its zero-resistance characteristics. However, the Meissner effect of superconductivity might negatively impact the performance of superconductors since a changing external magnetic field will induce a screening current in superconductors, which shows a diamagnetism and is the source of the Meissner effect. The higher the induced screening current, the lower the critical current density of superconductors. This is why the critical current density decreases with the external magnetic fields. Therefore, it is highly recommended that REBCO materials be protected from being influenced by external magnetic fields as much as possible. This is the significance of exploring suitable REBCO cabling methods that can achieve inductance balance and magnetic diffusion. On the other hand, REBCO materials are ceramic materials with fragile mechanical behavior that is quite different from

the metal Nb_3Sn or Nb-Ti conductors. The fabrication of REBCO materials into superconducting wires is challenging and costs around 20 years, from discovering superconductivity in REBCO materials to the practical applications of REBCO coated conductors.

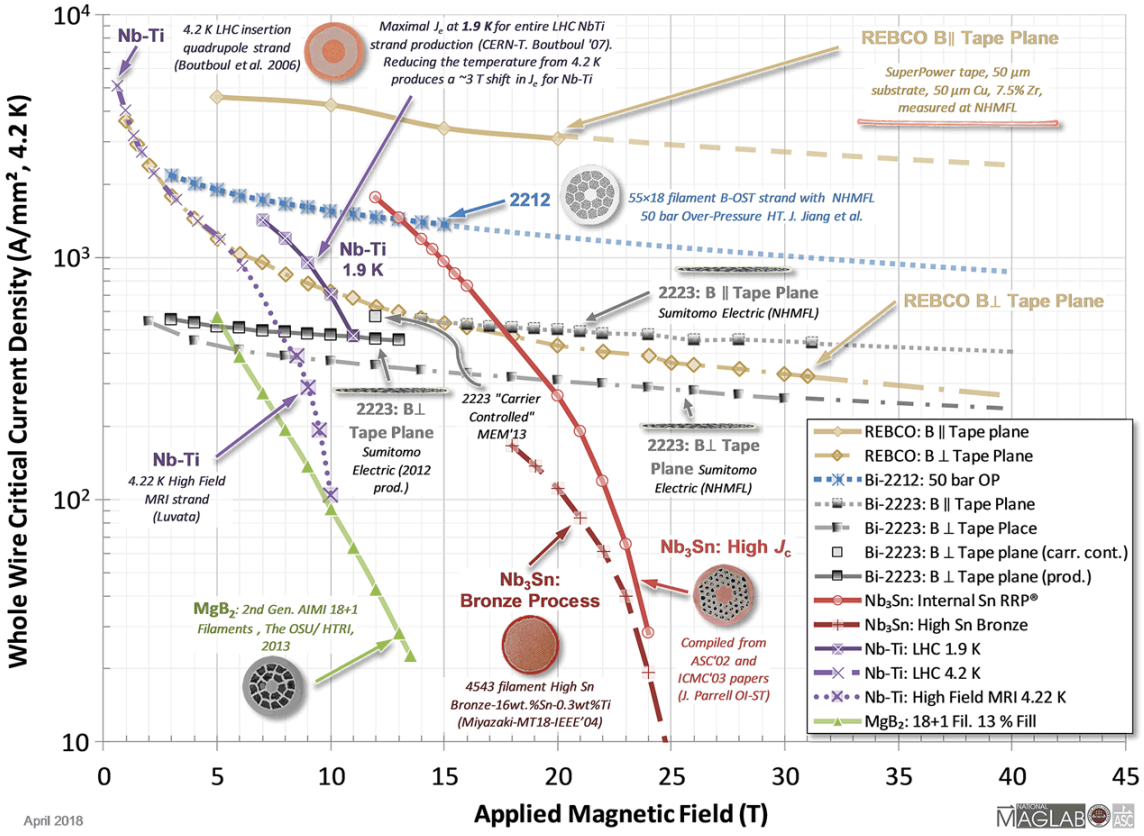

Fig.1 The relationship between critical current density and applied magnetic fields for superconductors. Courtesy of Peter J. Lee, Applied Superconductivity Center at the National High Magnetic Field Laboratory.

1.2 The elaboration of REBCO coated conductors

The architecture of REBCO coated conductors is complicated, as shown in Fig.2 [15]. Considering that the REBCO materials have very brittle mechanical properties, the thin REBCO layer with around 1 µm is laid on the 50 µm thick Hastelloy layer with excellent malleability by using the ion-beam-assisted deposition (IBAD) method [16]. This innovation invests REBCO materials with strength and bending functions, like wires. The silver layers have a current-sharing function, while the copper layers add thermal stability. The elaboration of REBCO coated conductors in 2006 enabled a large amount of high-temperature low-field applications such as motors and generators [17] [18], fault current limiters and transformers [19] [20], current lead and induction heaters [21] [22] and magneto-hydrodynamic pumps and drivers [23] [24] to be developed. The magnetic field strength requirements of these applications are conventionally at the level of several Tesla and, therefore, can be achieved within the current-carrying capacity of single tapes. However, an ultra-high field of more than 20 Tesla requires extremely high engineering current-carrying capacity that can only be possibly achieved by the cabling solution.

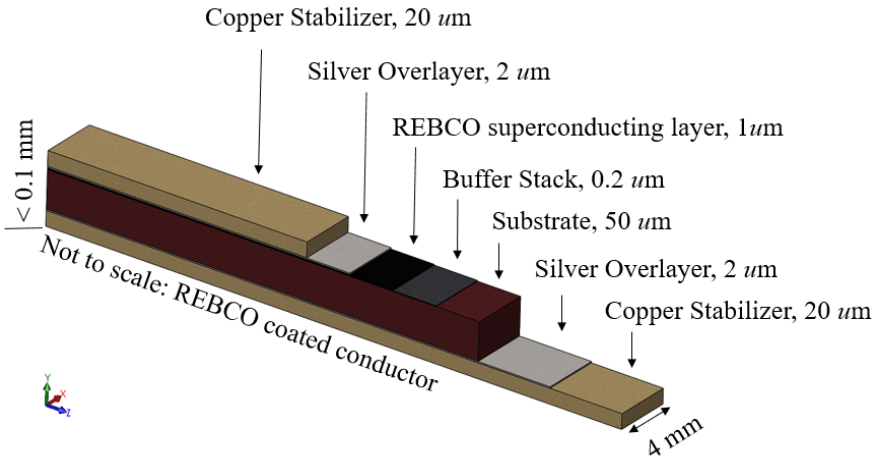

Fig.2 The multi-layer structure of a REBCO coated conductor produced by Super-Power using ion-beam-assisted deposition (IBAD) method.

1.3 State-of-the art: REBCO cabling methods

Five REBCO cabling strategies were developed after the elaboration of REBCO coated conductors; these cabling methods are all based on the cable-in-conduit conductor derived from the LTS cables. Specifically, these cabling methods are conductor on round core (CORC) cable, twisted stacked tape conductor (TSTC) cable, REBCO Roebel cable, REBCO Rutherford cable, and non-twisted cable. This section will discuss the current-carrying capacity of these cables under high fields.

1.3.1 Conductor on round core (CORC) cables

The development of CORC cables started in 2008; the primary purpose of the concept is to decrease AC losses and increase current-carrying capability by bending and winding REBCO coated conductors on a round core former to achieve transposition [25]. A configuration of the cable concept can be seen in Fig.3 [26]. The measurement of the critical current in CORC cables with a background magnetic field of 20 T at 4.2 K demonstrates that the critical current of the CORC cable with 52 tapes wound in 17 layers can reach 5.0 kA [27]. Subsequently, the critical current of a CORC cable with 50 tapes in 20 layers wound using the cable machine reached 7.0 kA under a background magnetic field of 17.0 Tesla at 4.2 K [28]. To find the dependence of critical current on magnetic fields, a CORC cable consisting of 15 tapes arranged in 5 layers with a winding angle of 45° produced by advanced conductor technology (ACT) was tested at KIT [29]. In a temperature environment of 4.2 K, the critical current of the cable decreases from 7.0 kA to 2.8 kA while the external field increases from 2.0 T to 12.0 T. The relationship between the critical current and the background magnetic field is demonstrated to follow a reciprocal dependence. In addition, an experimental study executed by MIT found the inductance stability of the CORC cable while increasing the current ramping rate from 2.0 A/s to 67.8 kA/s under a background

magnetic field up to 19 Tesla [30], which demonstrates its viability for applications in low-inductance magnets. A study carried out by ACT found that the critical current of the CORC cable can be increased by decreasing the substrate layer of the REBCO coated conductor from 50 μm to 38 μm, which allows an engineering current density of the CORC cable above 200 A/mm2, with a background magnetic field of 20 T at 4.2 K [31]. This idea eventually led to the development of STAR wires.

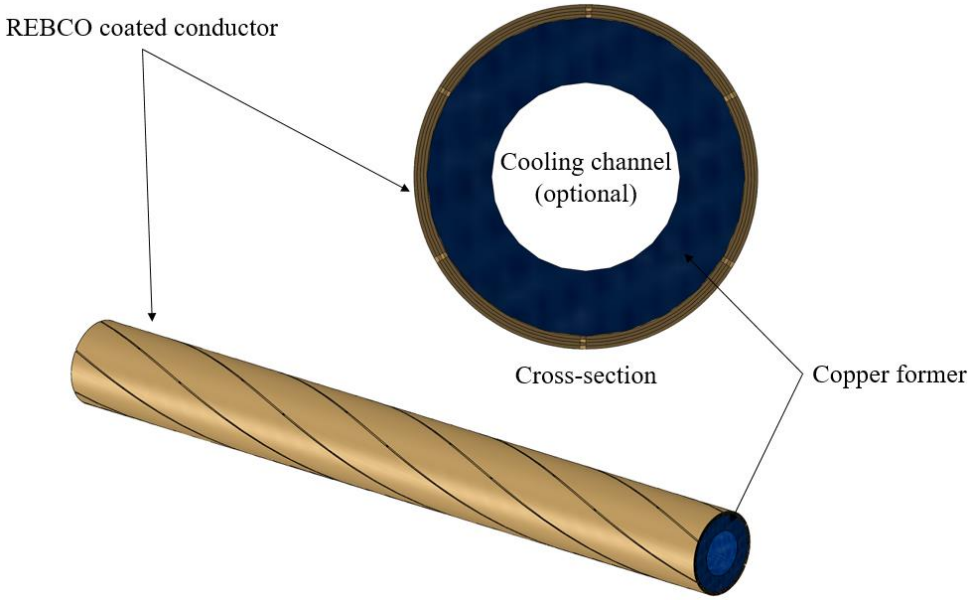

Fig.3 A CORC cable with 4 mm-width REBCO coated conductor being wound on the copper former.

The STAR wire is a CORC cable, but the STAR wire employs REBCO coated conductors with a symmetric structure arranged as Cu-Ag-REBCO-Buffer layer-Hastelloy-Ag-Cu as shown in the diagram of the STAR wire in Fig. 4. The Hastelloy layer in the conductor is only 20 μm thick [32]; it is reduced by more than half compared with conventional REBCO coated conductors. The reduced thickness compensates for the complement of copper layers that are used for current sharing. Structure optimization was performed based on CORC cables. For example, the space between each tape round is increased in comparison with the CORC cable, which is beneficial to the reduction of AC losses [33]. Optimizations of the REBCO coated conductor and the structure have significantly improved the electromechanical behavior of the cable. It is demonstrated that a STAR wire with six superconducting tapes under a bending radius of 15 mm can exhibit a critical current of 586.4 A/mm^2 at 20 Tesla, 4.2 K. A STAR wire with 12 superconducting tapes under the same conditions can present a critical current of 871.3 A/mm^2, the highest engineering critical current value ever reported for REBCO round wires [34]. Likewise, a type of STAR wire with a bending radius of 10 mm can sustain an engineering critical current of 333 A/mm^2 under 20 T, 4.2 K, and 412.7 A/mm^2 under 15 T, 4.2 K [35]. In addition, after several power cycles, the critical current of the cable drops by less than 1% and can still maintain around 300 A/mm^2 with a background field of more than 31 T. This demonstrates the excellent robustness of

the cable [36]. It has to be admitted that the behavior of STAR wires under ultra-high fields has been enhanced compared with the conventional CORC cables.

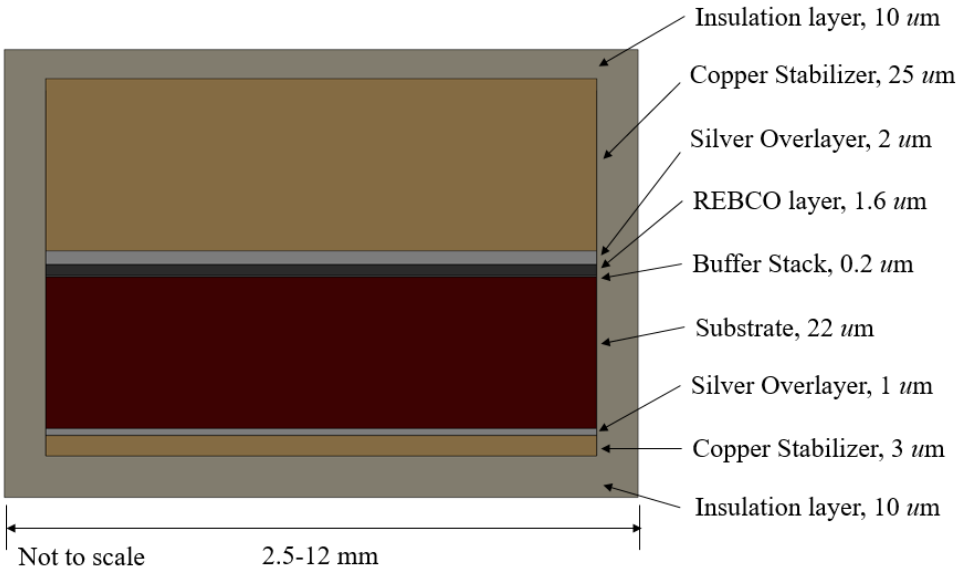

Fig.4 Cross-section of the STAR wire with a symmetric structure arranged as Cu-Ag-REBCO-Buffer layer-Hastelloy-Ag-Cu.

1.3.2 Twisted stacked tape conductor (TSTC) cables

The concept of a TSTC conductor was initially proposed by Takayasu *et al*. for high-field applications in 2012 [37]. Unlike CORC cables and STAR wires, which use bending and winding on a round core former to achieve transposition, the TSTC conductor adopts the twisting transposition approach, with the effect of reducing magnetic flux coupling loss. It has an advantage in increasing the current-carrying capability with the tapes stacked together to achieve a high engineering critical current density, showing great potential for ultra-high-field applications. The TSTC conductor has now evolved into the TSTC cable as shown in Fig.5, particularly the VIPER cable used for the feeder line of toroidal field coils in the SPARC project [38]. The current distribution along the TSTC conductor is non-uniform, as the conductor is not fully transposed. Therefore, the magnetic field distribution along the conductor can differ. The current-carrying capability of the TSTC cable is determined by the critical current density where the magnetic flux is concentrated, considering the conductor's anisotropy. It was found that TSTC conductors with multi-tapes show around 50% critical current degradation compared with non-twisted conductors under ultra-high fields, despite the critical current degradation of a single tape conductor not being observed from the transverse load [39]. Major studies also found that the critical current of a TSTC conductor with 50 tapes can reach 4.0 kA with a background magnetic field of 19.7 T at 4.2 K [40]. In addition, the critical current of a TSTC conductor with 40 tapes can reach 5.47 kA with external magnetic fields up to 12 Tesla at 4.2 K. Despite the Lorentz load up to 65.6 kN/m leading to irreversible

critical current degradation of 11.9% [41], these studies indicate that high Lorentz loads under high fields are the main factors that limit the current-carrying capability of the conductor.

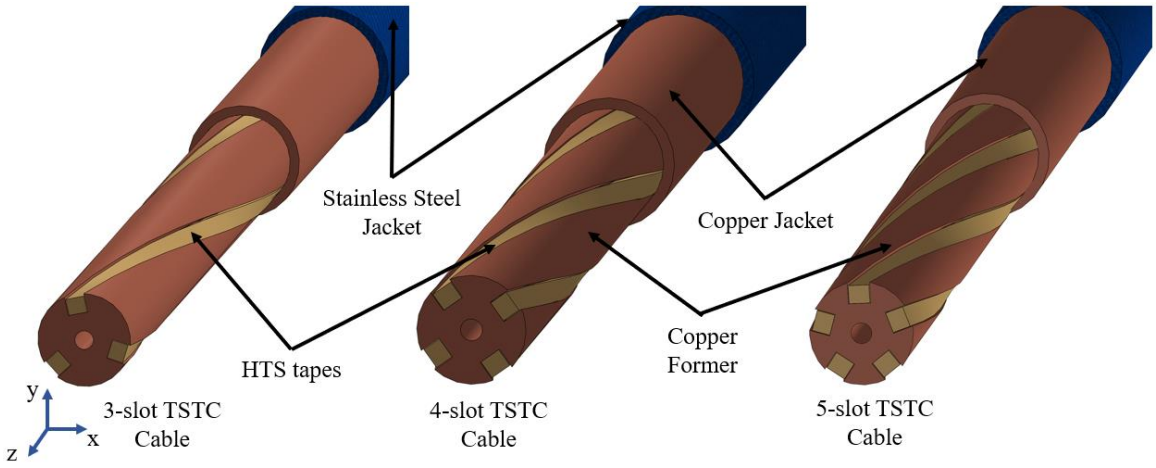

Fig.5 Configuration of the twisted stacked tape conductor (TSTC) cable for high-field superconducting fusion magnets.

The TSTC cable for the SPARC project has been developed for many years. Before the mature design of the VIPER cable, an industrially feasible TSTC cable for fusion was proposed by Celentano et al. [42]. It was experimentally estimated that the critical current of the TSTC cable is 20 kA with a background magnetic field of 15 Tesla at 4.2 K. The bending behavior of the cable was experimentally and numerically analyzed by Marzi et al. [43], and it was found that the bending diameter of the TSTC cable should be no less than 0.5 m to avoid irreversible I_c degradation. This may be why the TSTC cable can be used only as the current leads for toroidal field coils but has yet to be for the central solenoid coils in the SPARC project, in which the cable-bending processes can be avoided. Meanwhile, FEM analysis of the TSTC cable shows that the current distribution along the coated conductor is non-uniform, which might cause operating instability and lead to irreversible damage during operation [44]. The current-carrying capability and magnetic behavior of the TSTC cable with different slots were studied by Li et al. [45], and it was found that the 4-slot cable is the most suitable option when the same copper's former diameter is considered. Consequently, the TSTC cable is demonstrated as having a high current-carrying capability for fusion reactors. However, it is suggested only for use as the feeder line for the toroidal field coils since bending the cable might lead to irreversible critical current degradation.

1.3.3 REBCO Roebel cables

In 1914, Ludwig Roebel put forward a cable design to reduce eddy-current losses in copper wires by breaking down these wires into a series of insulated copper strands and twisting them to achieve complete transposition so that each position in the cable has the same operating periodicity under a time-varying current transmission condition. This invention successfully reduced AC losses and decreased

the operating temperature of sizeable electrical power generators [46]. In 2005, the Roebel cable concept was demonstrated as a practical approach offering complete transposition to REBCO coated conductors [47] [48]. The composition principle of the REBCO Roebel cable can be seen in Fig.6 [46]. It can achieve an extremely high engineering current density, thanks to the superiority of the cable at reducing AC losses. The cable is demonstrated to be feasible for high-temperature, low-field AC current applications. Challenges with the cable mainly relate to the mechanical stress associated with enormous Lorentz force under ultra-high fields and the bending strain caused by the tight bending radius for accelerator and fusion magnets with ultra-high fields.

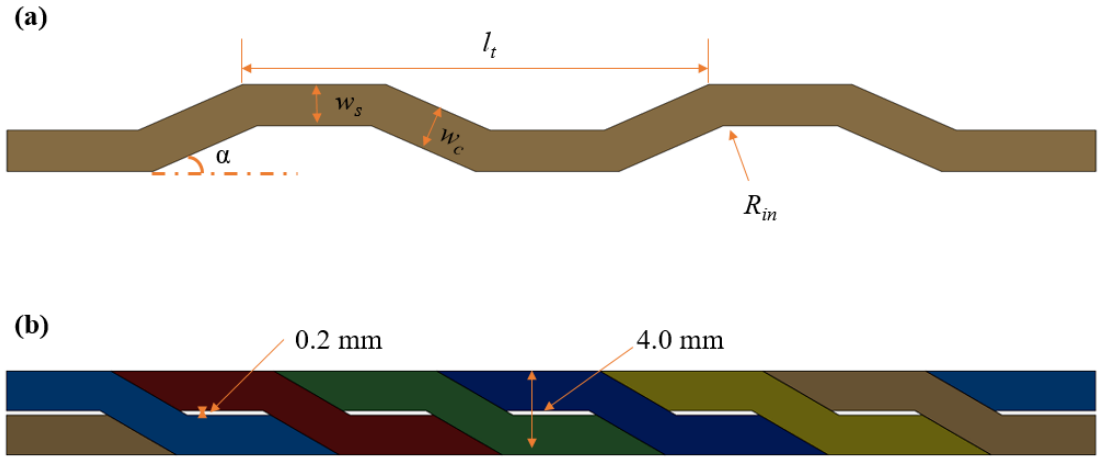

Fig.6 (a) A REBCO Roebel cutting pattern. (b) Assembly of a REBCO Roebel cable with six strands.

Critical currents of Roebel cables with 10 and 15 strands under external magnetic fields up to 9.6 T were measured at 4.2 K by J Fleiter et al. [49]. It was demonstrated that the maximum critical current of Roebel cables can reach 11.7 kA under a parallel field of 7.5 T. In comparison, the value decreases to 3.4 kA under a perpendicular field of 9.6 T. However, it was also demonstrated that an average transverse compressive stress of 45 MPa caused no critical current decay. In addition, a 7-turn, robust pancake coil wound with 15-strand Roebel cables was demonstrated to have an Ic of 1.5 kA under 8 T at 50 K [50]. Meanwhile, Roebel cables with 9-strand and 16-strand REBCO coated conductors containing copper stabilizers were investigated. The critical current of the 9-strand cables can reach 15 kA with the self-field, at 12.6 kA under an external parallel field of 7.0 T, but fall to 2.3 kA under an external perpendicular field of 9.6 T. The critical current of the 16-strand cables can reach 2.9 kA with an external perpendicular field of 9.6 T. An I_c degradation caused by an average transverse compressive stress of 40 MPa was detected [51]. The study shows that the function of a copper stabilizer in protecting against current decay caused by the transverse compressive stress under ultra-high fields is questionable. It should be concluded that the REBCO Roebel cable might have better performance for high-temperature, low-field applications such as generators, owing to its advantages in reducing AC losses. However, the electromechanical behavior of the cable associated with the unavoidable transverse

compressive stress caused by enormous Lorentz force under high fields is shown to be sensitive. Therefore, it might be a questionable solution for low-temperature, high-field applications, such as fusion magnets or magnets for accelerators.

1.3.4 REBCO Rutherford cables

The name of the Rutherford cable is taken from the Rutherford laboratory, whose purpose is the design of superconducting cables with extremely high current-carrying capability to realize ultra-high fields for dipole and quadrupole accelerator magnets [52]. The idea has been successfully achieved using multi-strand niobium-tin superconducting wires, from which current transposition can be fully realized. Drawing on the successful application of Rutherford cables for low-temperature superconductors (LTS), the possibility of using high-temperature superconducting REBCO coated conductors to achieve a REBCO Rutherford cable design with high current-carrying capability and low AC loss characteristics has been investigated by the HTS community. A type of HTS REBCO Rutherford cable can be viewed in Fig.7. The difference between LTS and HTS Rutherford cables is that a large, flat, metal former, which can support as many REBCO coated conductors as possible, is conventionally required for REBCO Rutherford cables. However, mounting a flat REBCO conductor with a round edge on a flat former is challenging. One possible way to use REBCO coated conductors as strands for the Rutherford cable is to stack them as taped stacks with a certain twisted angle or to employ REBCO conductors that have no backbone support, such as the Roebel cable, as strands on the former metal. A representative design of the REBCO Rutherford cable is the 60 kA REBCO coated conductor cable proposed by the Swiss Plasma Center (SPC) [53]. With an advantage in achieving ultra-high critical current density, there will be a lot of design work on this cable soon.

The critical current of the Roebel on Rutherford cable with self-field was tested in a liquid nitrogen environment [54]. The critical current of the Rutherford cable assembled with Roebel strands was found to be around 450 A, which is about 30% lower than the total critical current of the individual Roebel strands. There is currently no experimental data for the critical current of the cable under ultra-high fields. The critical current of the Rutherford cable developed by SPC can range from 30 kA to 70 kA with an external background magnetic field from 8 Tesla to 12 Tesla at 4.2 K [55]. The flat-type Rutherford cable is a cable concept proposed by Takayasu at MIT; the critical current test and bending experiments under ultra-high fields have yet to be investigated [56]. In brief, the research and development of the REBCO Rutherford cable is still at an early stage. Considering the superiority of Rutherford cables in terms of high current-carrying capability, the cable form is highly recommended for ultra-high-field applications in fusion and accelerator magnets.

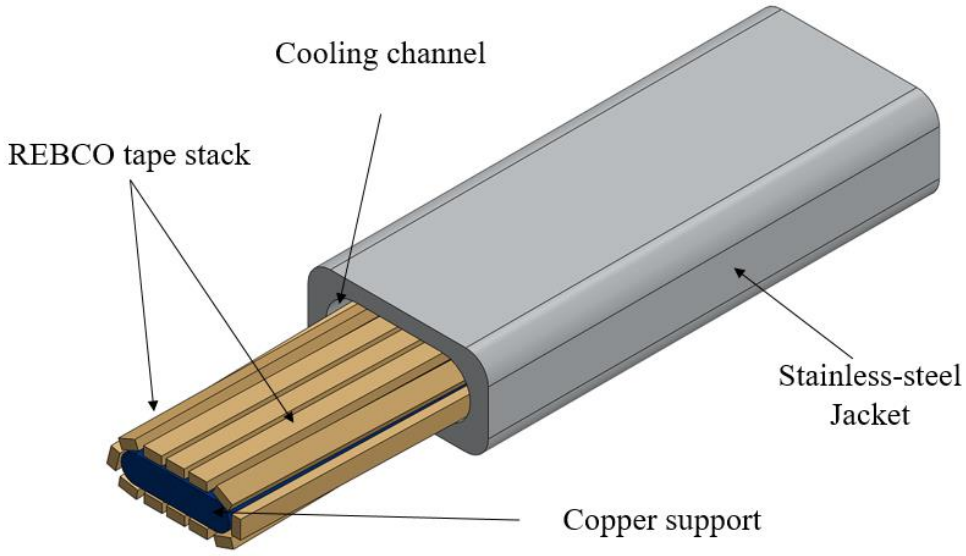

Fig.7 A type of REBCO Rutherford cable design with high current-carrying capacity.

1.3.5 Non-twisted REBCO cables

Non-twisted REBCO cables are commonly used in high-temperature, low-field applications. A representative, non-twisted cable design is the racetrack coil, which can be used as the stator of electrical machines or the magnet for electrodynamic suspension [57] [58]. However, the non-twisted cable configuration has not been fully considered for low-temperature, high-field applications. The main argument focuses on the imbalanced inductance; the magnetic diffusion might lead to an increasing perpendicular field component that causes higher AC losses. In addition, the negative screening current might cause the charging time of the coil to be extremely long. However, a study carried out by Lelekhov shows that the negative effect of screening current would be significantly reduced, owing to the wave-like magnetic field distribution along the non-twisted cables [59], revealing the possibility of using the non-twisted cable for ultra-high-field applications. In addition, Uglietti *et al*. studied the inductance and AC losses of the non-twisted stacked cable [60]. Results show that the twisted-stacked option might be superfluous because the inductance, AC losses, and operating stability might be marginally affected by the twisted structure. The potential advantage of the non-twisting architecture is that it has a higher tolerance to transverse stresses.

Meanwhile, the uninsulated option's critical current density in the non-twisted cable can be incredible. The development of the spherical Tokamak REBCO magnet demonstrator at Tokamak Energy in the UK was approved using non-twisted, partially insulated coils for the toroidal field coil design [61]. The SPARC project operated by MIT employed the non-twisted, uninsulated REBCO stack-in-plate channel design for the toroidal field coil. It demonstrated that the winding pack can achieve a peak magnetic field of 20 Tesla with an operating terminal current of 40 kA at 20 K [62]. These results indicate that the REBCO coated conductor cables might not be sensitive to current transposition. In addition, the non-

twisted cable design can primarily protect the REBCO ceramic conductor from mechanical destruction. This facilitates maximum release of the current-carrying capability of REBCO coated conductors. Therefore, employing the non-twisted REBCO taped stacks as components to develop novel REBCO cables for ultra-high-field applications is highly recommended. A representative non-twisted cable design can be seen in Fig. 8 [63].

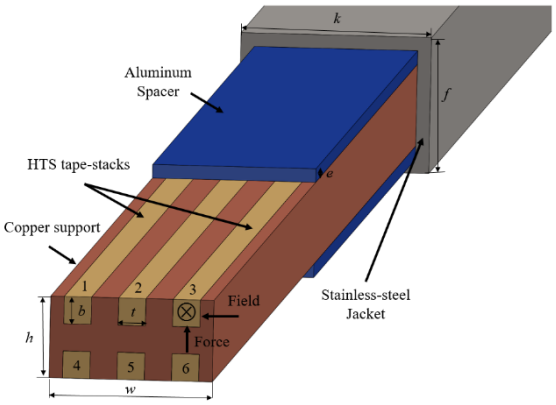

Fig.8 A representative non-twisted cable design featuring tape stacks of REBCO coated conductors embedded in a copper support.

1.3.6 Conclusion

This section has comprehensively reviewed the cutting-edge cabling techniques for REBCO conductors. A significant hurdle in utilizing REBCO cables for ultra-high magnetic fields lies in their mechanical components. To maintain inductance balance, these cables often undergo twisting or bending, actions that can severely compromise the ceramic superconductor layer's mechanical integrity within the REBCO coated conductors. Consequently, it is advisable to minimize twisting in the design phase of REBCO cabling strategies. Nonetheless, achieving a high inductance balance remains a crucial design objective. The insights and findings from this discussion have been synthesized into the manuscript titled " REBCO coated conductors for high-field fusion: state-of-the-art, challenges and perspectives," which is presently undergoing peer review at the journal *Superconductor Science and Technology*.

2 Experiments and simulation methodologies

This research was conducted through a combination of experiments and simulations. Experiments to measure the critical current density in REBCO-coated conductors were performed at Theva Dünnschichttechnik GmbH. A benchmark model for the REBCO-coated conductor's empirical equation was developed using this experimental data. To solve the equations, we employed finite element methods based on **H**-formulation, **T-A** formulation, and **A-V** formulation. These methodologies are discussed in detail in this section.

2.1 Experiments on the critical current in REBCO-coated conductors

The critical current density in REBCO-coated conductors was measured using the four-lead method, as illustrated in Figure 9. Voltage taps, affixed to the sample with soldering tin, measured the voltage across the conductor's ends. The conductor was subjected to DC transport at a current increase rate of 1 A/s via copper lead.

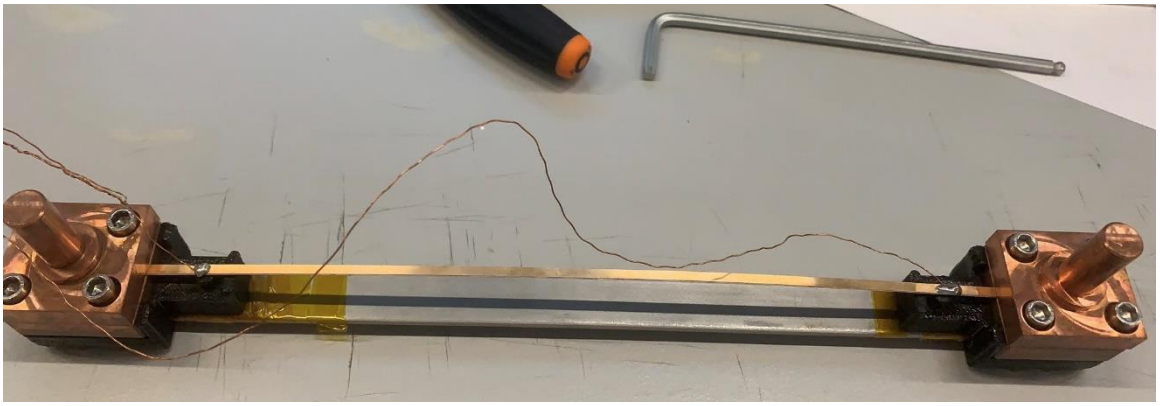

Fig.9 Experiment test of the critical current density in the REBCO coated conductor using the four-lead method.

The critical current for the REBCO coated conductor, when tested under self-field conditions in a liquid nitrogen environment, was determined to be 112 A. With the conductor tape measuring 4 mm in width and the superconducting layer being 1 µm thick, the resulting critical current density in a liquid nitrogen environment (77 K) under self-field conditions is calculated as 112 A divided by 4 mm and further divided by 1 µm, yielding a value of 2.8×10^{10} A/m^2. This critical current density value has been utilized in developing a benchmark finite element model for REBCO coated conductors.

2.2 Construction of the benchmarked model

The **E-J** relationship in REBCO coated conductors has been observed experimentally to follow an exponential relation as:

$$\mathbf{E} = E_0 \left| \frac{J}{J_c(B_{\parallel}, B_{\perp}, T)} \right|^n \cdot \frac{\mathbf{J}}{|J|} \tag{1}$$

This model has proven to align well with theories of superconductivity, addressing magnetic flux penetration, susceptibility to AC loss, flux creep, and critical state analysis, as referenced in [64]. From equation (1), we can infer that the nonlinear resistivity of the REBCO coated conductor is as follows:

$$\rho = \frac{E_0}{J_c(B_{\parallel}, B_{\perp}, T)} \cdot \left| \frac{J}{J_c(B_{\parallel}, B_{\perp}, T)} \right|^{n-1} \tag{2}$$

The relationship between the critical current density and the magnetic field can be modeled through the Kim model [65], incorporating temperature effects as follows:

$$J_c(B_{\parallel}, B_{\perp}, T) = \frac{J_{c0}}{\left[1 + \sqrt{(kB_{\parallel})^2 + B_{\perp}^2} / B_0\right]^{\alpha}} \cdot [1 - (\frac{T}{T_c})^2]^{3/2} \tag{3}$$

These equations delineate the E-J relationship in superconductors, highlighting the critical current density's sensitivity to external magnetic fields and operating temperatures. Detailed descriptions and values for these parameters are presented in Table 1.

Table 1 Description and values of parameters in the model.

Parameter	Description	Value
E_0	Electric field constant in equation (1)	1×10^{-4} V/m
n	n-value in equation (1) and equation (2)	29
B_0	Magnetic flux density constant in equation (3)	0.04265 T
k	Constant in equation (3)	0.29515
α	Index in equation (3)	0.5
J_{c0}	Critical current density of the REBCO coated conductor at 77 K.	2.8×10^{10} A/m^2
v	The thickness of the superconducting layer in the REBCO coated conductor	1×10^{-6} m

w	The thickness of the REBCO coated conductor	1×10^{-4} m
ρ_{co}	Resistivity of copper at 4.2 K	1.97×10^{-9} Ω/m
T_c	Critical temperature of REBCO coated conductors	92 K
ρ_r	Density of the REBCO coated conductor	8.0×10^{3} kg/m^3
ρ_c	Density of the copper former	8.96×10^{3} kg/m^3
E_r	Young's modulus of the REBCO coated conductor	1.40×10^{11} Pa
E_c	Young's modulus of the copper former	1.30×10^{11} Pa
P_r	Poisson's ratio of the REBCO coated conductor	0.3
P_c	Poisson's ratio of the copper former	0.34

2.3 Governing equations

The solution of partial differential equations, related to Maxwell's equations and the nonlinear **E-J** relationship on superconductivity, relies highly on certain variables. In recent years, three main finite element methods have been developed to solve the electromagnetic behavior of superconductivity. Specifically, there are **H**-formulation [66][67][68], **T-A** formulation [69][70][71], and **A-V** formulation [72][73][74]. These formulation-based finite element methods are mainly studied and discussed in this section.

2.3.1 H-formulation

In the **H**-formulation, **H** stands fort the magnetic field strength in the solving domain. The current density **J** in the solution domain can be derived via the quasi-static approximation of the Maxwell-Ampere's law as:

$$\nabla \times \mathbf{H} = \mathbf{J} \tag{4}$$

The electromagnetic behavior of the solution domain should satisfy the Maxwell-Faraday's law as:

$$\nabla \times \mathbf{E} = -\frac{\partial \mathbf{B}}{\partial t} \tag{5}$$

Therefore, we can solve equation (5) with the dependent variable **H** as:

$$\frac{\partial(\mu_0 \mu_r \mathbf{H})}{\partial t} + \nabla \times (\rho \nabla \times \mathbf{H}) = 0 \tag{6}$$

Here μ_0 and μ_r stand respectively for the magnetic and relative permeability of the free space. The advantage of the **H**-formulation is that since there is only one variable for the solution domain, it is not difficult to combine the method with other partial differential equations to solve the multi-physics problem in superconductivity. As it can be deduced from equation (4) and (5) that the power loss in superconductivity can be represented as:

$$Q = \mathbf{E} \cdot \mathbf{J} \tag{7}$$

A typical thermal model combines with the electromagnetic model of superconductivity can be solved by using the equation:

$$C_v \frac{\partial T}{\partial t} = \nabla \cdot (\lambda \nabla T) + Q \tag{8}$$

However, the disadvantage of using **H**-formulation for the solution is that since the resistivity of REBCO coated conductors is strongly non-linear, the air domain with a constant resistivity has to be solved together with the superconducting domain. Therefore, the computation efficiency of using **H** formulation can be low. In comparison, the **T**-**A** formulation which uses thin-strip approximation to simplify the meshing issues of superconductivity has a higher computational efficiency.

2.3.2 T-A formulation

In the **T**-**A** formulation, **T** represents the current vector potential, and **A** stands for the magnetic vector potential. The current density in REBCO coated conductors can be described as:

$$\mathbf{J} = \nabla \times \mathbf{T} \tag{9}$$

The magnetic field **H** in the solution domain can be solved by the magnetic vector potential **A** as:

$$\mathbf{H} = \frac{\mathbf{B}}{\mu_0} = \frac{\nabla \times \mathbf{A}}{\mu_0} \tag{10}$$

In addition, the Coulomb gauge has been used for the vector potential. The whole solution domain should satisfy the Maxwell-Ampere's circuital law as:

$$\nabla \times \nabla \times \mathbf{A} = \mu_0 \mu_r \mathbf{J} \tag{11}$$

It should be mentioned that in a three-dimensional model, equation (9) can be written as:

$$\begin{bmatrix} J_x \\ J_y \\ J_z \end{bmatrix} = \begin{bmatrix} \frac{\partial (T \cdot n_z)}{\partial y} - \frac{\partial (T \cdot n_y)}{\partial z} \\ \frac{\partial (T \cdot n_x)}{\partial z} - \frac{\partial (T \cdot n_z)}{\partial x} \\ \frac{\partial (T \cdot n_y)}{\partial x} - \frac{\partial (T \cdot n_x)}{\partial y} \end{bmatrix} \tag{12}$$

Therefore, the implementation of Faraday's law in the superconducting domain can be described as:

$$\begin{bmatrix} \frac{\partial E_z}{\partial y} - \frac{\partial E_y}{\partial z} \\ \frac{\partial E_x}{\partial z} - \frac{\partial E_z}{\partial x} \\ \frac{\partial E_y}{\partial x} - \frac{\partial E_x}{\partial y} \end{bmatrix} \cdot \mathbf{n} + \begin{bmatrix} \frac{\partial B_x}{\partial t} \\ \frac{\partial B_y}{\partial t} \\ \frac{\partial B_z}{\partial t} \end{bmatrix} \cdot \mathbf{n} = 0 \tag{13}$$

The soul of the **T-A** formulation is that it uses thin-strip approximation which decreases the modeling of REBCO coated conductor tapes from two-dimension to one-dimension that solves the meshing issue of REBCO coated conductors caused by the large aspect ratio. However, the distribution of current density is non-linear with the **E-J** relationship, it means that the computational accuracy of **T-A** formulation using the decreasing dimension method might not be high enough. In specifically, the thin-strip approximation might not be able to solve the screening current issues, especially the London penetration depth caused by magnetization in REBCO coated conductors.

The **T-A** formulation and the **H**-formulation are conventionally used for the calculation of REBCO coated conductors with limited number of tapes. In large-scale computation of REBCO coated conductors with many tapes such as the toroidal field coils of ultra-high-field magnetic-confinement plasma devices, the **A-V** formulation has to be considered.

2.3.3 A-V formulation

In the **A-V** formulation, **A** stands for the magnetic vector potential, and **V** is the electrostatic contribution. The Maxwell-Faraday's equation (5) for the electrical field **E** can be expressed as:

$$\mathbf{E} = -\frac{\partial \mathbf{A}}{\partial t} - \nabla \varphi \tag{14}$$

Combining the **E-J** power law in equations (1) and (14) we can derive:

$$J = J_c(B_{\parallel}, B_{\perp}, T) \sqrt[n]{-\frac{\partial A}{\partial t E_0}} \tag{15}$$

The problem in equation (15) is that the curve associated with the equation is not smooth while $\partial A / \partial t$ equals to zero. Considering the n value is an odd number, equation (15) can be converted into the hyperbolic tangent function, which has no such defect and can be described as:

$$J = J_c(B_{\parallel}, B_{\perp}, T) \tanh(-\frac{\partial A}{\partial t E_0}) \tag{16}$$

However, the collinearity between the current density and the electric field should be ensured by the proportionality rule as:

$$\partial A_x : \partial A_y : \partial A_z = J_x : J_y : J_z \tag{17}$$

In addition, the limitation on the superconducting state is defined by the current density as:

$$\sqrt{J_x^2 + J_y^2 + J_z^2} \le J_c(B_{\parallel}, B_{\perp}, T) \tag{18}$$

Therefore, the current density of a REBCO coated conductor which is used in the 3D computation of the toroidal field coils can be defined by combining equations (16)-(18) as:

$$J = \frac{J_c(B_{\parallel}, B_{\perp}, T)}{|E|}\left[|E_x| \tanh(\frac{E_x}{E_0})\mathbf{i} + |E_y| \tanh(\frac{E_y}{E_0})\mathbf{j} + |E_z| \tanh(\frac{E_z}{E_0})\mathbf{k} \right] \tag{19}$$

In the study of using **A-V** formulation for the calculation of electromechanical behavior in the toroidal field coils of magnetic-confinement plasma devices, the Maxwell stress has been employed and it can be defined as:

$$\mathbf{n}T_2 = -\frac{1}{2}\mathbf{n}(\mathbf{E}\cdot\mathbf{D}) + (\mathbf{n}\cdot\mathbf{E})\mathbf{D}^{\mathbf{T}} \tag{20}$$

$$\mathbf{n}T_2 = -\frac{1}{2}\mathbf{n}(\mathbf{H}\cdot\mathbf{B}) + (\mathbf{n}\cdot\mathbf{H})\mathbf{B}^{\mathbf{T}} \tag{21}$$

Here **E** is the electric field, **D** is the electric displacement, **B** represents the magnetic flux density and **H** stands for the magnetic field. T_2 is the stress tensor and can be described by the matrix. We define **n** here as the downward surface normal from the object.

In addition, the multi-physics coupling between the magnetic fields and the solid mechanics is realized by the Lorentz force:

$$\mathbf{F} = \mathbf{J} \times \mathbf{B} \tag{22}$$

Therefore, the relationship between the stress **S**, the displacement **u** and the Lorentz force **F** should satisfy:

$$\rho \cdot \frac{\partial^2 \mathbf{u}}{\partial t^2} = \nabla \cdot \mathbf{S} + \mathbf{F} \tag{23}$$

Here ρ is the density, and the relationship between the stress **S** and the strain ε should obey Hooke's law as:

$$S - (S_0 + S_{ext} + S_q) = \mathbf{C} : (\varepsilon_e - (\varepsilon_0 + \varepsilon_t + \varepsilon_h + \varepsilon_p + \varepsilon_c)) \tag{24}$$

S_0 stands for the prestress, Sext means the external stress and S_q represents the viscous stress, which is conventionally used in fluid dynamics, so that the viscous stress in the solution domain should be 0. **C** means the elastic matrix, ε_e is the elastic strain, ε_0 is the prestrain, ε_t is the thermal strain, ε_h means the infiltration swelling when the materials are absorbed with liquid. ε_p is the plastic deformation and ε_c is

the creep deformation that equals to 0. The relationship between the total strain ε and the displacement **u** can be described as:

$$\varepsilon = \frac{1}{2}\left[(\nabla \mathbf{u})^T + \nabla \mathbf{u}\right] \tag{25}$$

2.4 Boundary conditions

In finite element analysis, boundary conditions are the premise that the governing equations can have a certain solution. The boundary values should be known for a solution domain which is described with governing equations, in specifically, these equations are ordinary differential equations or partial differential equations [75]. As the initial condition describes the initial state of a time-dependent problem, the boundary condition should define the boundary values of a space region. There are mainly five types of boundary conditions: the Dirichlet boundary condition, the Neumann boundary condition, the Robin boundary condition, the mixed boundary and the Cauchy boundary condition.

The Dirichlet boundary condition, which is also known as the first boundary condition, defines the value along the boundary of the domain governed by the unknown governing equations [76]. For example, in the Laplace equation, the Dirichlet boundary condition used to describe the boundary value can be defined as:

$$\Delta\varphi(x) = 0 \qquad \forall x \in \Omega \tag{26}$$

$$\varphi(x) = f(x) \qquad \forall x \in \partial\Omega \tag{27}$$

Here φ is the governing equation, x is the independent variable, Ω is the solution domain, and $\partial\Omega$ is the boundary condition of the solution domain. Therefore, $f(x)$ is defined as the boundary scalar function on $\partial\Omega$. In finite element analysis, the Dirichlet boundary condition is conventionally imposed into the algebraic system which are aimed to be solved. For example, if we have an algebraic system which can be described as:

$$\begin{bmatrix} k_{1,1} & k_{1,2} & \cdot & k_{1,m-1} & k_{1,m} \\ k_{2,1} & k_{2,2} & \cdot & k_{2,m-1} & k_{2,m} \\ \cdot & \cdot & \cdot & \cdot & \cdot \\ k_{m-1,1} & k_{m-1,2} & \cdot & k_{m-1,m-1} & k_{m-1,m} \\ k_{m,1} & k_{m,2} & \cdot & k_{m,m-1} & k_{m,m} \end{bmatrix} \cdot \begin{bmatrix} x_1 \\ x_2 \\ \cdot \\ x_{n-1} \\ x_n \end{bmatrix} = \begin{bmatrix} a_1 \\ a_2 \\ \cdot \\ a_{m-1} \\ a_m \end{bmatrix} \tag{28}$$

k_{ij} stands for the elements of the algebraic operator, x_i means the degree of freedom of the solving problem, and a_i is the known terms. A better method to impose the Dirichlet boundary condition on the solution domain with *n* degree of freedoms is to modify the system as:

$$\begin{bmatrix} k_{1,1} & \cdot & \cdot & \cdot & k_{1,m} \\ \cdot & \cdot & \cdot & \cdot & \cdot \\ 0 & 0 & 1 & 0 & 0 \\ \cdot & \cdot & \cdot & \cdot & \cdot \\ k_{m,1} & \cdot & \cdot & \cdot & k_{m,m} \end{bmatrix} \begin{bmatrix} x_1 \\ \cdot \\ x_n \\ \cdot \\ x_m \end{bmatrix} = \begin{bmatrix} a_1 \\ \cdot \\ f \\ \cdot \\ a_m \end{bmatrix} \tag{29}$$

f is the value of the boundary on the solution domain with *n* degree of freedoms. The Dirichlet boundary condition adds values on the boundary of the solution domain, we can also add the derivative of a solution on the boundary of the domain, which can be called as the Neumann boundary condition, it is also known as the second boundary condition [77]. As the same problem shown in the Laplace equation in equation (22), the boundary value solved by using the Neumann boundary condition can be descripted as:

$$\frac{\partial \varphi(x)}{\partial n} = f(x) \qquad \forall x \in \partial\Omega \tag{30}$$

Here *n* is the unit which is normal to the boundary surface. The Neumann boundary are often used to solve the weak formulation in any finite element approach by rewriting the equation from a strong differential form to a weak integral form with two-step transformation. For example, when we have a simple equation:

$$-u''(x) = p(x) \qquad \forall x \in R \tag{31}$$

We define $u(x)$ as the unknown scalar field and $p(x)$ as the given scalar equation. The equation can be integrated as:

$$-\int_a^b u''(x)v(x)dx = \int_a^b p(x)v(x)dx \tag{32}$$

Here $v(x)$ is the shape function. The Green theorem can be employed to avoid higher order derivatives as:

$$\int_a^b u'(x)v'(x)dx = \int_a^b p(x)v(x)dx + \left[u'(x)v(x)\right]_a^b \tag{33}$$

Therefore, a term with the derivative of the unknown scalar field is appeared. It refers to the extremes of the interval in one dimensional issues, and the contour of the domain for two dimensional issues, while the boundary surfaces for the three-dimensional problems.

The Robin boundary condition is proposed for the finite element solution of electromagnetic scattering problems in open boundary domains [78]. It can be described by a linear combination of the field values and its derivatives on the boundary. For instance, the boundary value of the Laplace equation (22) can be written with the Robin boundary condition form as:

$$a\varphi(x) + b\frac{\partial\varphi(x)}{\partial n} = f(x) \qquad \forall x \in \partial\Omega \tag{34}$$

The mixed boundary condition can be used to determine the electromagnetic field in the presence of one or several bodies of revolution [79]. It uses different types of boundary conditions to different parts of the solution domain, so that the whole solution domain can be solved in total. In addition, the Cauchy boundary condition is a combination of the Dirichlet boundary condition and the Neumann boundary condition. It is used very often in solving heat transfer issues [80][81] and mechanical problems [82]. The electromagnetic problems are conventionally been solved by using the Dirichlet boundary condition, the Neumann boundary condition and the Robin boundary condition.

The **H**-formulation based finite element method uses the Dirichlet boundary condition to define the critical density distribution in REBCO coated conductors by using a pointwise constraint. The **T-A** formulation uses the Dirichlet boundary condition to define the current transmission in REBCO coated conductors by imposing a critical density in the tape to accommodate for the thin strip approximation. However, the **T-A** homogeneous model uses actually the Cauchy boundary condition by adding a Dirichlet boundary condition for current transmission in the REBCO stacked tapes and a Neumann boundary condition to define a zero flux on the direction which is perpendicular to the tape surface. This is the reason that the **T-A** formulation has no function in calculating the magnetization effect of REBCO coated conductors. The **A-V** formulation can actually be decoupled, since the electric potential can be solved by using the Laplace equation as:

$$V = \Delta\varphi = 0 \tag{35}$$

When current transportation is added to the boundary of the solution domain by using **A-V** formulation, Dirichlet boundary conditions are normally been employed. The conductor can be a perfect insulator when the Neumann boundary conditions are added. In addition, Robin boundary conditions are generally be used to solve the impedance of an electric circuit.

2.5 Mesh sensitivity analysis

In the studying of electromechanical behavior in REBCO coated conductor-based ultra-high-field magnet, meshing is an art. Firstly, the electromagnetic behavior of REBCO coated conductors based on the **E-J** relationship is strongly nonlinear. It means that the solution might not be so easily to achieve convergence in the process of iterative calculations. In addition, the REBCO coated conductor has a very high aspect ratio since its width is around 4 mm, but its thickness can be limited to 1 *u*m, which causes a meshing issue. The **T-A** formulation has solved the meshing issue by using the dimension reduction method without considering the thickness of the REBCO coated conductor. In the study of electromechanical behavior of REBCO coated conductors by using the **H**-formulation and the **A-V** formulation, a homogeneous model which consider the REBCO stacked tapes as a superconducting bulk

with anisotropic electromagnetic behavior has been employed. The solutions solve the meshing issues caused by the non-linear **E-J** behavior and the large aspect ratio of the REBCO coated conductors.

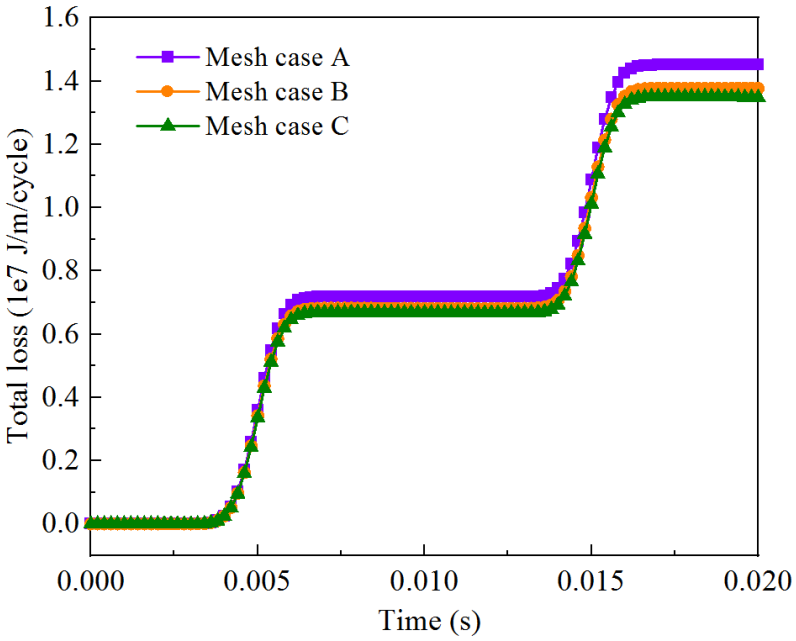

Fig.10 Mesh case studies of the total loss in the star-link cable during a time-varying sinusoidal current transmission with a peak current of 480 A and a frequency of 50 Hz under liquid helium environment**.**

It is regarded that the finer the mesh, the more accuracy the results in finite element analysis, but a finer mesh also results in a long-time computational process. For instance, In order to ensure the goodness of results on the losses of the star-link cable, a series of convergence studies based on mesh sensitivity have been carried out as shown in Table 2. Since the **T-A** homogeneous formulation and the **H**-homogeneous formulation are based on the same meshing scheme. Here we choose **H**-homogeneous formulation as the cases, and total losses which contain AC losses in REBCO coated conductors and eddy-current losses in the copper former calculated from these mesh cases have been presented in Fig.10. The results should be more accuracy if the meshes are finer, but the computational efficiency can also be reduced. It can be discovered from Fig.10 that the calculation results of mesh case B and mesh case C are approximately the same, but the calculation time of mesh case B is considerably reduced. Therefore, mesh case B has been chosen for the analysis of AC losses and eddy-current losses.

Table 2 Case studies in mesh sensitivity analysis.

	Mesh case A	Mesh case B	Mesh case C
Mesh elements	33371	41995	46239
Minimum quality	0.4385	0.5	0.4487

Average quality	0.8831	0.8896	0.8909
Computation time	2629 s	5591 s	8122 s

2.6 Summary

The studies were carried out by using COMSOL Multiphysics operated in a node of the COOLMUC2 InfiniBand cluster with the SLES15 SP1 Linux system in Leibniz Superconducting Centre (LRZ). There are 812 nodes in the COOLMUC2 cluster system and each node has a memory of 64 GB with a bandwidth of 120 GB/s.

This section described in detail the experimental and numerical studying methods in the development of REBCO coated conductor magnet systems for ultra-high field magnetic confinement plasma devices. The experimental studies are mainly related to the test of critical current density in REBCO coated conductors at liquid nitrogen environment by using the four lead method. The experimental data are used for the benchmark of the numerical model. Numerical studies are mainly based on finite element analysis using **H**-formulation, **T**-**A** formulation and **A**-**V** formulation based governing equations. These methodologies are of great significance in the design and analysis of the electromagnetic behavior of REBCO cables and the toroidal field coils and central solenoid coils of ultra-high-field magnetic-confinement plasma devices.

3 Current-carrying capacity and magnetic behavior in the advanced twisted-stacked tape conductor cable

The concept of the high temperature superconducting (HTS) twisted stacked tape conductor (TSTC) cable for fusion has been developed during recent years. The cable is demonstrated to have a stable cable critical current under extreme trial conditions with high electromagnetic force levels and multiple cryogenic thermal cycles. The remaining question is how to enhance the current-carrying capability and magnetic properties of the cable. In this article, three specific TSTC cables with the same twist pitch have been designed. Numerical studies of current-carrying capability and magnetic behavior of these cables have been carried out by employing a **T**-**A** formulation model and an **H**-homogenized formulation model which are based on the finite element method. The two models consider the variation of the critical current density with perpendicular and parallel magnetic fields, and temperature influence on the critical current density has been considered as well. These models have been validated with experiment data and a good fitting curve was obtained. Results show that the 4-slot TSTC cable has a better magnetic behavior compared to the 3-slot and 5-slot TSTC cables, in spite of a better current-carrying capability of the 5-slot cable. The study is of great significance for the research and development of the TSTC cables for compact fusion reactors.

The TSTC cable with 4-slot is currently under development in MIT for the SPARC compact fusion reactor. The cable has outstanding current-carrying capacity, but it might be quite difficult to employ the cable as the component of the toroidal field or central solenoid coils. Since a second bending process will cause stress concentration along the cable which might lead to an irreversible critical current degradation. Nevertheless, the TSTC cable is feasible to be employed as the current lead for ultra-high-field large-scale applications. In fact, it is currently employed as the feeder line of the toroidal field module coil in the SPARC project. In addition, it has large potential to be used as the superconducting cable for long-distance power transmission with the advantage of ultra-high current-carrying capacity. The study is aimed to lay a good foundation for the authors to develop novel REBCO coated conductor cables with outstanding current-carrying capacity for ultra-high-field magnetic-confinement plasma devices.

The individual contributions of the candidate with percentages for the research include: 100% of development and conceptual design, 100% of gathering data, 100% of analysis and interpretation of data, 100% of drafting of the manuscript and 20% of review work. The research has been published with the title: current-carrying capability and magnetic behavior of the HTS twisted stacked tape conductor cable for the compact fusion reactor in *IEEE Transactions on Applied Superconductivity*.

3.1 Introduction

The story starts in 1998, when the concept of HTS Tokamak was first proposed by Ando *et al* for the vector reactor design [83]. The possibility of using high-temperature superconductors for fusion magnets has been studied since then. Presently after more than two decades, with the maturity of HTS fabrication process and the production of HTS tapes with enormous increased critical current density, HTS cables have become a promising option in the field of nuclear fusion [16][84]. Many future fusion devices such as, the CFETR project in China [85], the SPARC tokamak project in USA [86], the DEMOnstration Power Plant in Europe [87], the helical fusion reactor in Japan [63], the fusion device in Russia [6] and the spherical tokamak project in UK [88] have considered to depend on the HTS cables to make further progress. A three-dimensional perspective of the HTS magnet system has been represented in Fig.11.

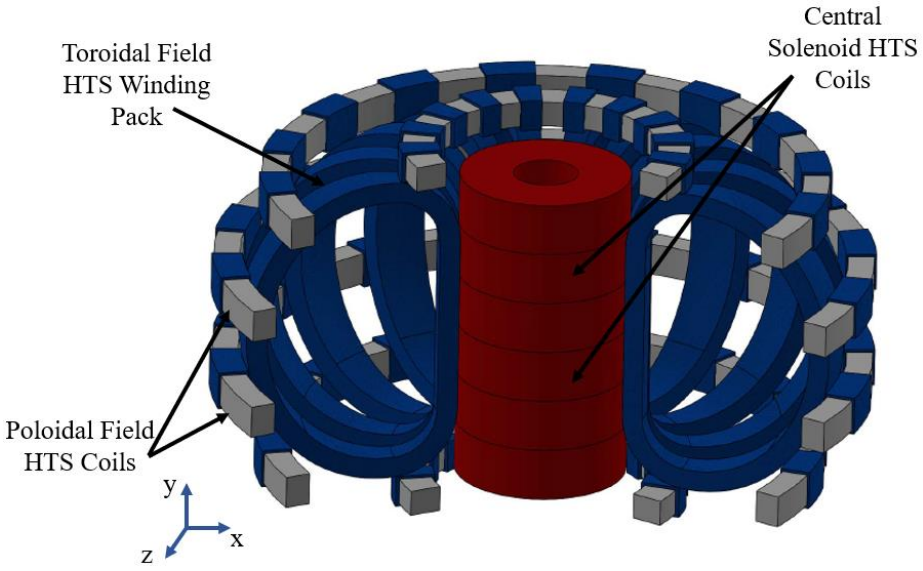

Fig.11 The geometrical perspective of the HTS magnet system for compact fusion reactors. The toroidal field coils and poloidal field coils are transported with DC currents, while the central solenoid coils are transported with pulse currents.

Because of the brittleness of oxidized ceramic materials, HTS material (ReBCO) must be deposited on substrates with better ductility, such as hastelloy, when they are made into superconducting wires. It means that the high temperature superconductor must be operated in the form of tapes, which is quite different from the Nb_3Sn compound superconductor-based low temperature superconducting (LTS) wires. It also implies that the mature cable-in-conduit-conductor (CICC) technology for LTS wires in the field of fusion is no longer suitable for the manufacture of HTS cables, and new cable technology for HTS tapes must be elaborated.

The concept of the HTS TSTC cable was first invented in a single-slot version in 2012 by Makoto Takayasu *et al* from MIT, USA [89]. It was then developed into a 5-slot version in 2014 by G. Celentano *et al* from the ENEA, Italy [42]. Later in 2016, the HTS TSTC technology was verified to meet the bending requirements of the high-field magnet design [43]. In 2017, it was found that the Lorentz load

degradation of the TSTC conductor was negligible according to the experimental evaluation of a 40-tape TSTC conductor at fields up to 17 Tesla at 4.2 K [90]. In 2020, a 4-slot TSTC cable named VIPER was demonstrated to have better cryo-stability and high mechanical strength [38]. In 2021, a 2D finite element model based on the T-A formulation has been developed to describe the experimental V-I curve in a 5-slot TSTC cable [44].

This article studied the difference of current-carrying capability and magnetic behavior among the 3-slot, 4-slot, and 5-slot TSTC cables. Based on which a developed H-homogeneous model and a modified T-A formulation-based model subject to the finite element method have been further studied. These models have been validated with the experimental data in [44] and a reasonable fit curve was obtained.

3.2 Cable design

Three layouts of HTS TSTC cables with 3-slot, 4-slot and 5-slot that are operated in the liquid nitrogen temperature region were designed in the light of the cables in [38] and [42] in this article. To trial the current-carrying capability of each cable, 20-tape, 30-tape, and 40-tape superconducting stacks are inserted respectively into the slot of each cable. In addition, the main features of the designed cable have been displayed in Fig.5, and detailed parameters of these cables can be found in Table 3.

Table 3 The main parameters of the HTS TSTC cables.

Parameter	Description
HTS tape	SuperPower SCS4050
Tape width	4 mm
Tape thickness	0.1 mm
Tape I_c at 77 K	140 A
Cable twist pitch	500 mm
Cable diameter	20 mm
Cable cryogenic tube diameter	4 mm
Cable slot width	4.3 mm
Cable slot hight	4.3 mm
Number of tapes per stack	20, 30, 40
Number of stacks per cable	3, 4, 5

3.3 Numerical Scheme

The **T**-**A** formulation which aims to use current vector potential **T** to solve the nonlinear E-J relationship of HTS tapes and magnetic vector potential **A** to solve the magnetic field in the solution domain was firstly developed by Min Zhang and Weijia Yuan's research group in 2017 [69][71]. The method uses

thin-strip approximation to simplify the geometry of HTS tapes, which eliminates the meshing problem caused by the large aspect ratio (more than 10^3) of superconducting tapes. It has sped up the computation efficiency comparably. In this article, the **E-J** non-linear relationship of the HTS tape can be described as shown in equation (1), chapter 2.2. The **T-A** formulation is further developed with the consideration of a variable critical current density J_c on the dependence of the magnetic flux density and temperature as shown in equation (3), chapter 2.2. It should be clarified that the **E-J** relationship is used to describe the electromagnetic behavior of superconducting layers in the tape. Since the other layers do not contribute to the shaping of the magnetic field [91], they are neglected in the model. The other components of **T-A** formulation can be found in [24]. The model is validated with the experimental data in [44] and a better fitting curve was obtained by adjusting essential parameters appropriately.

The **H**-homogeneous model is evolved from the **H**-formulation model, which uses the magnetic field **H** to solve the current distribution, electrical field and magnetic flux of high temperature superconductors determined from Maxwell's equations. The main idea of the **H**-homogeneous model is to build an anisotropic superconducting bulk which could represent the overall electromagnetic behavior of the HTS taped stacks. It retains the global electromagnetic behavior of the previous taped stack by considering a modified kim model as it is presented in equation (36) but loses the sight of the geometrical layout of substrate, metallic and insulating layers. It was first developed by Victor M. R. Zermeno *et al* [68][92]. In this article, a scale factor was introduced to the model to make it better exhibit the current distribution of the TSTC cables. The critical current density J_c can thereby be expressed as:

$$J_c(B_{\parallel}, B_{\perp}, T) = \frac{J_{c0}}{\left[1+\sqrt{(kB_{\parallel})^2 + B_{\perp}^2}\,/\,B_0\right]^{\alpha}} \cdot [1-(\frac{T}{T_c})^2]^{3/2} \cdot f \tag{36}$$

The **E-J** relationship of HTS taped stacks applied here is consistent with equation (1). Here J_{cb} represents the initial critical current density of the homogenized superconducting taped stack. Likewise, the relationship between J_{c0} and J_{cb} can be described as:

$$J_{cb} = \frac{J_{c0} \cdot u \cdot v}{w} \tag{37}$$

Particularly, u stands for the number of tapes in a stack, v represents the thickness of the superconducting layer in a superconducting tape, while w means the thickness of a superconducting tape.

The current ramping rate is given as 20 A/s during the simulation process, which is in accord with the experiment process in [44]. Meanwhile, Table 4 shows the values of essential parameters applied in the modeling. The study is carried out in the commercially available finite element modeling package COMSOL Multiphysics 5.6.

Table 4 Descriptions and values of parameters in the model.

Parameter	Description	Value
T_n	Temperature in liquid nitrogen environment	77 [K]
T_h	Temperature in liquid helium environment	4 [K]
f	Scale factor in equation (36)	0.046
u	The number of tapes in a stack	40
v	The thickness of the superconducting layer in a tape	1×10^{-6} m
w	The thickness of a superconducting tape	1×10^{-4} m

3.4 Model validation

3.4.1 Validation of current-carrying capability

The critical current of a 20-tape stacked cable under liquid nitrogen temperature region was detected by experiments in [44]. The experiment data was borrowed in this article. Two models with 20-tape stacks in a cable were separately established by using **H**-homogeneous formulation and **T-A** formulation. The power term n indicates the anisotropy properties of the HTS coated conductor, but it may have minor effect on determining the current-carrying capability and magnetic behavior of the tape. In addition, the higher the n-value, the tougher the calculation tends to converge, while the computation speed will slow down accordingly. Therefore, the n-value was finally determined with 29 in the models, which is quite different from the value of 49 in the article [44]. This may be the consideration for the difference between the numerical solutions and the experimental curve as it is shown in Fig.12.

In addition, due to the introduction of scale factor in the **H**-homogeneous model, the volt ampere characteristic curves calculated by the two model show some differences. Despite these differences are quite small, it can still be assured that the extremely accurate results should be somewhere between the two curves, which condition is quite similar with the pinch theorem in mathematical theory.

3.4.2 Validation of magnetic behavior

A desirable outcome of the magnetic flux density calculated by the two models was acquired as it is exposed in Fig.13. Since the **T-A** formulation is based on the thin strip approximation method, the overall appearance of Fig. 13(b) is a little bit darker compared with Fig. 13(a). But it can still be realized that the magnetic flux penetration region calculated by the **H**-homogeneous model is basically the same as that obtained by the **T-A** formulation.

In addition, it should be mentioned that the magnetic flux density calculated by the two models is also well matched with the simulation results calculated in [44] under the case of a 20-tape HTS stack.

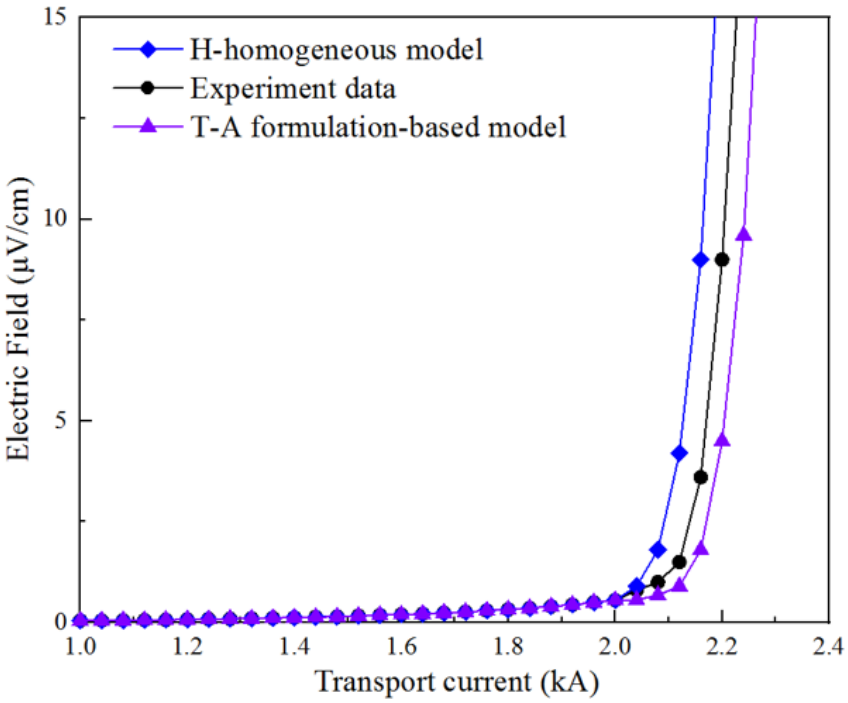

Fig. 12 The volt ampere characteristic curve of a 20-tape stack under liquid nitrogen operating condition.

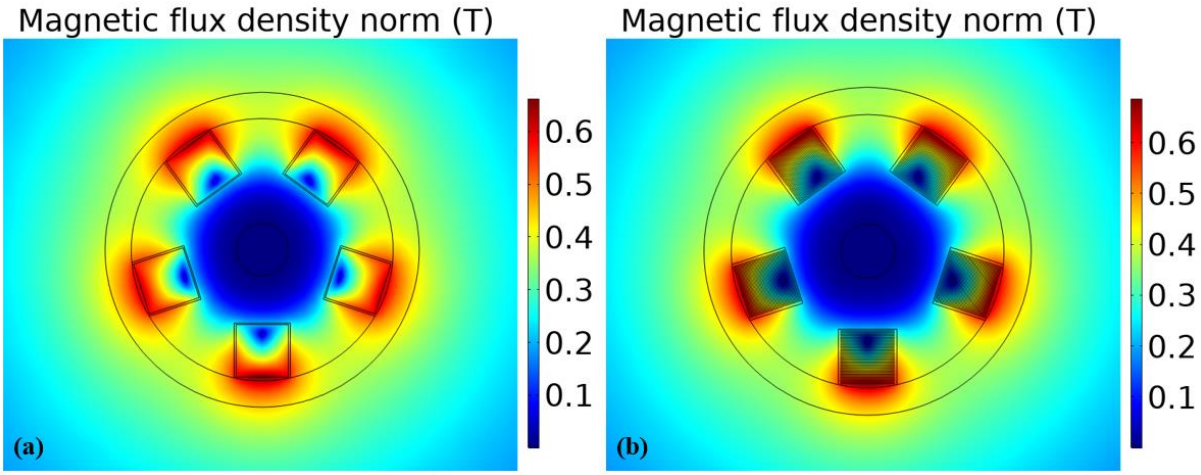

Fig. 13 The magnetic flux density of a 5-slot 40-tape per stack HTS TSTC cable calculated by (a) H-homogeneous model and (b) T-A formulation-based model.

3.5 Results and Discussion

3.5.1 Study of the current-carrying capability

In this section, the critical current of a single tape under liquid nitrogen environment has been studied. In addition, it is assumed that the external magnetic field has a negative effect on the critical current of the tape as it is shown in equation (3) and equation (36). Therefore, the relationship between the tape

transport current and the stack transport current has been represented in Fig.14(a), while the relationship between the tape transport current and the cable transport current has been presented in Fig.14(b). From which it can be concluded that the current-carrying capability of an HTS TSTC cable depends largely on the number of tapes in a stack and the number of slots in a cable.

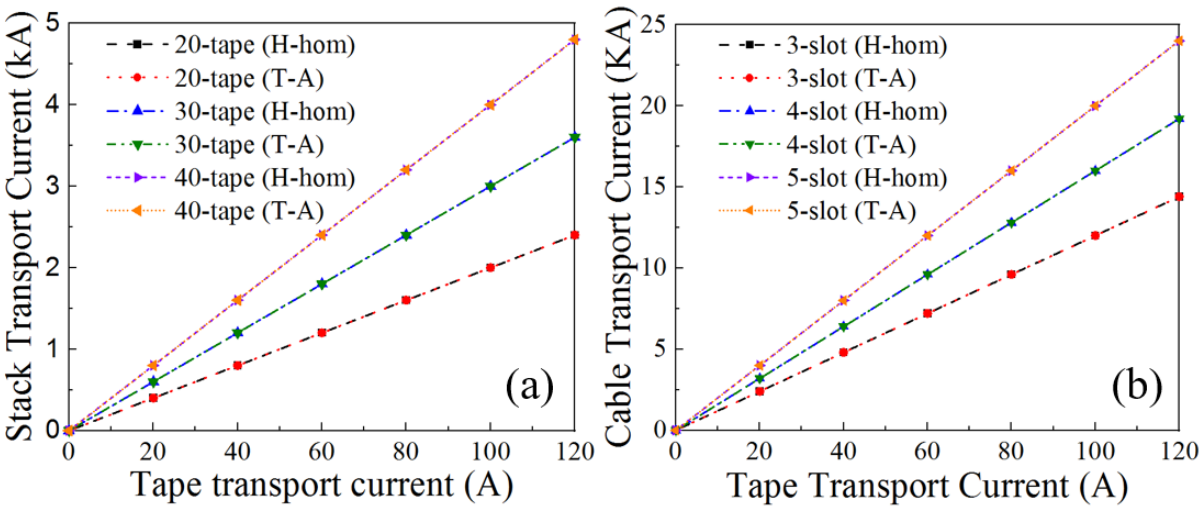

Fig. 14 Current-carrying capability of the HTS TSTC Cables. (a) The stack transport current varies with the tape transport current. (b) The total cable current varies with the tape transport current in a 40-tape stacked cable.

The study also found that the relationship among the tape transport current, the stack transport current and the cable transport current is almost linear, which has similar consequence with [44]. It indicates that the influence of external magnetic field on the critical current of the cable is not obvious under the liquid nitrogen condition.

3.5.2 Study of the magnetic behavior

Intriguingly, magnetic deflection was detected in the magnetic flux density of the 3-slot and 5-slot cables, but such phenomenon was not found in the 4-slot cable as it is shown in Fig.15, which may be associated with the geometric symmetry of the slotted cable.

The magnetic field deviation of the 3-slot cable occurs at the position of 120°, 240°, 360°, which is not symmetrical in space. The magnetic fields are thereby shifted due to mutual attraction or repulsion. The phenomenon can also be distinguished on the 5-slot cable. For example, the magnetic field does not deviate at the 90° position, where the symmetric center is placed. But the magnetic field at 18°, 162°, 234° and 306°, where the asymmetric areas are, are all deflected. To the contrary, the 4-slot cable shows a better magnetic behavior due to its structure symmetry. It may be concluded that cables with even-numbered slots and the geometric structure are symmetrically distributed in space could have a better magnetic field performance.

Considering the best condition of using a 40-tape per slot and 4-slot cable, the magnetic flux density produced under liquid nitrogen condition may be not high enough for the application of fusion magnets.

Therefore, magnetic behavior of the same cable has been studied under the liquid helium condition, and relevant results could be seen in Fig.16.

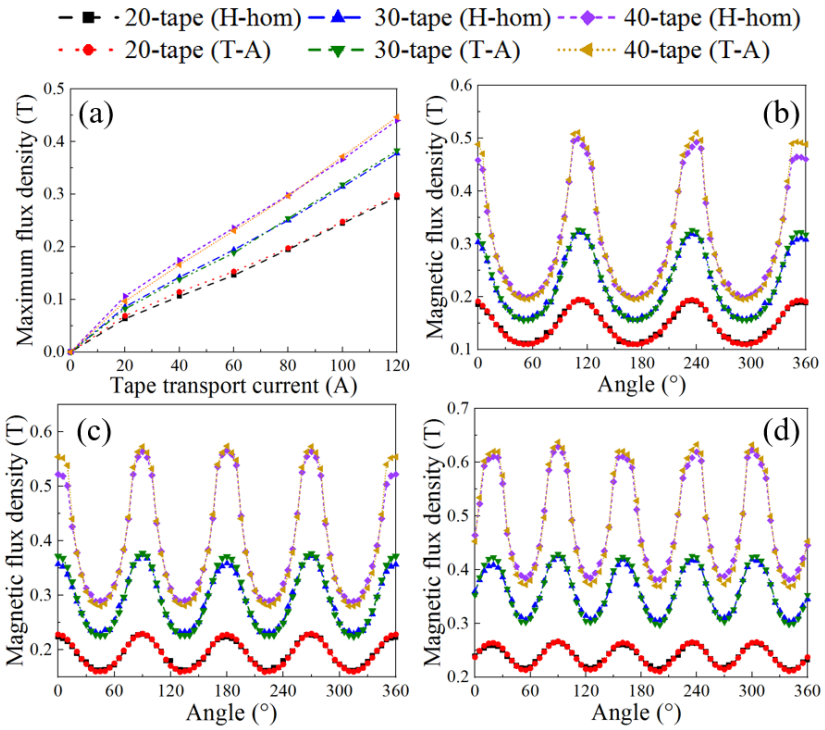

Fig.15 Magnetic flux density of the cable. (a) Maximum magnetic flux density produced by the single taped stack. (b) magnetic flux density of a 3-slot cable, the corresponding transported current in the cable for the 40-tape condition is 14.4 kA. (c) magnetic flux density of a 4-slot cable, the corresponding transported current in the cable for the 40-tape condition is 19.2 kA. (d) magnetic flux density of a 5-slot cable, the corresponding transported current in the cable for the 40-tape condition is 24 kA.

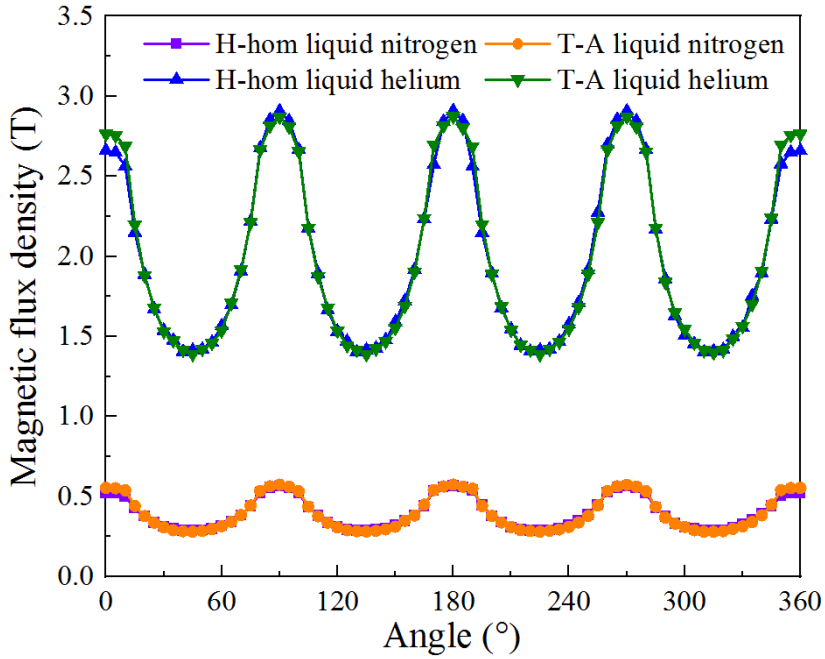

Fig. 16 Magnetic flux density of the 40-tape per slot, 4-slot cable under liquid nitrogen and liquid helium temperature zone. The corresponding transport current in the cable under liquid nitrogen condition is 19.2 kA, while the corresponding transport current in the cable under liquid helium condition is 95.78 kA.

3.6 Summary

Current-carrying capability and magnetic behavior of the HTS TSTC cable have been evaluated in this article. Two kinds of FEM methods are further developed based on the principle that the accuracy of the model should be verified. The influence of slots on the performance of the cable has been figured out by developing cables with 3-slot, 4-slot, and 5-slot. It is indicated that the 4-slot cable has a better performance compared to the 3-slot and 5-slot cable, no matter from the perspective of current-carrying economic aspect or from the side of the cable magnetic behavior.

It is quite challenge for the HTS TSTC cable-assembled winding pack to generate a sufficiently high magnetic field (larger than 20 Tesla) to maintain the operation of nuclear fusion with present HTS engineering critical current density under liquid nitrogen temperature region, but the situation could be changed while the operating environment could be transferred to liquid helium temperature zone, under which condition the critical current density of the HTS magnets could be further improved. The other solution is to use a larger diameter cable which contains more (6-8) slots, but in this case, whether to choose a 4-mm width HTS tape or a 12-mm width HTS which could be stacked with more layers is a well-worth studying question.

4 Elaboration of the non-twisted cable and its application to the ultra-high-field toroidal field module coils

The development of rare-earth barium copper oxide (REBCO) coated conductors with an extremely high critical current density under ultra-high fields opens up a high-field path towards large-scale fusion. The latest technology has inspired cable-in-conduit conductors (CICC) such as conductor on round core (CORC) wires, twisted stacked tape conductor (TSTC) cables and Rutherford cables with outstanding current-carrying capacities. In order to realize an inductance balance and decrease magnetic diffusion, these cables have been twisted or folded to a certain extent, thus breaking the mechanical behavior of the ceramic superconductor and limiting their potential for ultra-high-field applications. One possible solution is to employ a non-twisted cable, which offers maximum protection of its mechanical properties and enables a parallel orientation of the toroidal field vector to the surface of REBCO coated conductors, and at the same time decreases the influence of perpendicular fields on the critical current of REBCO cables. However, the applied physics community's attitude towards using non-twisted, parallel REBCO stacked-tape cables is one of skepticism, the main argument being that the nonlinear E-J behavior associated with screening current in the parallel stack might lead to a field distortion and reduce the performance of superconductivity. Recent analyses have demonstrated that the effect of screening current decreases significantly owing to a wavelike magnetic field distribution along the cable. The authors obtained similar results using **H**-formulation and **T**-**A** formulation based finite element methods and demonstrated that the non-twisted cable may be feasible for DC current transmission toroidal field coils in magnetic-confinement devices. Furthermore, the electromechanical behavior of toroidal field coils has been evaluated via the Maxwell stress, solved by using an **A**-**V** formulation. It was discovered that the stress generated by the toroidal field coils is within the stress tolerance of the REBCO coated conductor, something which is of great significance in promoting the application of REBCO coated conductors for ultra-high-field magnetic-confinement plasma devices.

The individual contributions of the candidate with percentages for the research include 100% of development and conceptual design, 100% of acquisition data, 100% of data evaluation, 100% of drafting of the manuscript and 20% of review work. The research has been published with the title: electromechanical behavior of REBCO coated conductor toroidal field coils for ultra-high-field magnetic-confinement plasma devices in *Journal of Physics D: Applied Physics*.

4.1 Introduction

The global race for fusion energy on earth is mainly a story of magnetic-confinement plasma [93]. Ultra-high magnetic fields can decrease particle drifting and disruption, and significantly increase the possibility of fusion reactions. For instance, the international thermonuclear experimental reactor (ITER) has a fusion energy gain factor of 10 and aims to achieve a peak magnetic flux density of 11.8 Tesla by using low temperature superconducting Nb_3Sn conductors [94]. However, things may change with the emergence of the second-generation high temperature superconducting REBCO coated conductor, a technique that was not introduced when the ITER project was launched but which has reached a certain degree of maturity so that there are now tens of manufacturers worldwide [95]. Over the last 15 years, REBCO coated conductors have made great strides toward potential applications in motors [17], fault current limiters [96], magnetic energy storage systems [97], transformers [20], wind turbine generators [98], MRI machines and so on [99]. They are regarded as a breakthrough for the new generation of ultra-high-field (> 20 Tesla) fusion power plants [83]. The current baseline design for the toroidal field coils and central solenoid coils of EU-DEMO reactor is based on Nb_3Sn conductors. High temperature superconductor activities have been pursued in parallel to the LTS coils, the mid-term target has been focused on determining the best REBCO cable option for fusion magnets [100]. The CFETR-Phase II fusion project aims to enhance the magnet system by using REBCO magnets [101] [102]. In addition, REBCO coated conductor cables with a current capacity of 100 kA are being built and tested for the magnet system of the force-free helical reactor (FFHR) in Japan [103][104][105]. A helical current-carrying element made of REBCO coated conductors is also under development for the fusion neutron source in Russia [106]. Since a compact fusion reactor project relying entirely on REBCO magnets was launched in the United States in 2020 [86], the design of REBCO cables for large-scale fusion reactors has got into full swing. At present, existing REBCO cabling methods for fusion are mainly based on the cable-in-conduit conductor (CICC) technique, which is derived from cable designs such as twisted stacked tape conductor cables [38][42], CORC cables [107], Rutherford cables [55] and star conductors [108]. In our previous study, the current-carrying capacity and magnetic behaviour of TSTC cables were estimated by finite element methods; it was discovered that the REBCO cable has a high-current-carrying capacity in a low-temperature cooling environment [45]. However, it might be quite challenging to employ the cable as a component for toroidal field coils in a compact fusion reactor because mechanical issues caused by bending after twisting might lead to an enormous critical current degradation. In addition, experiments show that the bending strain and the twist pitch have a negative impact on the current-carrying capacity of TSTC cables [43][44]. The degradation of I_c in CORC cables caused by mechanical pinching has also been detected [109]. An I_c reduction was observed during the cyclic transverse load in experimental tests [55]. The non-twisted, star cable seems to have a predictable and stable electromechanical performance [108]. Nevertheless, the high copper ratio in the cable might lead to high eddy-current losses under current ramping conditions.

The advantage of the non-twisted cable design is its high tolerance to transverse stress [60] and extremely high critical current density, since there is no critical current decay caused by torsion. A recent analysis proposed the possibility of using non-twisted paralleled REBCO stacked tape as the cable for toroidal field coils [59], and it has been demonstrated that a wavelike magnetic field distribution along the conductor can significantly decrease the negative effect of the screening currents induced during charging. In this article, a similar wavelike magnetic field was obtained by using **T**-**A** formulation and **H**-formulation based finite element methods. In addition, the electromechanical behaviour of toroidal field coils consisting of non-twisted CICC cables has been studied further using an **A**-**V** formulation. The results demonstrate the feasibility of employing non-twisted CICC cables for ultra-high-field magnetic-confinement plasma devices.

4.2 Numerical scheme

The studies were carried out by using **H**-formulation [66][67][68], **T**-**A** formulation [69][70] and **A**-**V** formulation [72][73] based finite element methods. **H**-formulation and **T**-**A** formulation are employed to study power loss, eddy-current loss, and magnetic behavior of the non-twisted cable, while **A**-**V** formulation is mainly used for the analysis of magnetic and mechanical behavior of the large-scale toroidal field module coils.

The studies were carried out in the commercial finite element modelling package COMSOL Multiphysics. The physical parameters of the REBCO coated conductor refer to the experimental data at Theva Dünnschichttechnik GmbH. Specific parameters described above are presented in Table 1.

4.3 System design

4.3.1 Cable design

The inspiration for the cable comes from combining the advantages of the viper-shaped cable and the star cable [38][103]. It is assumed that the cable should avoid conductor torsion to protect the fragile mechanical behavior of REBCO ceramic layers in coated conductors [110] when they are assembled into toroidal field coils. In addition, it is suggested that the number of stacked tapes mounted on the copper former should be more to reduce the proportion of copper, so that eddy-current loss induced in the copper former can be decreased. Considering the toroidal field coils are transported with DC current, the inductance induced in the cable can be ignored. Nevertheless, Joule heat generated in the non-twisted cable during charging will be studied further in the coming section. The diagram of the non-twisted cable is presented in Fig.8, and geometric parameters of the cable are shown in Table 5.

The cable has 6 stacks of tapes mounted on the copper former, with each stack containing 40 REBCO coated conductors of 4 mm in width, leading to a higher current-carrying capacity compared to the star cable. The 4 mm coated conductor was used instead of the 12 mm coated conductor to allow a reduction

of the screening current along the surface of the conductor during current charging. Meanwhile, the straight-forward rectangular cable configuration can avoid the problem of uneven stress distribution. In addition, the cooling channel system has been moved out and arranged on the outside of the entire magnet system to avoid the possibility of damage by excessive stress on the cooling channels due to the large Lorentz force acting on the cable. As a result, our cable design has a few potential advantages, such as a high current-carrying capacity, great flexibility, and reliability, while it is also robust and cost-effective.

Table 5 Descriptions of the geometric parameters of the non-twisted cable and the toroidal field coil.

Parameter	Description	Value
b	Height of the copper support slot	4.2 mm
e	Thickness of the aluminum spacer	2.0 mm
f	Height of the stainless-steel jacket	20.0 mm
h	Height of the copper support	12.0 mm
k	Width of the stainless-steel jacket	28.0 mm
t	Width of the copper support slot	4.2 mm
w	Width of the copper support	24.0 mm
v	Width of the REBCO stacked tape	4.0 mm
l	Thickness of the REBCO coated conductor	0.1 mm
ri	Inner radius of the inboard leg cross-section	1000 mm
ro	Outer radius of the inboard leg cross-section	1900 mm
nu	Number of REBCO coated conductors in each taped stack	40
nc	Number of cables in a winding pack	560

4.3.2 Toroidal field system design

The maximum magnetic flux density produced by the toroidal field winding pack aims to reach 20 Tesla by employing the non-twisted cable. The layout of the cabling system in the winding pack has been established to meet the design target and the configuration of the magnet system is shown in Fig.17. Considering the high cryogenic stability of REBCO coated conductors, an indirect cooling system is

established, and the non-twisted cables are cooled by thermal conduction. The helium cooling channel is on the outside of the magnet for the concern that the enormous mechanical stress generated under ultra-high fields should have a small effect on the cooling system. The cooling system design has some similarities with the magnet system for the helical fusion reactor in [105]. The geometric parameters of the toroidal field winding pack are presented in Table 5. The total number of non-twisted cables in a toroidal field coil is 560, and each cable contains 240 stacked-tape REBCO coated conductors.

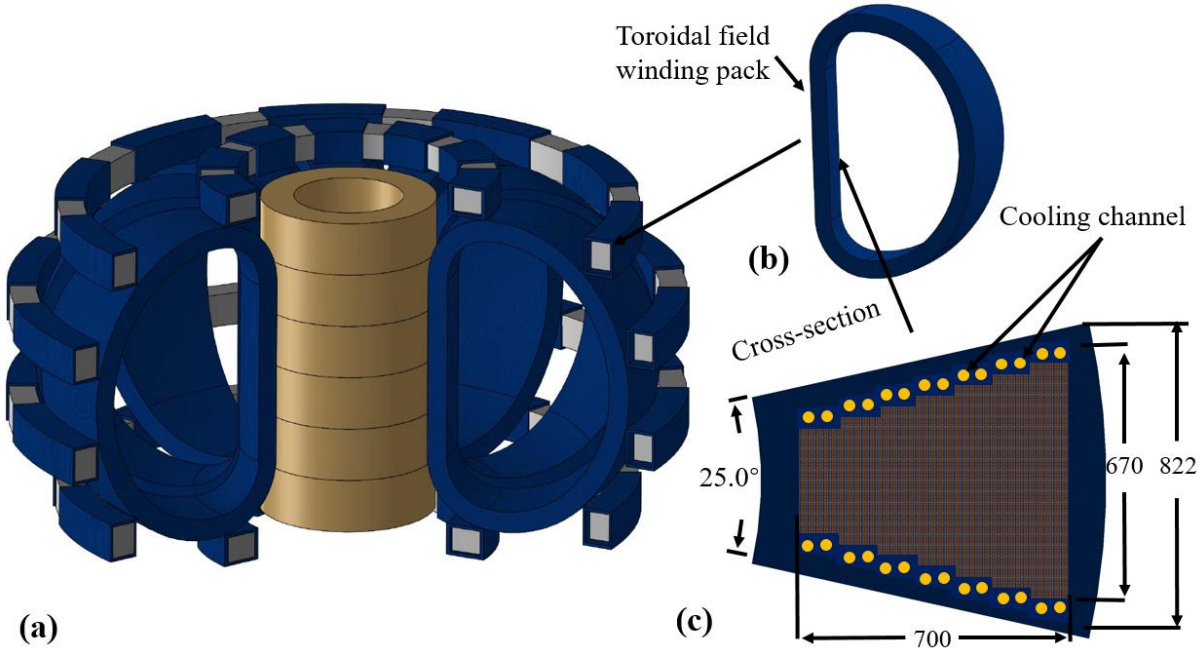

Fig. 17 Diagram of the REBCO compact fusion reactor system. (a) The compact fusion reactor. (b) The toroidal field winding pack. (c) Layout of the toroidal field winding pack's inboard leg cross-section in the equatorial plane.

4.4 Power loss and eddy-current loss of the non-twisted cable during the transient current charging procedure

The critical current of the REBCO coated conductor has been identified as being 112 A in a liquid nitrogen environment with a self-field in THEVA. The value determines that the critical current density of the conductor at 77 K can reach 2.8×10^{10} A/m^2, which has been adopted for modelling the non-twisted cable by considering the temperature dependence. During the modelling procedure, a current ramping rate of 40 A/s was defined, and the charging time of the cable determined as 6 s while maintaining a current margin of more than 20%. Justification for the high ramping rate is to study the threshold power loss and dynamic magnetic flux characteristics during cable transient charging. The purpose of this section is to compare the power loss in the REBCO coated conductors and eddy-current loss in the copper support and other materials to ensure that power loss is the main loss in the cable during the transient current charging procedure, which may demonstrate that the cable design is reasonable. In addition, one concern with the non-twisted cable is that the power loss and eddy-current loss in the cable

might influence the magnetic behavior of the cable during the transient charging procedure; these effects are studied further using the **H**-formulation based finite element method.

AC current periodically reverses direction with time while DC current flows only in one direction. In the AC current transmission condition, power dissipation in REBCO coated conductors is conventionally evaluated by AC loss. However, it was discovered that the power loss in REBCO conductors is relatively small when DC current is transmitted in the conductor. The amount of power loss in REBCO stacks during the transient charging is within 10 J/m/s that is equivalent to 10 W/m, as shown in Fig.18. However, the cooling power of 1- m superfluid helium cooling channel can reach 1.2×10^4 W/m [111]; which is three orders of magnitude higher than the required cooling power by the non-twisted cable.

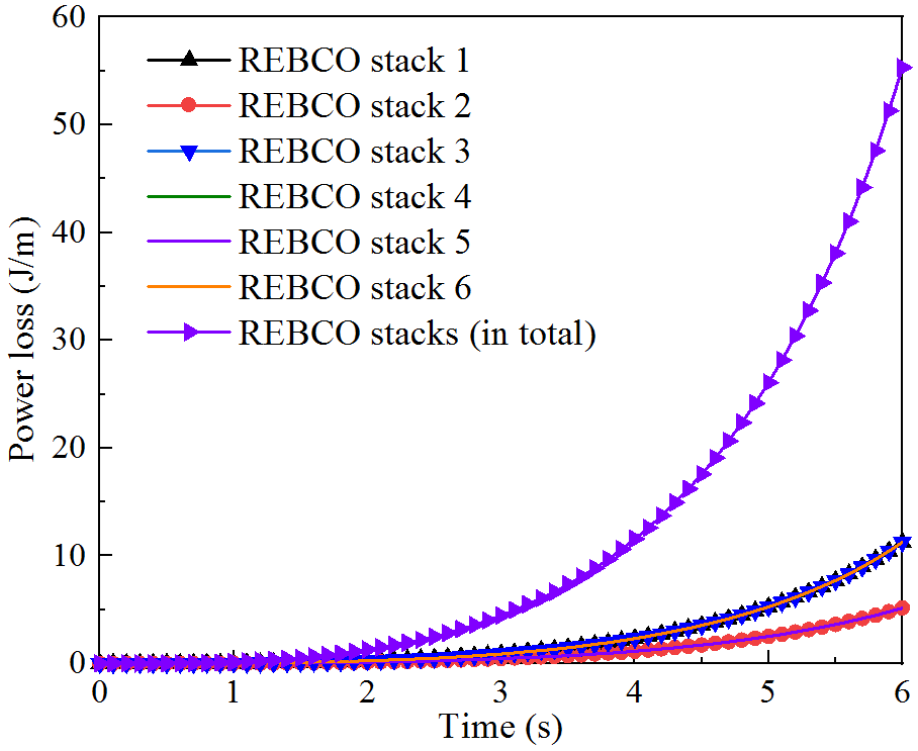

Fig. 18 Power loss of the REBCO stacks in the cable during current charging at 4.2 K.

The eddy-current loss in the copper former, the aluminum spacer and the stainless-steel jacket is also studied, as shown in Fig.19. The total eddy-current loss is approximately equivalent to the power loss in one REBCO stack that is in the edge area of the conductor. It means that the main loss generated in the conductor during the transient charging procedure will still be the power loss in REBCO coated conductors. Eddy-current loss in other materials is probably 1/6 of the power loss in REBCO coated conductors. However, the loss value is small and controllable under the DC current transmission condition. It also demonstrates, however, that the Joule heat associated with power loss and eddy-current loss generated in the cable is very small under the DC current charging condition. This can be removed

rapidly by ensuring the heat-exchange capacity of liquid helium in the cooling channel to avoid quenching in superconductors.

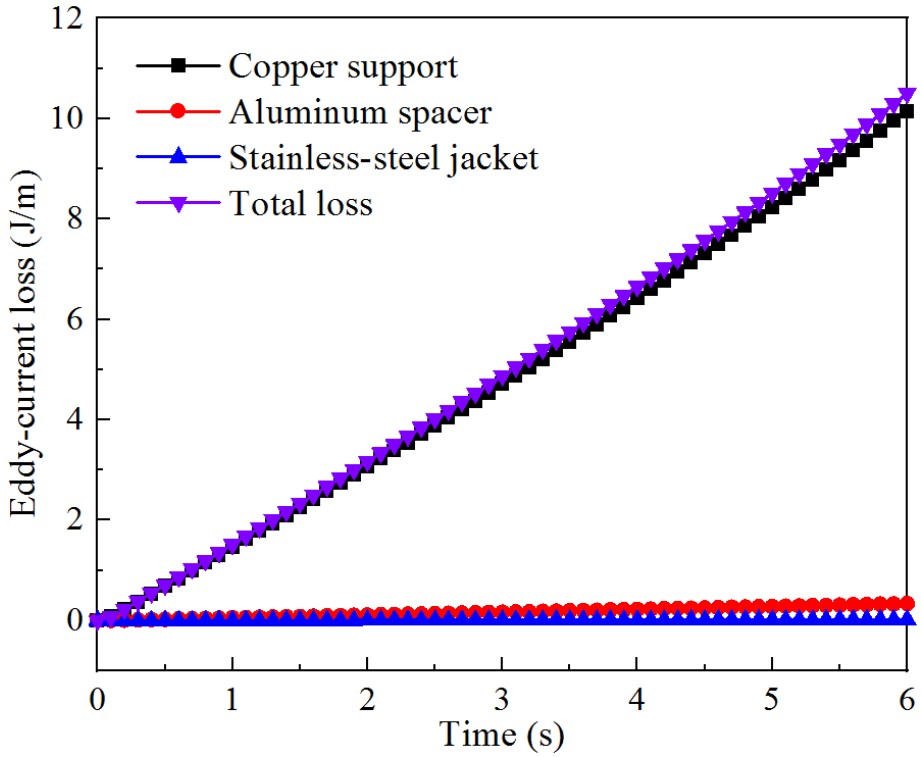

Fig. 19 Eddy-current loss in the copper support, the aluminum spacer, and the stainless-steel jacket during current charging in the conductor.

4.5 Magnetic behavior and temperature dependence of the non-twisted cable

The magnetic behavior of the non-twisted cable is regarded as an essential factor and should be analyzed before systematically studying the electromechanical behavior of the toroidal field coils assembled from non-twisted cables. This section thus studies the magnetic behavior of the non-twisted cable during the transient current charging procedure at 4.2 K and the maximum magnetic flux density produced by the cable under different operational temperature environments using **T**-**A** formulation and **H**-formulation based finite element methods. The **T**-**A** formulation, which is based on the thin-strip approximation, treats each REBCO coated conductor as a line strip. Therefore, the **T**-**A** formulation model can be considered an insulating stacked-tape coil model. However, the **H**-formulation treats the stacked-tape conductor as an equivalent anisotropic superconducting bulk. Hence, the **H**-formulation model can be regarded as a non-insulating stacked-tape coil model. It can be seen from Fig.20 and Fig.21 that the magnetic flux density calculated using the **H**-formulation seems to be slightly higher than the magnetic flux density calculated with the **T**-**A** formulation. A comparison of the two shows the superiority of the non-insulating coils to achieve higher fields due to current sharing between conductors. However, the

differences between the two methods are relatively small. This can thus be considered negligible in the large-scale computation in the coming section.

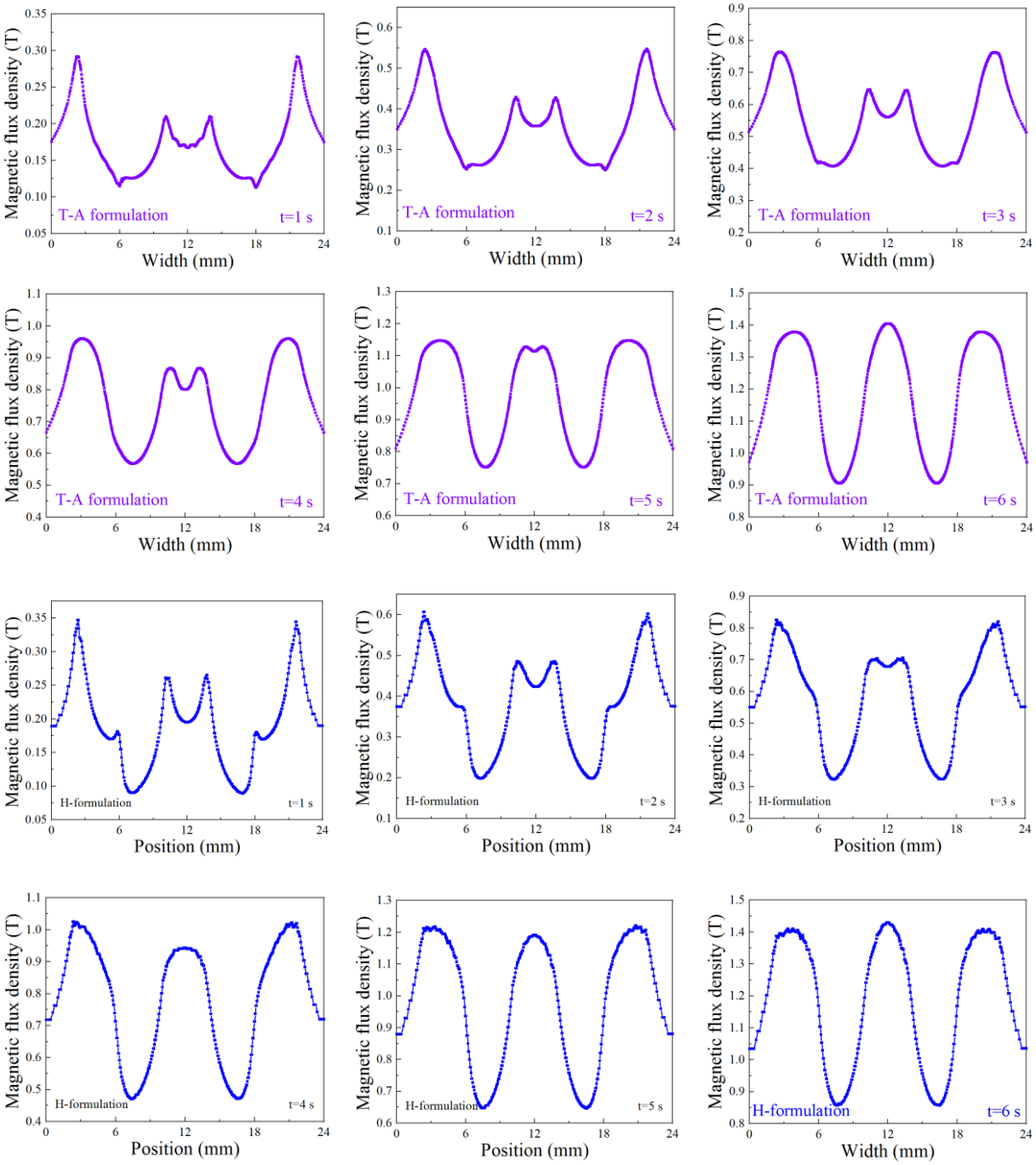

Fig. 20 Wave-like magnetic fields detected from the magnet charging of the non-twisted cable by using the **H**-formulation and **T**-**A** formulation based finite element methods at 4.2 K.

If the cable is charging with a current ramping rate of 40 A/s at 4.2 K, a magnetic field distribution along the length of the conductor can be detected, as shown in Fig.20. The field distribution initially appears to be an anomaly, but it eventually shows up as a regular wave-like shape over time. This should be an effect of the counter electromotive force resulting from the transient effect, which is calculated from Maxwell's equations considering a nonlinear current density that is, in turn, a function of the magnetic

field. It indicates that the nonlinear **E-J** behavior of superconductivity can lead to a field distortion in the initial stage of charging. However, a steady-state, wave-like magnetic field distribution along the cable at the end of charging indicates that the negative effect of the strong nonlinear **E-J** relationship on the magnetic field disappears. Consequently, the charging for non-twisted cables can be successful. The phenomenon detected in this article has some similar inferences with the analytical solution in [59]. It demonstrates the feasibility of using non-twisted REBCO cables for the toroidal field coils of magnetic-confinement plasma devices.

The dependence of the maximum magnetic flux density of the cable on the operational temperature environment has been evaluated, as shown in Fig.21. To achieve an ideal toroidal field for ultra-high-field magnetic-confinement devices, it is suggested that the operational temperature for toroidal field coils should not exceed 30 K. This can be achieved by a supercritical helium flow environment. Therefore, the electromechanical behavior of toroidal field coils at 4.2 K and 30 K has been specifically studied in the coming section.

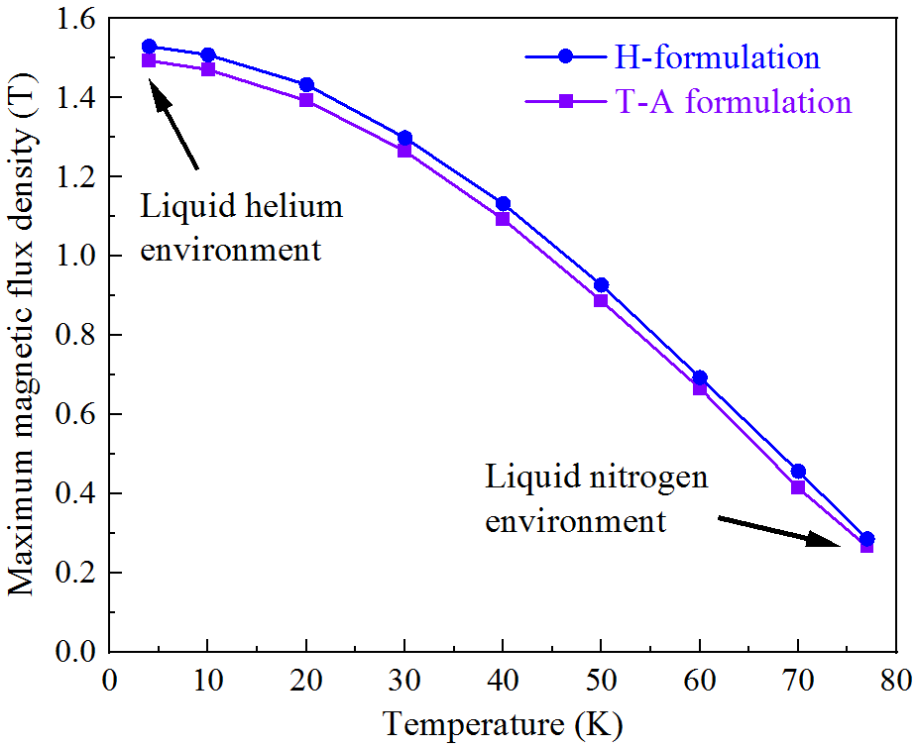

Fig. 21 The dependence of the maximum magnetic flux density produced by the non-twisted cable on the temperature.

4.6 Electromechanical behavior of the independent toroidal field coil

The critical current of the REBCO coated conductor is estimated to be 303.75 A at 4.2 K, 20 Tesla by referencing experimental data in [112]. It is rated to be 260 A at 30 K, 20 Tesla using the Kim model. Therefore, the operating current of the REBCO coated conductor in the toroidal field coil is estimated

to be 208 A at 30 K, 20 Tesla and 243 A at 4.2 K, 20 Tesla, with a 20% margin to the critical current. The magnetic behavior of the independent toroidal field winding pack has been evaluated using the **A-V** formulation. It could be demonstrated that the toroidal field coil assembled from non-twisted cables can achieve a maximum magnetic flux density of 17.61 Tesla at 30 K, as shown in Fig.22. However, the field can exceed 20 Tesla when the operating temperature drops to 4.2 K, as shown in Fig.23. The maximum magnetic flux density occurs on the edge of the toroidal field leg, which could lead to stress concentration, something that needs a specific analysis in the coming section. In addition, it can be seen from the cross-section area that cables arranged in the surroundings of the toroidal field coil could be subjected to a higher external magnetic flux density and will need to withstand more stress. If the same currents are transmitted in each conductor of the toroidal field system, cables on the edge area are more likely to be quenched.

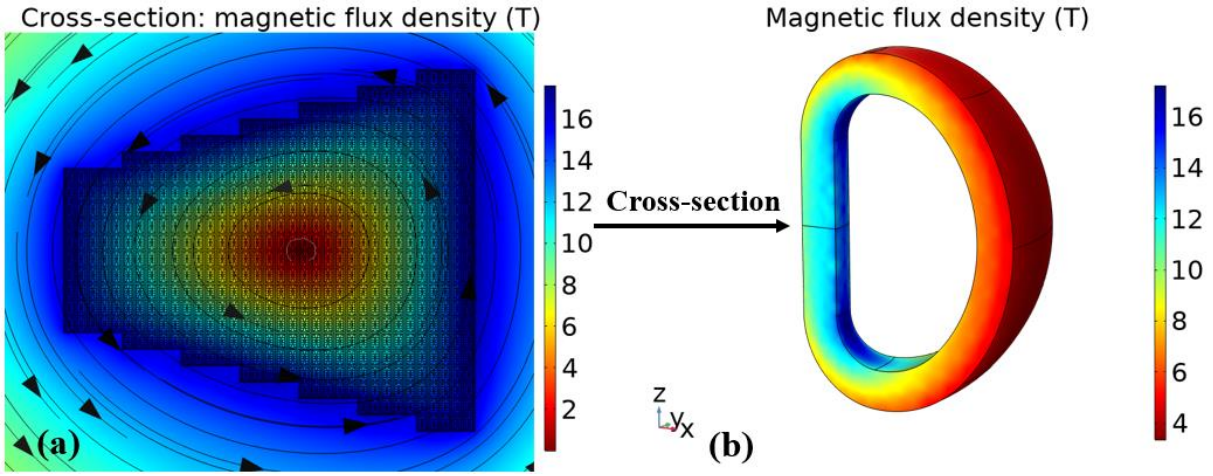

Fig. 22 The magnitude of magnetic flux density produced by the independent toroidal field coil at 30 K calculated by **A-V** formulation. (a) Magnetic flux distribution in the cross-section of the winding pack. (b) Magnetic flux distribution of the toroidal field coil.

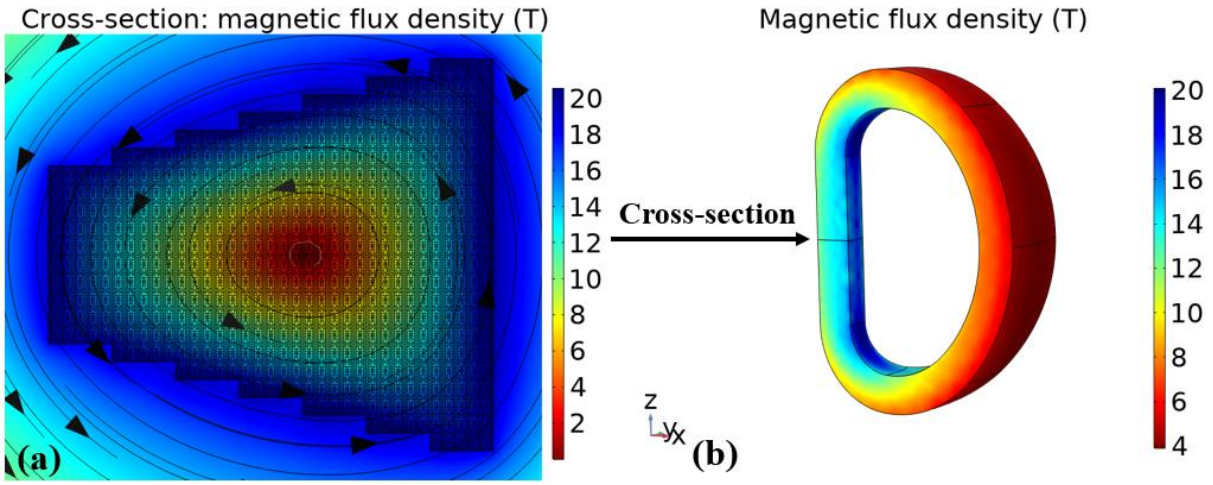

Fig. 23 The magnitude of magnetic flux density produced by the toroidal field coil at 4.2 K calculated by A-V formulation. (a) Magnetic flux distribution in the cross-section of the winding pack. (b) Magnetic flux distribution of the toroidal field coil.

In addition, the magnetic flux density generated by the REBCO coated conductor-based toroidal field coils may be even higher due to the magnetic superposition principle, but the critical current density of REBCO coated conductors may also fall with an increase in the external magnetic field. However, the ultra-high critical magnetic field of the REBCO conductor determines that an ultra-high field of more than 20 Tesla for toroidal field coil modules can be achieved, and that a high field path towards large-scale fusion is possible.

The electromagnetic forces on parallel, current-carrying cables can be evaluated based on the Maxwell stress tensor. The stress tolerance of CICC coated conductors is 680 MPa, and it is recommended that the stress distribution along the toroidal field coil should be less than 500 MPa [83]. The Maxwell stress tensor of the toroidal field coil and its component on the coordinate system, at 4.2 K and 30 K respectively, have been evaluated and presented in Fig.24 and Fig.25 to better determine the stress concentration in toroidal field coils. The direction of the surface normal is defined as downward as mentioned in section 2, meaning that Maxwell stresses which are in the same direction of the surface normal will be positive values. Otherwise, the values can be negative. It can be seen from the figures that the Maxwell stress of the toroidal field coil is concentrated on the inboard leg. But the maximum Maxwell stress on the toroidal field coil is within the stress tolerance of the REBCO coated conductors.

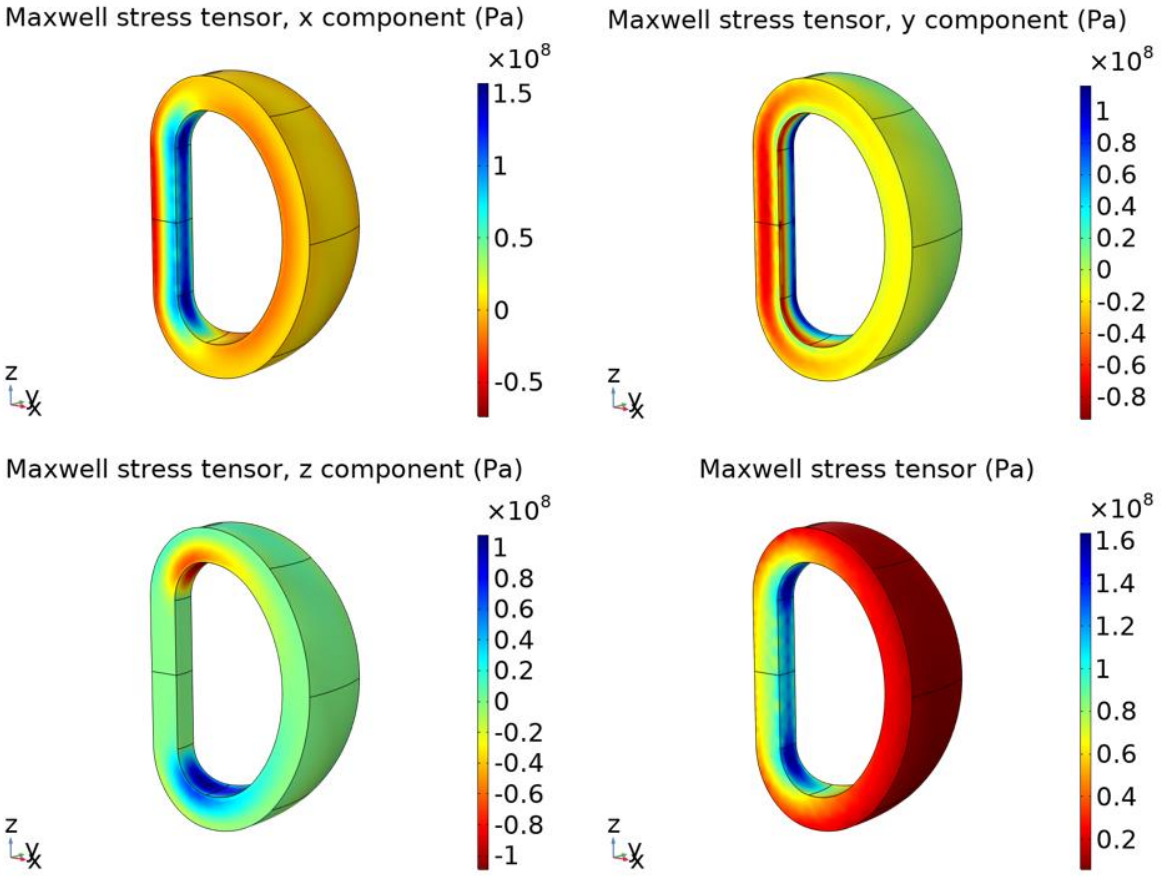

Fig. 24 The distribution of Maxwell stress tensor of the toroidal field coil at 4.2 K, from which it can be concluded that the maximum maxwell stress tensor of the toroidal field coil is around 160 MPa.

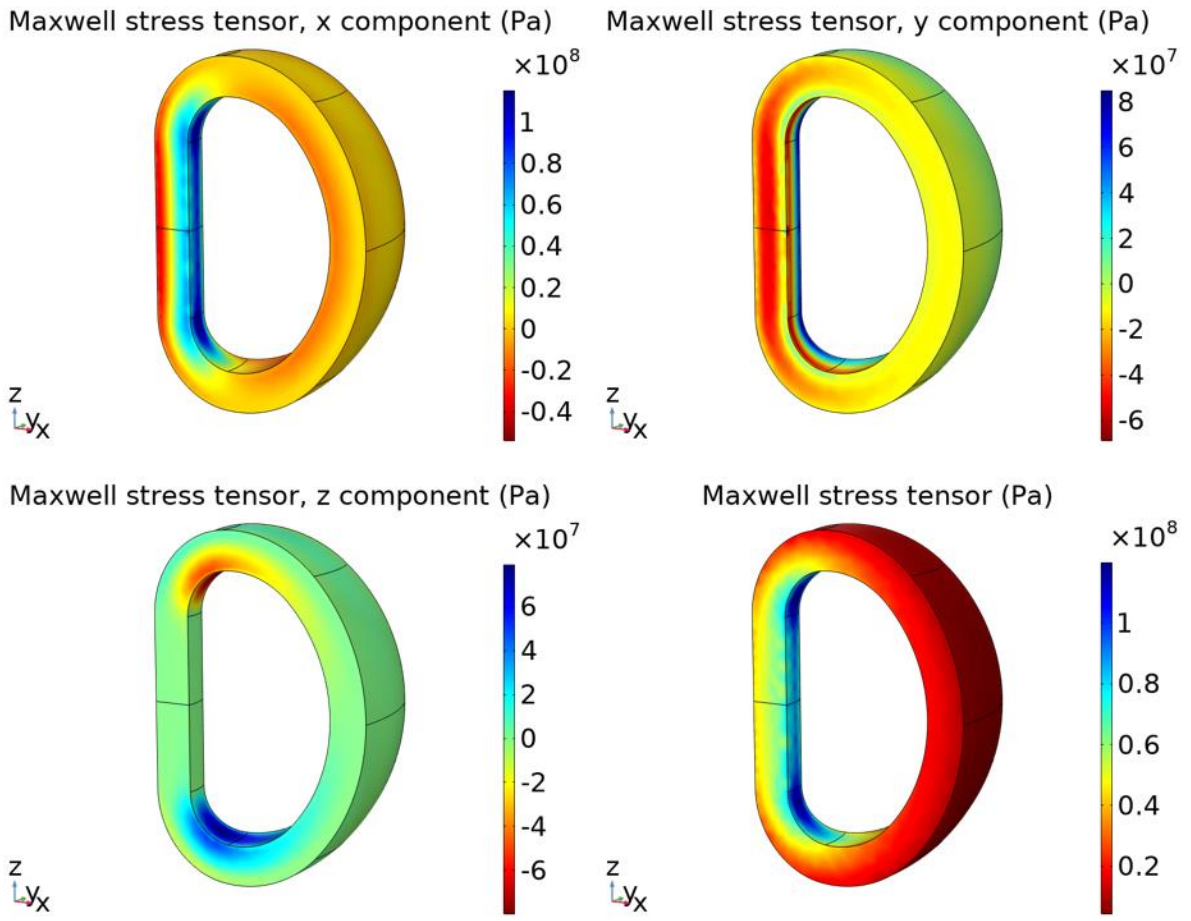

Fig. 25 The distribution of Maxwell stress tensor of the toroidal field coil at 30 K, from which it can be concluded that the maximum maxwell stress tensor of the toroidal field coil is around 100 MPa.

4.7 Electromechanical behavior of the toroidal field coil modules

The Maxwell stress tensor along the toroidal field coil would be higher if all the toroidal field coil modules were considered. Nevertheless, the critical current density of the coil modules will be mainly determined by temperature and external fields. In the same operational temperature environment, the critical current of the REBCO coated conductor can be defined by the interpolation method, with consideration of the external magnetic fields. The concern focuses on the increasing magnetic flux density caused by the magnetic superposition principle possibly leading to a critical current degradation. Consequently, the operating current in each REBCO coated conductor of the toroidal field coil modules is defined as 148 A at 30 K and 186 A at 4.2 K, with a safety margin of more than 20% to the critical current of the REBCO coated conductor in the independent toroidal field coil. The magnetic flux distribution of the toroidal field coil modules is presented in Fig.26. The upper line, middle line, and down line, which are distributed along the inner leg of the toroidal field coils in the figure have been selected as the stress concentration sites to evaluate the Maxwell stress tensor of the coil modules. In addition, a comparison of the magnetic flux density along the inner loop of the toroidal field coil modules at 4.2 K and 30 K is presented in Fig. 27. The measurement starting point 0 m has been marked in Fig.26,

and the measurement direction is clockwise, which means that the 8 m point is in the center of the inboard leg of the toroidal field coil.

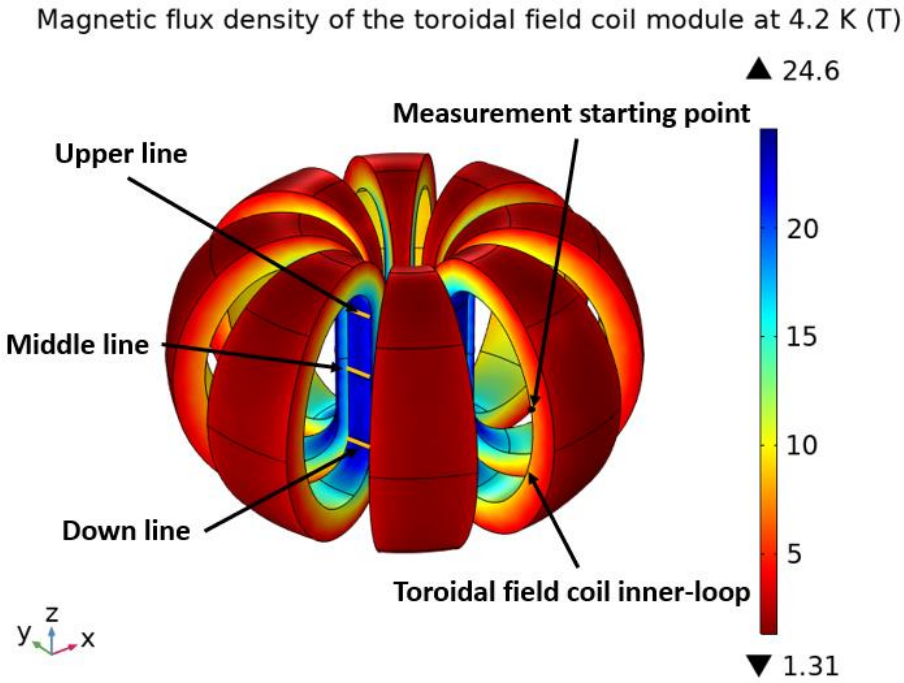

Fig. 26 Distribution of the magnitude of the magnetic flux density in the toroidal field coil modules at 4.2 K.

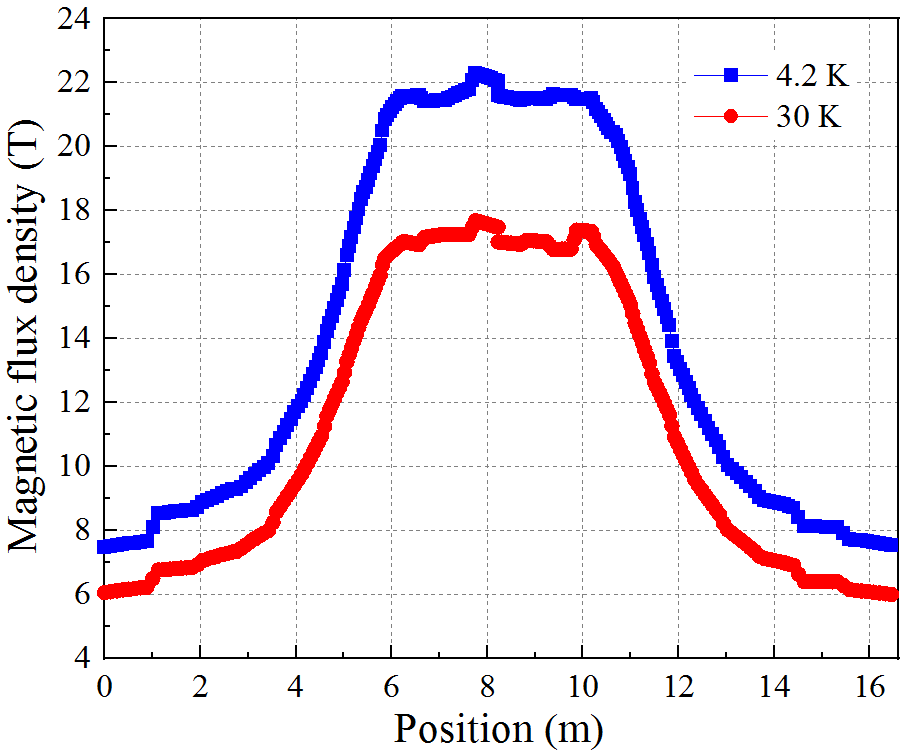

Fig. 27 The magnitude of the magnetic flux density along the toroidal field coil inner-loop at 4.2 K and 30 K.

It should be emphasized that the toroidal field coil modules are more likely to achieve a magnetic flux density of more than 20 Tesla with a relatively small transported current if an independent toroidal field coil can reach the threshold. In addition, it has been demonstrated in experiments that the independent toroidal field coil for the SPARC compact fusion reactor has achieved 20 Tesla if REBCO coated conductors are used [62]. This also demonstrates the feasibility of using REBCO coated conductors to achieve ultra-high fields for large-scale fusion reactors.

The Maxwell stress distribution along the upper line, middle-line, and downline of the inboard leg of toroidal field coils is shown in Fig.28. These lines have been marked in Fig.26. The measurement starts from the left side of the inboard leg, the 0 mm position as shown in Fig.28, and continues to the right side, the 800 mm position. The 400 mm position where the stress concentration occurs, is in the center of the line. It can be seen from this figure that the maximum Maxwell stress is concentrated on the upper line of the inboard leg, due to the smaller bending radius. The maximum stress value is 245 MPa, within the stress tolerance of REBCO coated conductors.

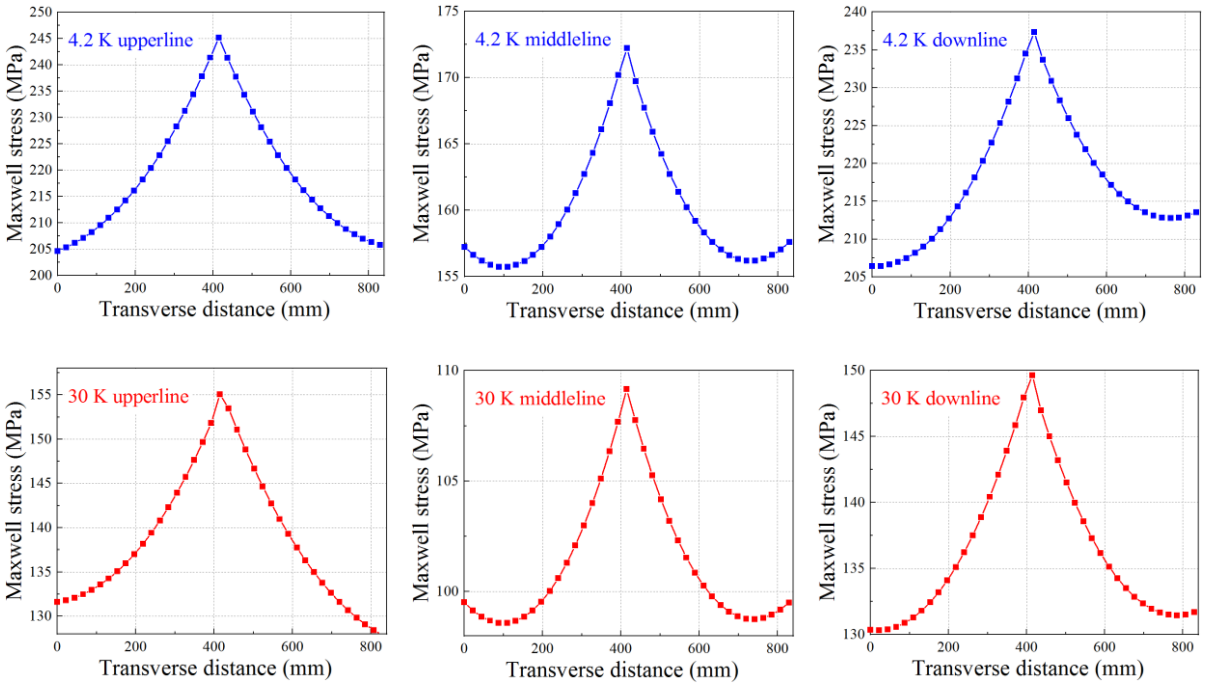

Fig. 28 The distribution of Maxwell stress along the line of the toroidal field coil in the module under 4.2 K and 30 K.

4.8 Summary

A high-field path towards large-scale fusion on earth would be a landmark for fusion energy with the assistance of REBCO coated conductors that have a highly critical current density under ultra-high fields. To achieve the target, this paper proposed a non-twisted REBCO cable with an outstanding DC current-carrying capacity. A layout for the toroidal field coils with the ability to achieve an ultra-high field of more than 20 Tesla has been designed based on this. To evaluate the electromagnetic behavior

of the cable, Joule heating, which is associated with power loss and eddy-current loss, and the magnetic behavior of the cable during transient charging, have been studied further using optimized **T-A** formulation and **H**-formulation based finite element methods, taking temperature into consideration. It could be demonstrated that the designed non-twisted cable is able to carry ultra-high DC currents to achieve a high magnetic field with an operational temperature environment of between 4.2 K and 30 K. In addition, the electromechanical behavior of the independent toroidal field coil and the toroidal field coil modules have been studied further using an **A-V** formulation-based finite element method. It was found that the independent toroidal field coil and the toroidal field module coils can generate a magnetic flux density of more than 20 Tesla within the stress tolerance of REBCO coated conductors on the premise that the coils do not quench.

The study is of great significance in demonstrating the feasibility of using non-twisted REBCO coated conductor cables as a component for toroidal field coils in ultra-high-field magnetic-confinement devices. It may provide effective references for designing new-generation compact and large-scale fusion reactors by using the second-generation REBCO coated conductors.

5 Evidence of AC losses reduction in HTS REBCO coated conductors using the hexagonal arrangement cabling method

High temperature superconducting (HTS) REBCO coated conductors with ultra-high critical current density under external fields of more than 20 Tesla bring a high-field path toward large-scale fusion. REBCO cabling methods such as conductor on round core (CORC) cables, twisted stacked tape conductor (TSTC) cables and Rutherford cables are based on the cable-in-conduit conductor (CICC) developed for low temperature superconducting (LTS) Nb_3Sn and Nb-Ti conductors. However, the REBCO coated conductor is a ceramic conductor and its cross-section is a rectangular shape that is different from these LTS metallic conductors with the round cross-section. It means that REBCO coated conductors might face an irreversible critical current degradation due to mechanical damaging caused by local stress concentration when they are assembled into CICC cables. In order to solve the problem, a star-link REBCO cabling method with the inherent advantage of mechanical protection and inductance balance has been proposed in this article. The electromagnetic behavior of REBCO coated conductors has been evaluated by using H-homogeneous and T-A homogeneous formulation based finite element methods. It is found that the cabling method can offer a stable electromagnetic environment for REBCO coated conductors under AC transmission environment, which has a large potential to be employed as the component of ultra-high-field applications, especially the central solenoid coils of thermonuclear fusion reactors. The study also shows great significance for promoting the employment of REBCO coated conductors for ultra-high field applications with a high-level inductance balance requirement.

This research developed a star-link cabling method with ultra-high inductance balance for the central solenoid coils of ultra-high-field magnetic-confinement plasma devices. Since the central solenoid coils are mainly used for plasma charging, an extremely high current ramping rate with 4 T/s is required. The star-link cabling method has a large potential to be employed as the component of the central solenoid coils. The preliminary work in this research focuses on the conception design and the analysis of its AC loss characteristics.

The individual contributions of the candidate with percentages for the research include: 100% of development and conceptual design, 100% of provision of data, 100% of analysis of data, 100% of drafting of the manuscript and 20% of review work. The manuscript entitled: evidence of AC losses reduction in HTS REBCO coated conductors using the hexagonal arrangement cabling method, which is associated with the research, has been finished and current is under review by the Journal *IEEE Transactions on Applied Superconductivity.*

5.1 Introduction

One sustainable energy development strategy to meet long-term energy needs on Earth is nuclear fusion. An uncontrollable fusion reaction for hydrogen nuclei has been realized using inertial confinement. A theoretically viable option to achieve controllable fusion is to use magnetic confinement [113]. In 1991, the Joint European Torus (JET), as the first large-scale magnetic-confinement device, produced 2 MW controlled fusion power with the deuterium-tritium (DT) reaction [93]. It spawned the largest international collaboration project ITER to demonstrate the feasibility of magnetic-confinement fusion in 2006 [114]. The magnet system for the ITER project took advantage of a mature cable-in-conduit conductor (CICC) cabling method developed for LTS Nb_3Sn and Nb-Ti superconductors [115]. In the same year, the second generation, high temperature superconducting REBCO coated conductor with high critical current density under ultra-high fields of more than 20 tesla was commercialized [16][95]. The elaboration of REBCO coated conductors brings us closer to the possibility of ultra-high-field magnetic confinement fusion. Fig.29 shows the configuration of a magnet system for magnetic-confinement devices using REBCO coated conductors.

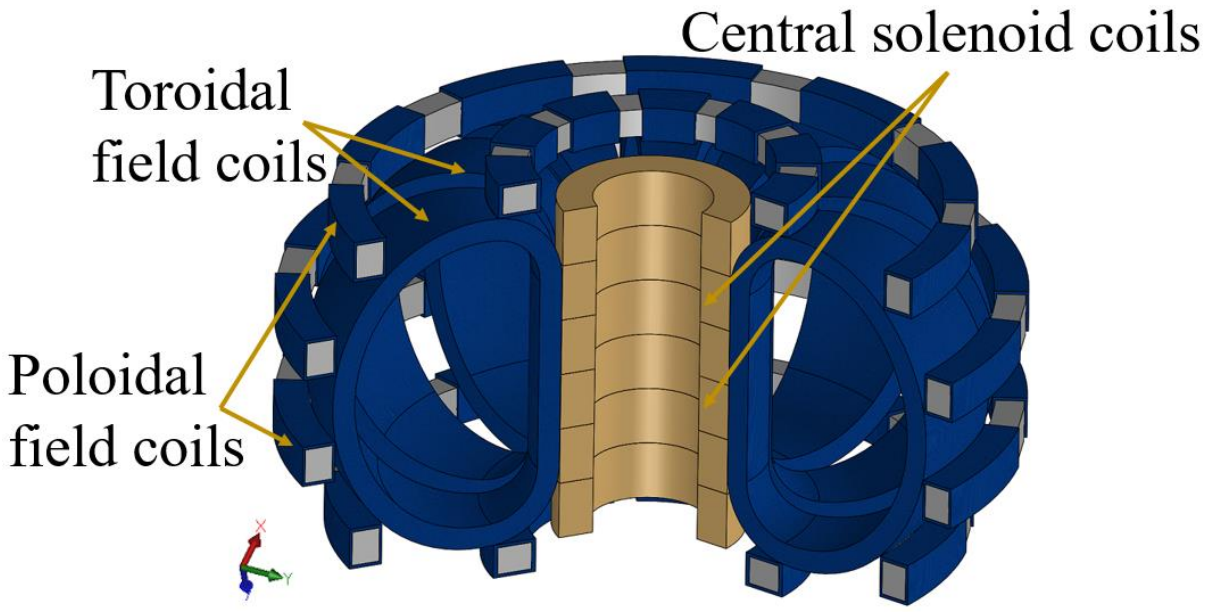

Fig. 29 A geometrical perspective of the REBCO magnet system for magnetic confinement devices.

To achieve an ultra-high-field path toward fusion, the SPARC project which relies entirely on the REBCO coated conductor has been launched at MIT in 2020 [86]. In the following year 2021, a break-through of 20 Tesla was achieved in the SPARC toroidal field model coil by the implementation of the non-twisted non-insulated coil with a current ramping rate of 0.28 mT/s [62]. This value was restricted due to a lack of current transposition and the REBCO coated conductors should be protected from quenching. The coming challenge is that the central solenoid coils, which are needed to transport pulse-field currents to induce plasma current, require an extremely high current ramping rate for REBCO

coated conductors. Therefore, a suitable REBCO cabling method that can achieve high current-carrying capacity as well as high inductance balance urgently needs to be developed by the applied superconductivity community [83]. This is one of the immediate, next research targets for the SPARC project.

In this article, a hexagonal arrangement REBCO cabling method with the function of achieving inductance balance and reducing AC losses is proposed. The inspiration of this cabling method is from the twisted stacked tape conductor (TSTC) cable and the non-twisted REBCO cable that were developed in our previous studies [45][116]. AC losses in the REBCO coated conductors and eddy-current losses of the copper formers in the cable are specifically analyzed using finite element methods.

5.2 The hexagonal arrangement cabling method

REBCO cabling, as a crucial step for exploiting REBCO coated conductors to increase engineering current-carrying capacity, often adopts the strategy of winding the REBCO coated conductors in spiral forms, such as the CORC cable, the TSTC cable, and the Rutherford cable. However, the main challenge is that the REBCO coated conductor is a ceramic material, and its mechanical behavior is quite fragile. Additionally, its rectangular cross-section makes it challenging to achieve current transposition through twisting and bending because mounting a flat tape on a round edge is challenging. Consequently, critical current degradation caused by stress concentration is often found in these REBCO cables.

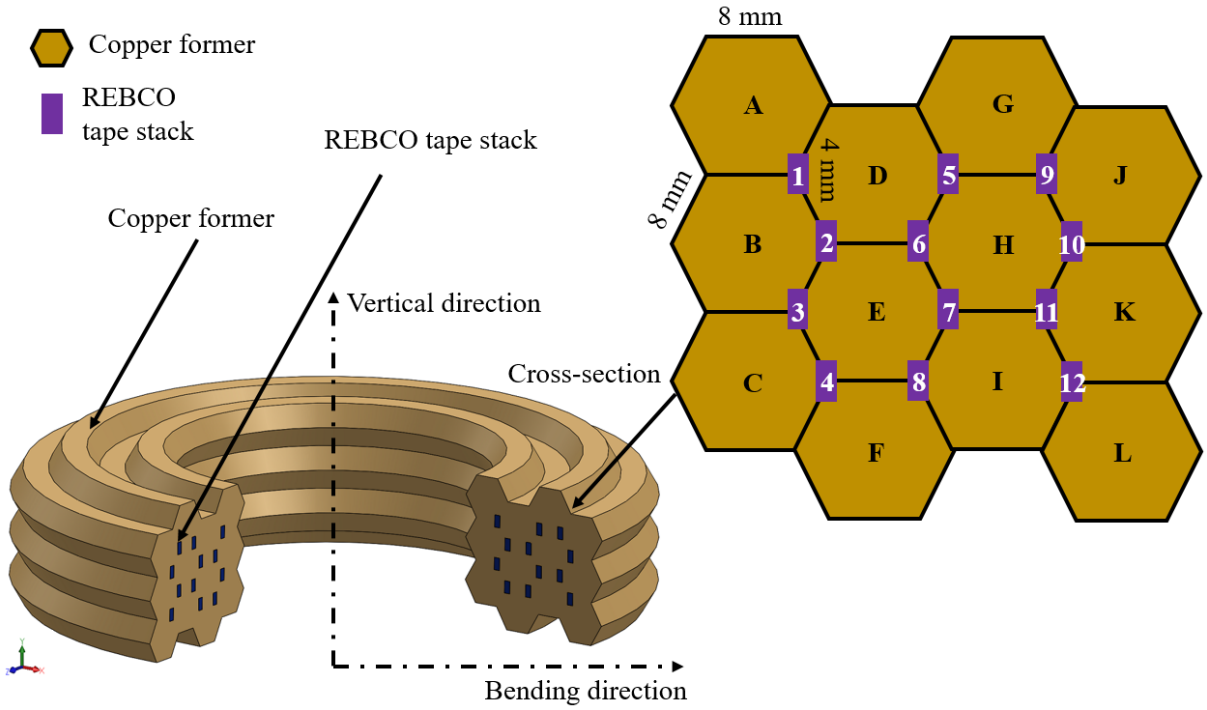

Fig. 30 Hexagonal arrangement REBCO cabling method for ultra-high field central solenoid coils of magnetic confinement devices. The center of the stack is in the intersection of the three regular hexagons. There are 20 REBCO coated conductors in one REBCO taped stack.

The hexagonal arrangement cabling method avoids using the spiral form for REBCO coated conductors to achieve current transposition and priorities protecting their mechanical properties. Although there is no current transposition, the hexagonal arrangement of REBCO stacks in the copper former can help achieve a maximal inductance balance that each REBCO stack in the magnet generates approximately the same AC losses, and eddy-current losses of the copper formers are dependent on the number of REBCO stacks that they encircle.

The REBCO stacks are soldered and arranged in a vertical direction, perpendicular to the bending direction of the tapes, as shown in Fig.30. The inductance balance is achieved by the arrangement of the REBCO stacks at the nodes of each hexagonal copper former from which each REBCO stack is subjected to a similar electromagnetic environment. The hexagonal arrangement REBCO cabling method belongs to the category of cable-in-conduit conductor (CICC) cables, and the conduits wrapped with REBCO coated conductors are located at the junction of the hexagonal copper nodes. Specific geometrical parameters of the cable are listed in Table 6.

Table 6 Main geometrical parameters of the hexagonal arrangement REBCO cable under investigation.

Parameter	Description
REBCO coated conductor	Theva Dünnschichttechnik GmbH
Conductor width	4 mm
Conductor thickness	0.1 mm
Number of conductors in a stack	20
Number of stacks	12
Number of copper formers	12
Copper former cross-section	Hexagonal
Copper former length	8 mm
Coil diameter	1250 mm

The studies were carried out using **H**-homogeneous and **T**-**A** homogeneous formulation base finite element methods. Modelling parameters are listed in Table 1.

5.3 Results and discussion

The current distribution and AC losses in REBCO tape stacks and eddy-current losses in the copper former were calculated. In addition, a comparison of the total losses in the hexagonal arrangement REBCO cable, the regular twisted REBCO cable, and the TSTC REBCO cable is presented.

5.3.1 Current density distribution

The current distribution in each REBCO tape stack has been studied using the **H**-homogeneous model, and the **T-A** homogeneous model [70] has been developed for comparison, as shown in Fig.31. As the current vector potential **T** solves the current density in the superconducting domain, the current density distribution of copper which is solved using the magnetic vector potential **A** is now shown in the **T-A** homogeneous model. The critical current density of REBCO coated conductor is estimated to be 500 A at 4.2 K using the Kim model and the finite element method. In addition, the results from both models show that the current density distribution in each REBCO tape stack is similar, which indicates that REBCO stacks in the cable have achieved a high-level inductance balance.

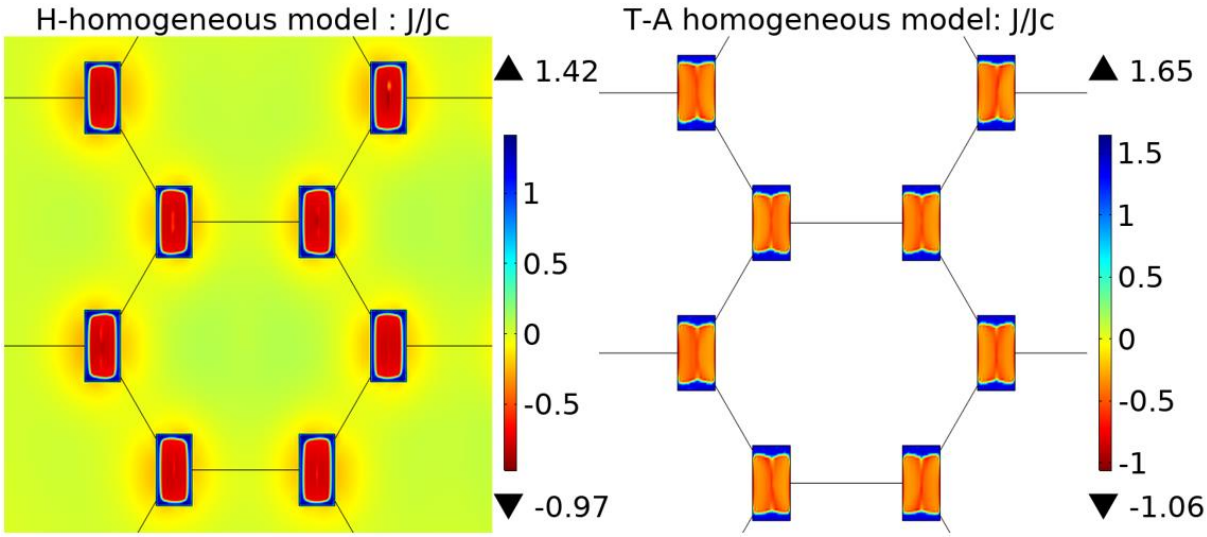

Fig. 31 Current density distribution of REBCO tape stacks at t=0.02 s calculated using the **H**-homogeneous model and **T-A** homogeneous model.

5.3.2 AC losses in the REBCO coated conductors

A time-varying AC current with a frequency of 50 Hz and a peak current of 480 A flows in each REBCO coated conductor at 4.2 K has been studied. As the REBCO stacks are initially in a virgin magnetization state at the first cycle, instantaneous power losses and AC losses of REBCO stacks over the second cycle have been respectively presented in Fig.32 and Fig.33. It is concluded that each REBCO stack is subjected to similar instantaneous power losses and AC losses, which indicates these REBCO stacks experience a similar electromagnetic environment under this AC current, results in a high-level inductance balance among REBCO stacks has been achieved.

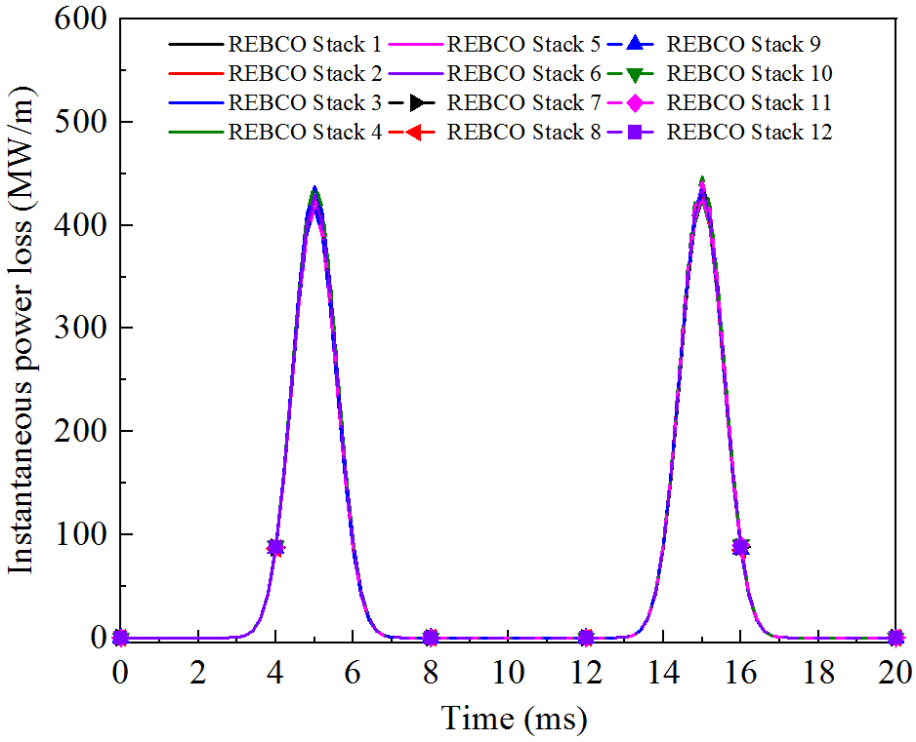

Fig. 32 Instantaneous power loss of REBCO stacks in the hexagonal arrangement REBCO module coil when a time-varying AC current with a frequency of 50 Hz and a peak current of 480 A is transported in each REBCO coated conductor at 4.2 K.

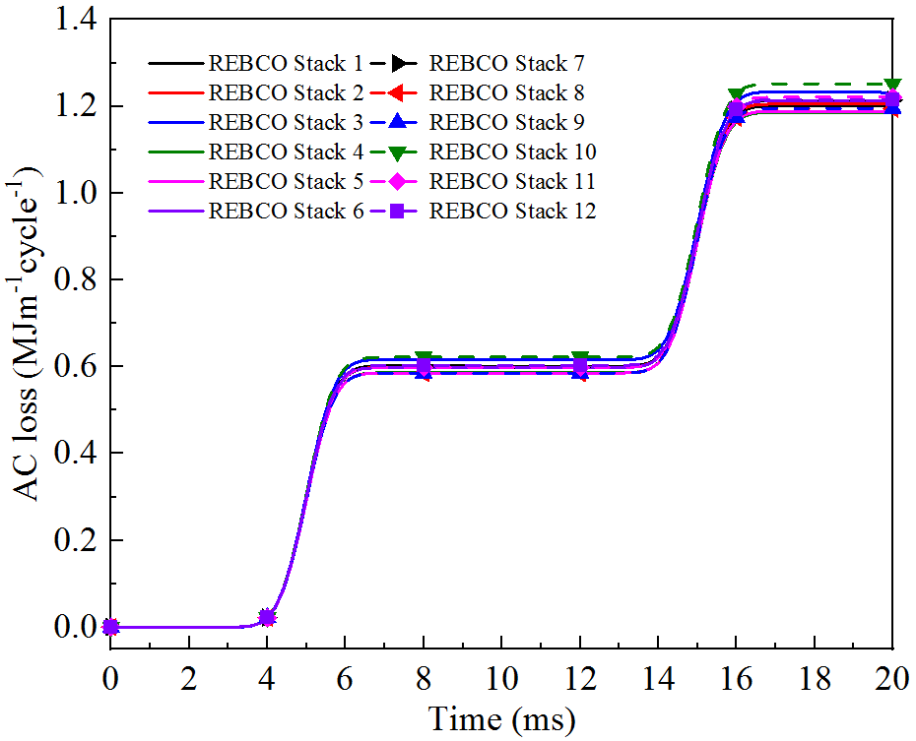

Fig. 33 AC loss of REBCO stacks in the hexagonal arrangement REBCO module coil when a time-varying AC current with a frequency of 50 Hz and a peak current of 480 A is transported in each REBCO coated conductor at 4.2 K.

5.3.3 Eddy-current losses in the copper former

The instantaneous power loss and the eddy-current loss in each copper former have been studied as shown in Fig.34 and Fig.35. As the eddy-current losses generated in the copper former are different between the first and second half-cycles, the model has been operated for 1.5 cycles to check the symmetric behavior after the first half-cycle. It can be discovered that the eddy-current loss is several orders of magnitude smaller than the AC loss and accounts for a small fraction of the total loss compared to Fig.33 and Fig.35. In addition, it appears that eddy-current losses induced in copper A and copper L, copper B and copper K, copper C and copper J, copper D and copper I, copper E and copper H, copper F and copper G, are respectively the same, which indicates that the induced current loss value shows a symmetrical distribution due to the symmetrical arrangement of copper formers in the hexagonal arrangement cabling method.

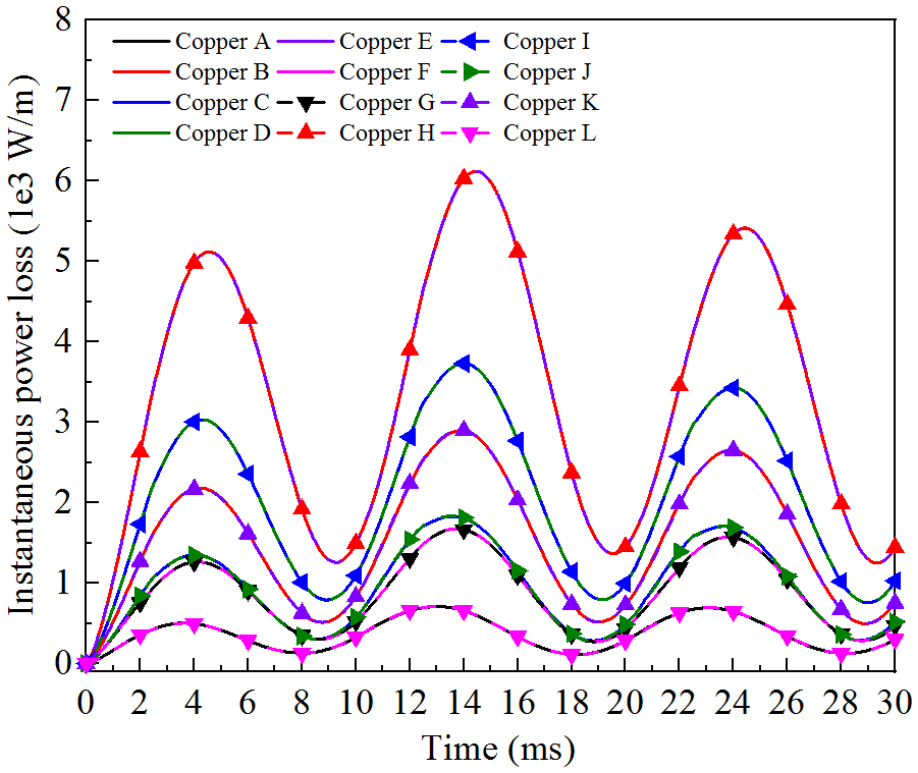

Fig. 34 Instantaneous power loss of the copper formers in the hexagonal arrangement REBCO module coil when a time-varying AC current with a frequency of 50 Hz and a peak current of 480 A is transported in each REBCO coated conductor at 4.2 K.

Eddy-current losses of the copper former are mainly determined by the number of REBCO stacks encircling it, as these REBCO stacks determine the external traveling magnetic fields surrounding the copper former. Therefore, copper formers with more REBCO stacks encircled can induce more eddy-current losses. In addition, despite the amount of copper accounts for a relatively high proportion in the hexagonal arrangement cabling approach, eddy-current losses induced in the copper former are relatively low compared with AC losses induced in REBCO stacks, indicating the cabling method's

reasonable design. Moreover, the copper former also functions as mechanical protection and electrical stabilization.

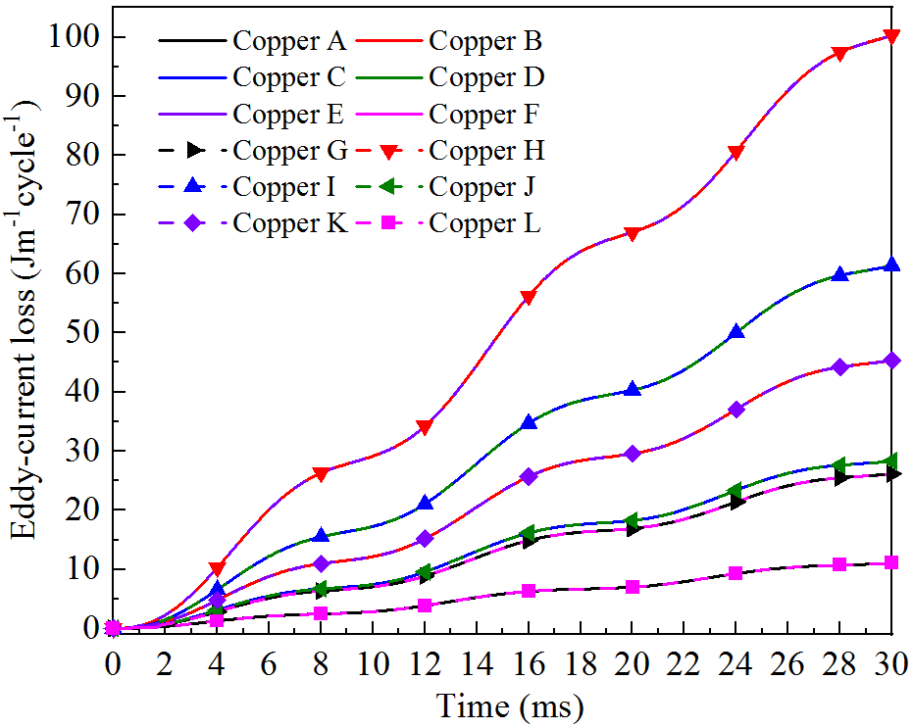

Fig. 35 Eddy-current loss of the copper formers in the hexagonal arrangement REBCO module coil when a time-varying AC current with a frequency of 50 Hz and a peak current of 480 A is transported in each REBCO coated conductor at 4.2 K**.**

5.3.4 Total losses comparing different cable architectures

A comparison of the total losses which contain AC losses in REBCO stacks and eddy-current losses in the copper former in the hexagonal arrangement cabling configuration, the regular non-twisted REBCO cabling configuration [116], and the twisted-stacked tape-conductor (TSTC) cabling configuration [45] has been carried out. In the condition that these cables have a similar packing density with REBCO coated conductors, and the number of REBCO coated conductors in a REBCO stack, the number of REBCO stacks in a cable, and the AC currents transmitted in these cables are the same, the total losses produced in a cycle by the hexagonal arrangement cable are around three-quarters of the TSTC cable and three-fifths of the regular non-twisted REBCO cable as shown in Fig.36. It indicates that the hexagonal arrangement cabling method has advantages in reducing AC losses compared with the regular non-twisted REBCO cable and the TSTC REBCO cable. Meanwhile, when the cables are wound into coils, the hexagonal arrangement cabling method and the regular non-twisted REBCO cable have the function of mechanical protection and, therefore, can avoid critical current degradation in REBCO coated conductors compared with the TSTC REBCO cables.

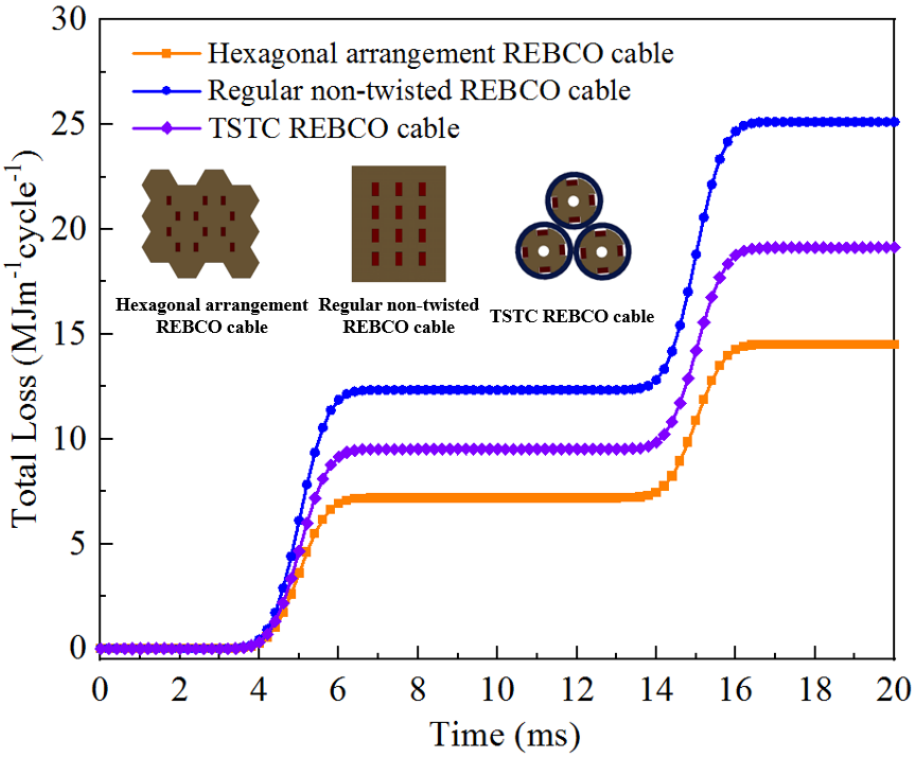

Fig. 36 A comparison of the total loss of the hexagonal arrangement REBCO module coil, the regular non-twisted REBCO module coil and the twisted-stacked tape-conductor (TSTC) coil when a time-varying AC current with a frequency of 50 Hz and a peak current of 480 A is transported in each REBCO coated conductor at 4.2 K.

5.4 Summary

A hexagonal arrangement REBCO cabling method with inductance balance and low AC loss characteristics for ultra-high-field current transmission has been proposed in this article. AC loss characteristics of the hexagonal arrangement REBCO cable have been evaluated using finite element methods. Studies of critical current density, AC losses in REBCO stacks, and eddy-current losses in copper formers demonstrate the reasonable feasibility of our cable design. As the hexagonal arrangement of REBCO stacks in the cable seems like a star-link, we renamed the hexagonal arrangement REBCO cable as the star-link REBCO cable. It is applicable for ultra-high-field applications in MRI machines, accelerators, fusion reactors and so on. It shows great potential to be applied to the central solenoid coils of ultra-high-field magnetic-confinement plasma devices with its superiority in achieving inductance balance and reducing AC losses. The study should significantly promote the development of REBCO coated conductors for ultra-high-field large-scale applications.

6 Electro-thermal-mechanical behavior of HTS REBCO coated conductor central solenoid coils for ultra-high-field thermonuclear fusion reactors

The second-generation high temperature superconducting (HTS) REBCO coated conductors, featuring extremely high engineering critical current density under ultra-high fields enable a high-field path toward compact and large-scale fusion reactors. A 20 Tesla toroidal field has been achieved experimentally by using the racetrack REBCO cabling method with a current ramping rate of 0.28 mT/s in the SPARC project. An essential issue that has not been solved is the cabling strategy for the central solenoid coils that are used for plasma charging. Since an extraordinarily high current ramping rate with 4.0 T/s is required in this process, a qualified cabling method should offer REBCO coated conductors inductance balance and reduce power losses as much as possible to avoid quench. In our study, a star-link REBCO cabling method in reducing AC losses of REBCO coated conductor coils has been developed, and the implementation of the star-link cabling method for the REBCO coated conductor central solenoid coils with the capacity of achieving ultra-high fields under high ramping rates has been elaborated in this article. Since there is no critical current degradation caused by torsion, the inherent superiority of the cabling method can be focused on mechanical protection. As a consequence, hysteresis losses, coupling-current losses and eddy current losses of the star-link cables in the central solenoid coils have been evaluated by using the H-formulation based finite element method. In order to assess the stress in REBCO coated conductors under ultra-high currents and fields, electromechanical behavior of REBCO coated conductors in the star-link cables has been studied by using the Wilson formula-based analytical method. Results show the advantages of the star-link cabling method in reducing AC losses and achieving inductance balance. The study demonstrates the feasibility of the star-link cabling method for ultra-high-field central solenoid coils and is of great significance for the R&D of the new generation of HTS REBCO magnets used for ultra-high-field large-scale fusion devices.

The individual contributions of the candidate with percentages for the research include: 100% of development and conceptual design, 100% of gathering data, 100% of evaluation data, 100% of drafting of the manuscript, and 20% of review work. The manuscript which is related to the research has been entitled: development of a star-link cabling method for the REBCO coated conductor central solenoid coils of ultra-high-field ultra-high-field thermonuclear fusion power plants and submitted to *Journal of Physics D: Applied Physics*.

6.1 Introduction

In the process of using REBCO coated conductors for ultra-high-field applications such as fusion devices and accelerator magnets, initially it can only be used as a component of the hybrid magnet toward ultra-high field magnets [117]. Until 2021, a SPARC toroidal field model coil of the magnetic-confinement device as shown in Fig.29 that relies entirely on REBCO coated conductors has been achieved 20 Tesla by means of the non-insulation non-twisted racetrack coils [118], which is a breakthrough and brings the possibility of achieving magnetic-confinement fusion with an ultra-high-field path. The entire charging and discharging process for the SPARC toroidal field module coil lasted for 100 hours, and the current ramping rate was around 0.28 mT/s. The charging model is feasible for the steady-state toroidal field coils, but it is difficult to be applied to the central solenoid coils, at a current ramping rate requirement of 4.0 T/s. The main reason is that the racetrack coil is a non-transposed coil and is unable to provide inductance balance for the entire central solenoid charging system.

In the application of using REBCO coated conductors for ultra-high-field large-scale fusion magnets, the critical current density of the REBCO coated conductor can hardly meet the current transmission requirement of these ultra-high-field magnetic-confinement devices. Therefore, a cabling method is necessary and essential in increasing the engineering critical current density of REBCO cables. In the past decades, five main REBCO cabling methods have been developed: the conductor on round core (CORC) cable [109], the twisted stacked tape conductor (TSTC) cable [45][90], the REBCO Roebel cable [48], the REBCO Rutherford cable [55] and the non-twisted cable [105][116], which are all based on the cable-in-conduit conductor (CICC) that was developed from the low temperature superconducting cabling technique. To decrease AC losses and achieve inductance balance, CORC cable, TSTC cable, and Rutherford cable have adopted a tape-twisting structure, which breaks the mechanical behavior of the ceramic superconducting layers in REBCO coated conductors and limits their potential for achieving ultra-high fields. The REBCO Roebel cable is a fully transposition cabling method and was developed based on a century-old copper cabling concept. The latter has advantages in reducing AC losses of superconductivity, but the main challenge limiting application to ultra-high fields is that the transverse stress generated under ultra-high Lorentz forces can lead to irreversible critical current degradation [119]. Therefore, the Roebel cable is feasible for high-temperature, low-field applications, but it can hardly meet the requirement of ultra-high-field applications due to stress concentration. The non-twisted cable can maximally protect the mechanical behavior of superconducting layers in REBCO coated conductors, but in electrical terms it has no function for achieving inductance balance and can only be applied to the toroidal field coils or poloidal field coils having steady-state magnetic fields that require an extremely low current ramping rate. Therefore, the research and development of REBCO coated conductor cables for the central solenoid coils is essential and would be the next development target for ultra-high-field magnetic-confinement devices.

The development of suitable high temperature superconducting REBCO coated conductor cabling methods for ultra-high-field magnetic-confinement devices has been carried on in our laboratory for some years. The current-carrying capability and magnetic behavior of the TSTC cable with different slots have primarily been studied. We found that the cable has a highly current-carrying capacity at an operating temperature environment of no more than 30 K [45]. But we also recognized that an enormous critical current degradation might arise when the TSTC cable is bent to the shape of the toroidal field coils, because the bending after twisting process can cause direct destruction of the mechanical behavior of REBCO coated conductors. Therefore, TSTC cable is recommended as the linear current lead for ultra-high-field large-scale fusion devices, but it might not be feasible for bending or curve applications like toroidal field or poloidal field coils. Thereafter, we developed a non-twisted cable having the advantages of excellent current-carrying capacity, great flexibility, and cost-effectiveness [116] for the toroidal field coils of ultra-high-field magnetic-confinement plasma devices. To achieve the maximum inductance balance while also offering the maximum mechanical protection for REBCO coated conductors, a star-link cabling method for the central solenoid coils of ultra-high-field magnetic-confinement devices has been developed as shown in Fig.30. The elaboration of the manufacturing process, and explanations of power loss characteristics and mechanical behavior of the star-link cabling central solenoid coils for ultra-high-field magnetic-confinement devices have been presented in this article. The star-link cabling method shows great potential regarding the design and manufacture of the new generation of ultra-high-field compact and large-scale fusion devices.

6.2 system design

The G-tune thermonuclear fusion reactor, as a concept fusion reactor proposed recently in our group, is an ultra-high-field large-scale reactor that relies entirely on the second-generation high temperature superconducting REBCO coated conductor magnet system. The volume of the G-tune fusion reactor is 5 times larger than the SPARC fusion reactor, and nearly the same as the International Thermonuclear Experimental Reactor (ITER). However, the maximum magnetic field produced by the G-tune fusion reactor is nearly twice that of the ITER fusion magnet by virtue of using REBCO coated conductors. It has been demonstrated that the achievable fusion power of a thermonuclear fusion reactor is proportional to the fourth power of the toroidal field [83]. Therefore, the gain of plasma heating power of the G-tune fusion reactor can be 16 times of the ITER fusion reactor. The aim for the G-tune fusion reactor is to build a connection between the compact fusion and the large-scale fusion reactors. In specific terms, it can be a reactor in the direction of large-scale fusion reactors and towards the Europe Demonstration (EU-DEMO) power plant. This section elaborates the central solenoid coil system of the G-tune thermonuclear fusion reactor using the star-link cabling method.

6.2.1 The star-link cabling method

The thickness of the superconducting layer in REBCO coated conductors is around one micron [16]. More importantly, the superconductor is a sort of oxide ceramic material with very fragile mechanical behavior. This means that REBCO coated conductors can be easily destroyed by man-made tensile or torsional stresses. Therefore, it is assumed that REBCO coated conductors should avoid twisting when they are being assembled into cables in order, that the mechanical behavior of REBCO coated conductors be maximally protected. Meanwhile, considering the requirement of inductance balance under ultra-high current ramping rate for central solenoid coils, it should be ensured that the electromagnetic environment to which each REBCO coated conductor is exposed should be similar. In this case, power losses during the transient charging can be minimized. The star-link cabling method was created after taking these factors into account. As shown in Fig.30, the star-link cabling method, which is based on the CICC structure, consists of copper former and REBCO stacked tapes. Adoption of the hexagonal copper former structure ensures that each hexagonal node has the same connection form with the surrounding nodes. The center of each REBCO taped stack is coincident with the hexagonal node, from which each REBCO taped stack is surrounded with a similar electromagnetic environment such that the maximum inductance balance of REBCO coated conductors can be achieved. The REBCO taped stack is composed of non-insulation REBCO coated conductors, but it is insulated with the copper former. There is no current transmission in the cooper former given the concern that the magnetic field produced by the copper might induce a screening current on the surface of REBCO coated conductors, which has a negative influence on the engineering critical current density of REBCO taped stacks.

The function of the copper former is to protect the mechanical behavior of REBCO coated conductors and simultaneously achieve conduction cooling for REBCO taped stacks. In general, the cooling channel for REBCO cables is arranged in the center area of the cabling system. In this case, however, the huge Lorentz force results from the combination of ultra-high currents and extremely strong magnetic fields might cause stress concentration around the cooling channel, leading to a risk of damaging. Therefore, considering the cryogenic stability of REBCO coated conductors under low temperature environment, an indirect cooling system has been adopted, and the cooling channel is arranged on the outside of the cabling system, which is another innovation by the star-link cabling method. Therefore, the star-link cabling method has many potential advantages, e.g., robust mechanical behavior, high-level inductance balance, easily assembly, high reliability, and cost-effectiveness.

6.2.2 The star-link cabling central solenoid coil system

A non-twisted cabling method used for the toroidal field coils of the G-tune thermonuclear fusion reactor has been developed in our previous study [116]. The external radius of the toroidal field coil is 5500 millimeters, and the overall height of the toroidal field coil is 8000 millimeters. Therefore, the overall

height of the central solenoid coil system is designed accordingly as 11785 millimeters, consisting of 6 coils with a height of 1964 millimeters for each coil. The inner diameter of the central solenoid coil is set as 1000 millimeters and the outer diameter of the central solenoid coil is set as 1550 millimeters, consisting of 378 star-link cabling units with 54 rows and 7 columns of units arranged in each coil. The configuration of the star-link cabling central solenoid coil system can be seen in Fig.37. Specific geometrical parameters of the ultra-high-field star-link cabling central solenoid coil are shown in Table 7.

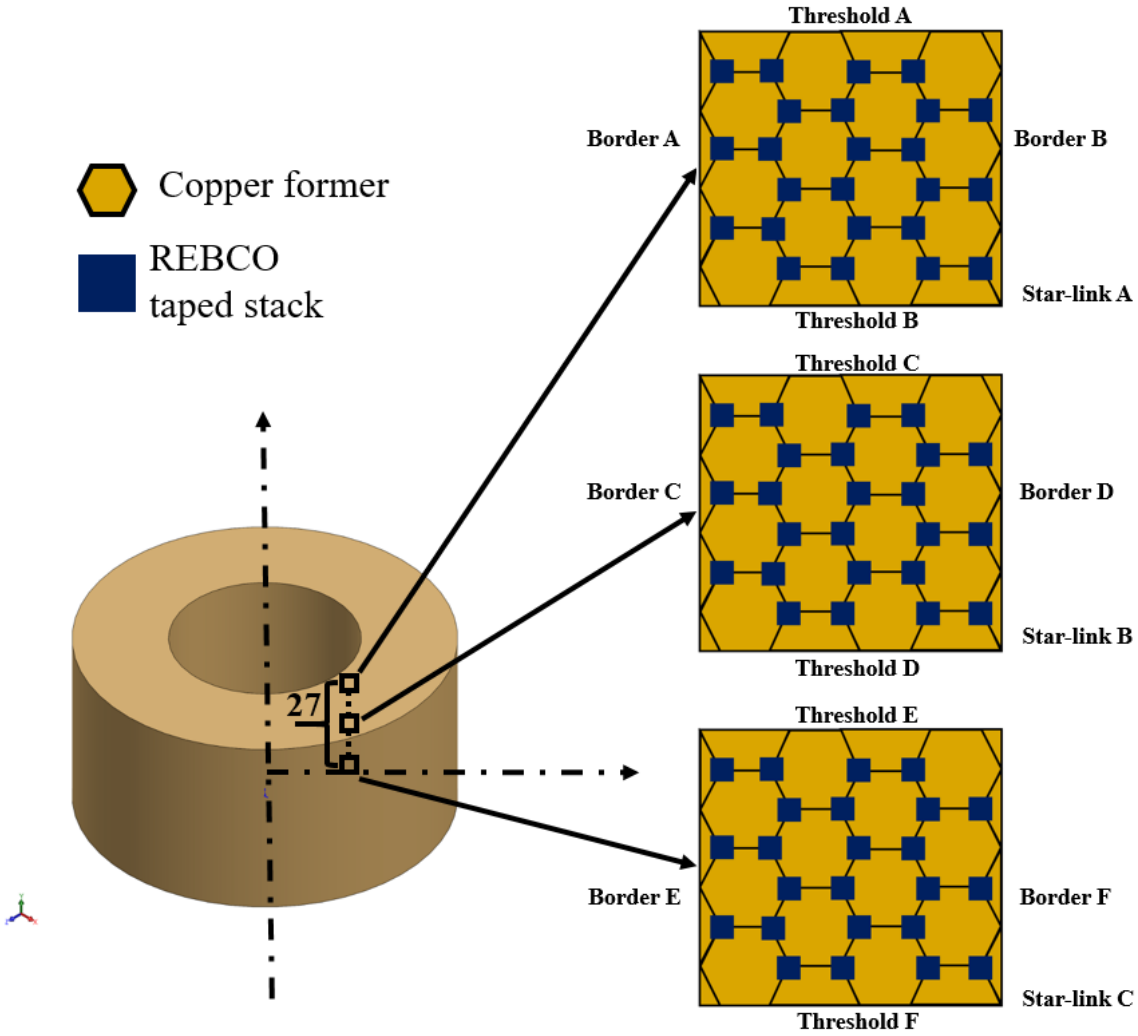

Fig. 37 The star-link cabling central solenoid coil system. Each central solenoid coil consists of 7 rows and 8 columns of star-link cabling units.

Table 7 Geometrical parameters of the ultra-high-field star-link cabling central solenoid coil.

Parameter	Description	Value
w	Width of the REBCO coated conductor	4 mm
t	Thickness of the REBCO coated conductor	0.1 mm

u	Number of REBCO coated conductors in a REBCO taped stack	40
r	Width of the regular hexagon copper former	6 mm
v	Number of REBCO taped stacks in a star-link cabling unit	24
p	Number of star-link cabling units in a central solenoid coil	378
q	Inner diameter of the central solenoid coil	1000 mm
k	Outer diameter of the central solenoid coil	1550 mm
a	Width of a star-link cabling unit	39 mm
b	Height of a star-link cabling unit	36.37 mm
e	Height of a half central solenoid coil	982 mm

6.3 Methodologies

The study is carried out using experiments and simulation. Experiment tests of the critical current density in REBCO coated conductors were carried out in Theva Dünnschichttechnik GmbH. A benchmark model of the empirical equation for the REBCO coated conductor was established using the experimental data. The equations were solved using the further developed **H**-formulation [67][68][120] and **A-V** formulation [121][122][123] based finite element methods with the consideration of the influence of operating temperature. A multi-physics model in solving the electromechanical behavior in REBCO coated conductors has been further developed using A-V formulation based finite element methods with the consideration of the Wilson formula [124]. The description of the models can be viewed in Section 2, and the detailed parameters in modelling the electromechanical behavior of the star-link cabling central solenoid coils can be viewed in Table 1.

6.4 Results and discussion

The study aims to evaluate the performance of the star-link cabling central solenoid system from the aspects of magnetic behavior, power dissipation during transient charging and mechanical behavior of the central solenoid coil system. Therefore, these parts have been studied carefully in this section.

6.4.1 Magnetic behavior of the central solenoid coil

The engineering critical current density of the second-generation high temperature superconducting REBCO coated conductor has been developed to a very high performance with over 1000 A/mm^2 at 20 K, 20 Tesla and over 2000 A/mm^2 at 4.2 K, 20 Tesla [6], that equals to an engineering critical current of more than 400 A at 20 K, 20 Tesla and more than 800 A at 4.2 K, 20 Tesla. But the REBCO coated conductors require a stability margin to be operated in energy terms. In our study, the operating current of the REBCO coated conductor was set as 120 A, and the central solenoid coils were operated in a liquid helium environment of 4.2 K. The main concern in the model setup was reducing the influence of magnetization effects which might cause quenching for REBCO coated conductors at an ultra-high field ramping rate. The transient charging duration for the magnet system was 5 seconds, at a current ramping rate of 24 A/s for each REBCO coated conductor. Therefore, the magnet system has the capacity to achieve 24.7 Tesla when current charging is completed, which means that the overall current ramping rate of the magnet system can reach 4.814 T/s. This rate meets the plasma charging requirement for ultra-high-field, large-scale fusion reactors.

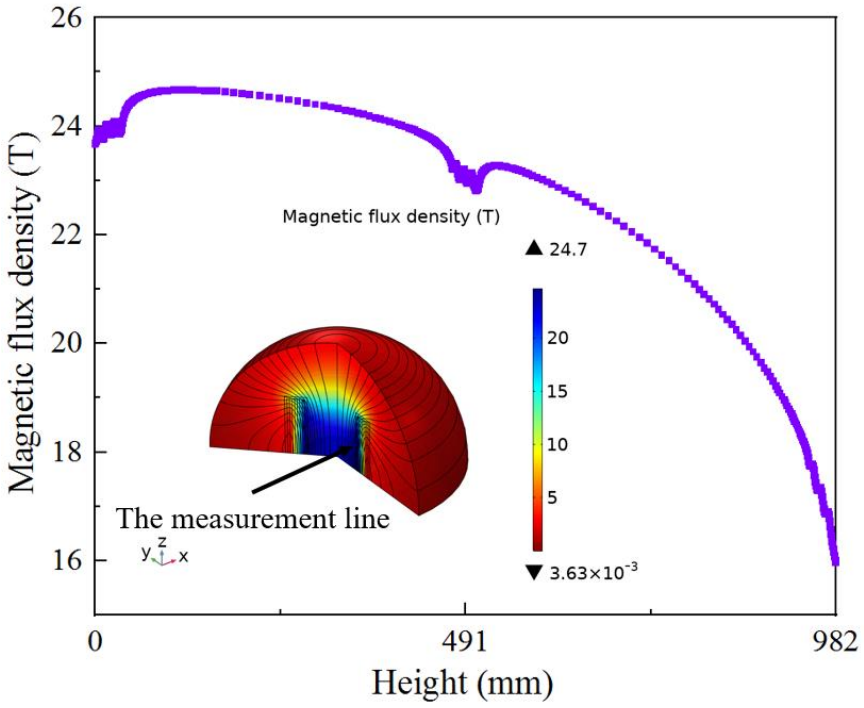

Fig.38. Magnetic behaviour of the central solenoid coil after transient charging. The measurement line is taken along the inside diameter of the coil.

The magnetic behavior of the central solenoid coil was measured and is shown in Fig.38. The measurement line is along the inner diameter of the coil. There were no charging challenges to the magnet system achieving an ultra-high stable magnetic field since the star-link cabling method has the specific capacity to achieve inductance balance. The critical issue in this charging process is that of avoiding quenching in superconductivity, which is the result of the resistive transition, possibly leading to temperature increase and cryogen expulsion. It is noteworthy that the critical temperature of low

temperature superconducting Nb_3Sn is 18.3 K [125], but the critical temperature of REBCO materials can reach 92 K [126]. It means that the REBCO superconductors have a high cryogenic stability compared with LTS Nb_3Sn superconductors, especially at 4.2 K. The quench protection in REBCO coated conductors requires an assessment of the power dissipation in the magnet system during transient charging. If the refrigeration power of the cooling system is greater than the heat dissipation generated by the magnet system during transient charging, then quench in superconductivity can be avoided and the transient charging process can be regarded as being successful. Therefore, the power dissipation of the magnet system during transient charging has been studied.

6.4.2 Power losses during transient charging

There are four main types of losses in REBCO coated conductors: hysteresis losses, transport current losses, eddy current losses and ferromagnetic losses [127][128]. Hysteresis losses are generated with external magnetic fields, which have a magnetization effect on REBCO coated conductors and can induce screening current that causes an induced electromotive force inside the conductor as well. Hysteresis losses can be very significant during transient charging in the central solenoid coil given the very high external magnetic fields. Transport current losses are generated in REBCO coated conductors during current transmission. The REBCO coated conductor consists of a copper layer, a Hastelloy substrate layer, a superconducting layer, a buffer layer, and a silver layer [129]. Given the premise that the superconductor does not quench, there is no power dissipation in the superconducting layer during current transmission. However, current sharing does exist between the superconducting layer and other conductive layers, which causes transport current losses. Eddy-current losses are mainly caused in the copper former of the star-link cabling unit. Regarding the design of the cabling method, inductance balance and mechanical behavior have been mainly considered, but this leads to a large quantity of copper in the cabling system. Therefore, it is essential to analyze the eddy current losses in the copper former to ensure that the proportion thereof accounts for a reasonable and qualified ratio. In addition, the Hastelloy substrate is a non-ferromagnetic material, and there are no ferromagnetic materials in the REBCO coated conductor, so the value of ferromagnetic losses can be ignored. This section analyses the hysteresis losses, transport current losses, and eddy current losses during transient charging.

6.4.2.1 Hysteresis losses

In a central solenoid coil, REBCO coated conductors that generate the most hysteresis losses should come from the inboard of the coil, where the magnetic flux density is higher. Therefore, these areas should be specifically analyzed. In our study, three specific star-link cabling units which are located on the inboard region of the coil were selected as shown in Fig.37. A ramping current rate of 24 A/s was conducted in each REBCO coated conductor, and the duration of the charging process was 5 seconds. Hysteresis losses were generated with screening currents, which are the induced currents in REBCO coated conductors changing with the external magnetic fields. A non-linear induced current density has been discovered in the star-link cabling units as shown in Fig.39. It was found that unit B induced the

most current density, and the influence of perpendicular fields on unit B might be higher than with another two units. In addition, the induced current density in unit A was also high, which might have been caused by the end effect of the central solenoid coil. The continuously rising induced current density in the star-link cabling units also indicates that the superconducting coils are working in a healthy condition and do not quench. The corresponding hysteresis losses in these three units are illustrated in Fig.40; the magnitude of the value is at 1×10^7 J/m, meaning that the magnetization effect of external ultra-high fields can be significant. The hysteresis losses in one star-link cabling unit of the central solenoid coil were within 2×10^7 J/m/s, which is equivalent to 2×10^7 W/m. There are 378 star-link cabling units in the central solenoid coil system. Therefore, the total hysteresis losses generated during transient charging can be within 7.56×10^9 W/m.

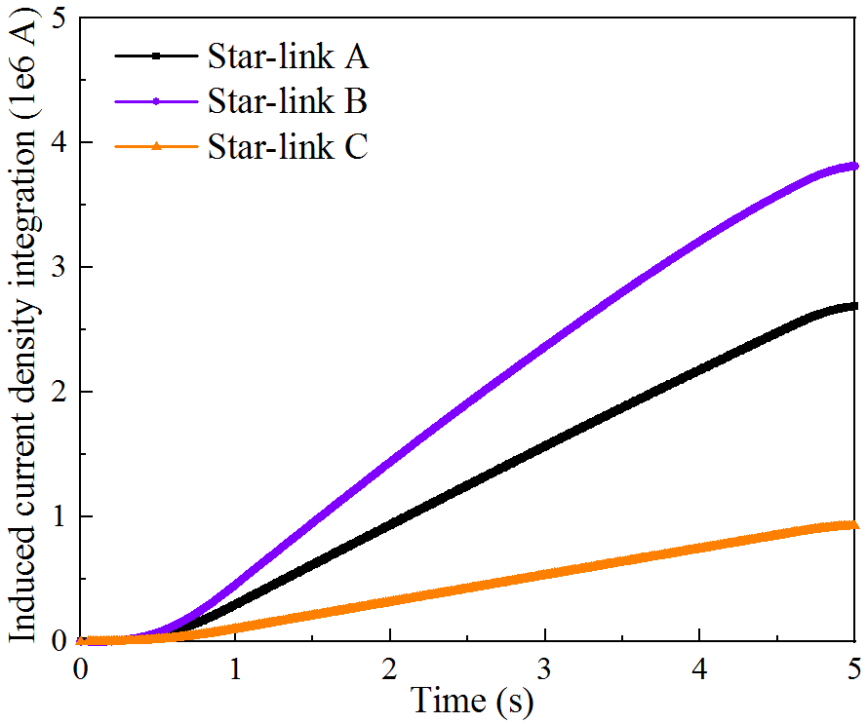

Fig.39. The integration of induced current density in REBCO coated conductors during the transient charging.

6.4.2.2 Transport current losses

The same current ramping model associated with plasma charging in the central solenoid coil was applied to REBCO taped stacks in the cabling units. Transport current losses in each star-link cabling unit were estimated without considering the external magnetic field. Since each REBCO coated conductor was transported at the same current, transport current losses in each unit appear to be the same, despite being non-linear given the highly non-linear **E-J** behavior of the REBCO coated conductor, as shown in Fig.41. As we define the transport current loss P_t as $P_t=\mathbf{E}\times\mathbf{J}$, and the current density in each REBCO taped stack should be the same, so the curve for the transmission current losses is consistent with the curve of the induced electromotive force of the REBCO coated conductor, and the relationship between them is basically multiplicative. The order of magnitude of transmission current

losses was 1×10^6 J/m, which was smaller than the order of magnitude of the hysteresis losses. It can be deduced that the total transport current losses in the central solenoid coil system was within 1.89×10^8 W/m.

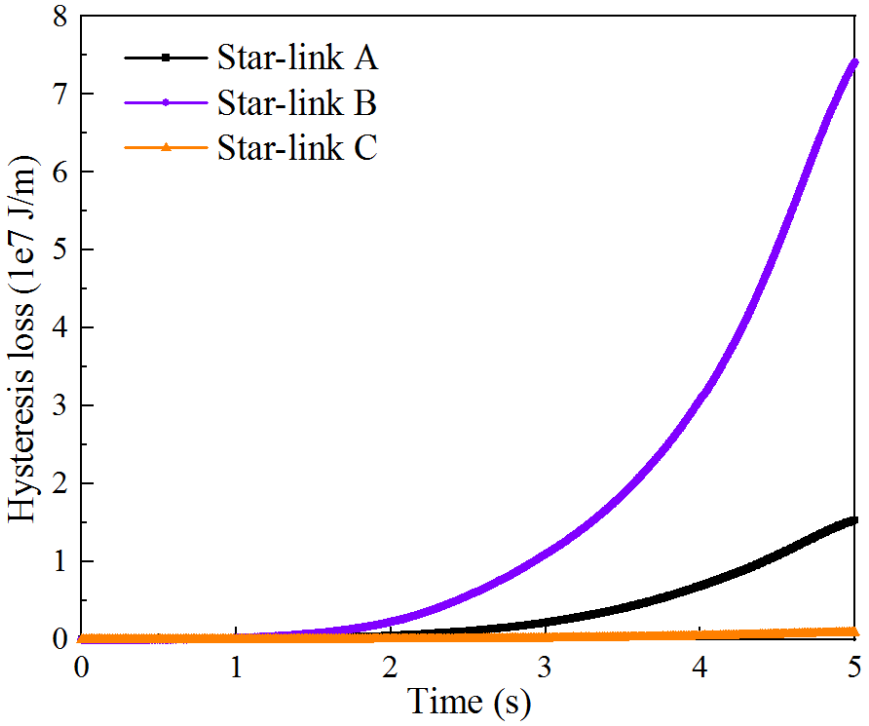

Fig.40. Hysteresis losses of REBCO coated conductors during the transient charging.

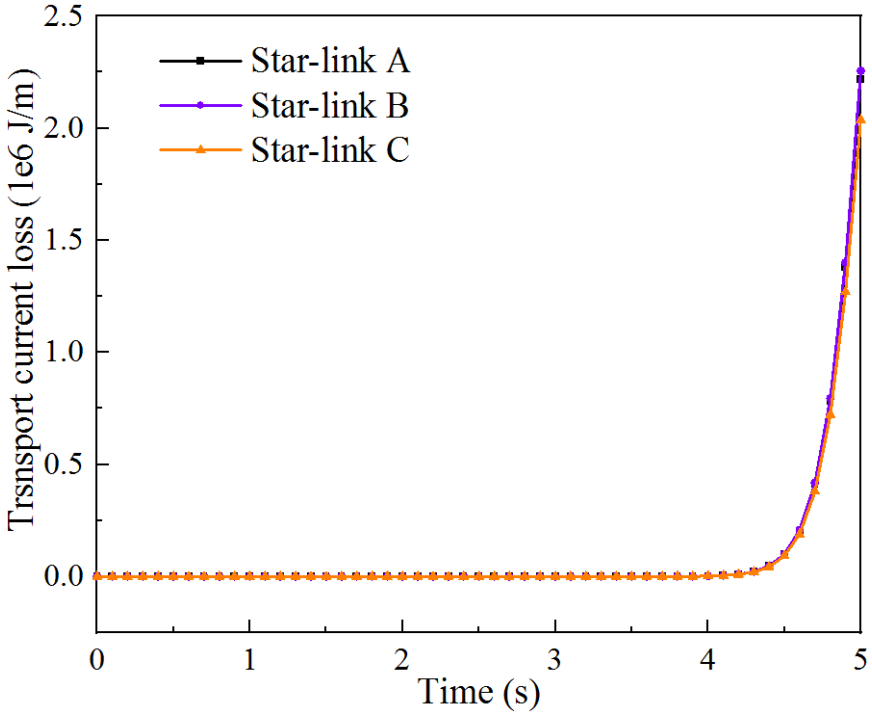

Fig.41. Transport current losses of REBCO coated conductors during transient charging.

6.4.2.3 Eddy-current losses

Eddy-current losses in the copper former were studied under a real-simulation of the ultra-high current ramping rate at 4.814 T/s and a transient charging duration of 5 seconds for the central solenoid coil. Since eddy current is a sort of induced current in metals with linear conductivity, it is essential to ensure the induced current density in the copper former during transient charging. It was found that the induced current density in the copper former tends to be saturated during the transient charging with an ultra-high current ramping rate as shown in Fig.42. The magnitude of the eddy current losses was smaller than the transport current losses in REBCO coated conductors as shown in Fig.43, an effect benefiting from the E-J linear behavior of copper and the saturation of induced current in the copper former. This outcome also demonstrates that the elaboration of the star-link cabling method is reasonable. It can be deduced that the total eddy-current losses in the central solenoid coil was within 7.56×10^{7} W/m.

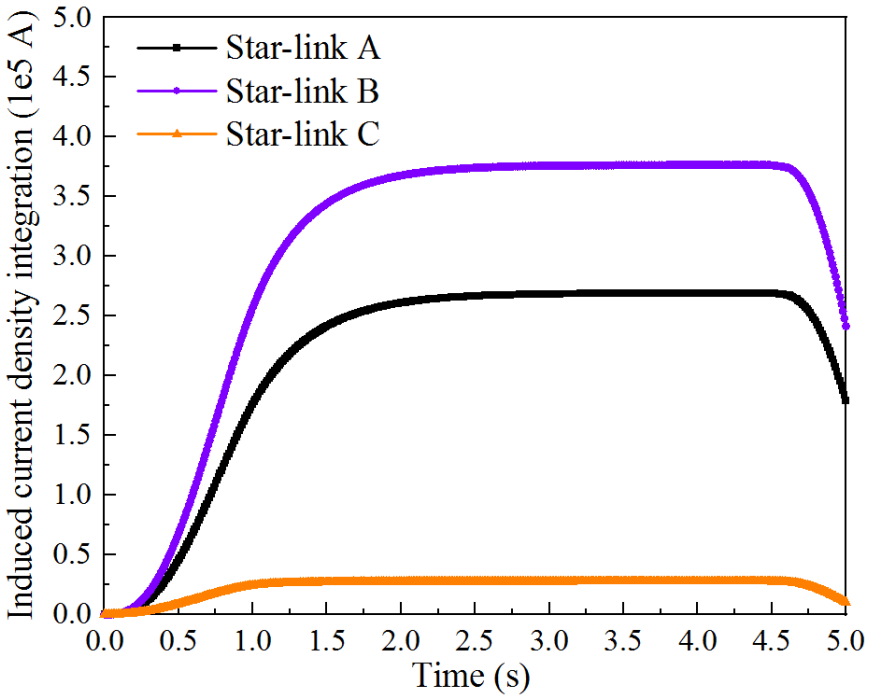

Fig.42. The integration of induced current density in the copper former during transient charging.

6.4.2.4 Brief summary

This section reports our study of three hysteresis losses, transport current losses and eddy-current losses in the star-link cabling central solenoid coil under an ultra-high-rate real current ramping environment for plasma charging. It was found that hysteresis losses were still the main losses for REBCO coated conductors. It was also demonstrated that the minimum loss incurred during transient charging were eddy-current losses, which is a testament to the soundness of the star-link cabling method. The total power losses of the central solenoid coil during ultra-high current ramping rate were within 7.82×10^{9} W/m. Therefore, the cooling power of the liquid helium cooling system should satisfy the cooling requirement of avoiding quenching during superconductivity.

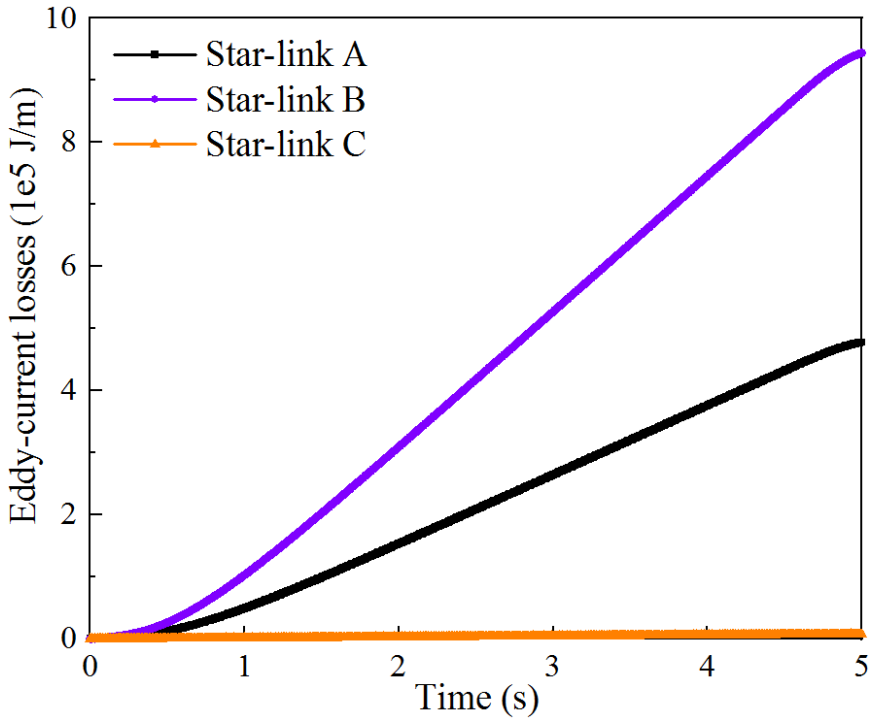

Fig.43. Eddy-current losses in the copper former during transient charging.

6.4.3 Mechanical behavior of the central solenoid coil system

The stress tolerance of REBCO coated conductors is 680 MPa, but it is highly suggested that the stress distribution along the central solenoid coil should be less than 500 MPa [83]. Therefore, it is essential to assess the stress distribution along the central solenoid coil, especially places where stress concentration may happen. It can be predicted that the stress concentration should occur in the inboard area of the central solenoid coil, where the magnetic field strength is extremely high. This section describes our detailed study of the hoop stress and radial stress in the star-link cabling units, as shown in Fig.30. The hoop stress of the central solenoid coil was a normal stress in the tangential direction, and the radial stress of the central solenoid coil was a normal stress in directions perpendicular to the symmetrical axis. The values of hoop stress and radial stress in a position should depend highly on the component of the magnetic flux density and the current density. To better study the stress distribution, we define the hoop direction of the star-link cabling units herein as thresholds and the radial direction of the star-link cabling units as borders. The stress distributions along these thresholds and borders were specifically studied.

6.4.3.1 Mechanical stress in thresholds

In general, the hoop stress in thresholds should depend highly on the longitudinal component of the magnetic field, and the radial stress in thresholds should be determined by the transverse component of the magnetic field. As shown in Fig.44, the stress distribution exhibited a certain degree of stabilization, meaning that the magnetic flux density along these distributions did not experience any significant

excursion in these directions. It was also found that the threshold, which is closer to the center of the solenoid coil, had a high-level stress. The maximum stress was the radial compressive stress along the threshold F, the value for which was around 100 MPa. This is well below the stress tolerance of REBCO coated conductors.

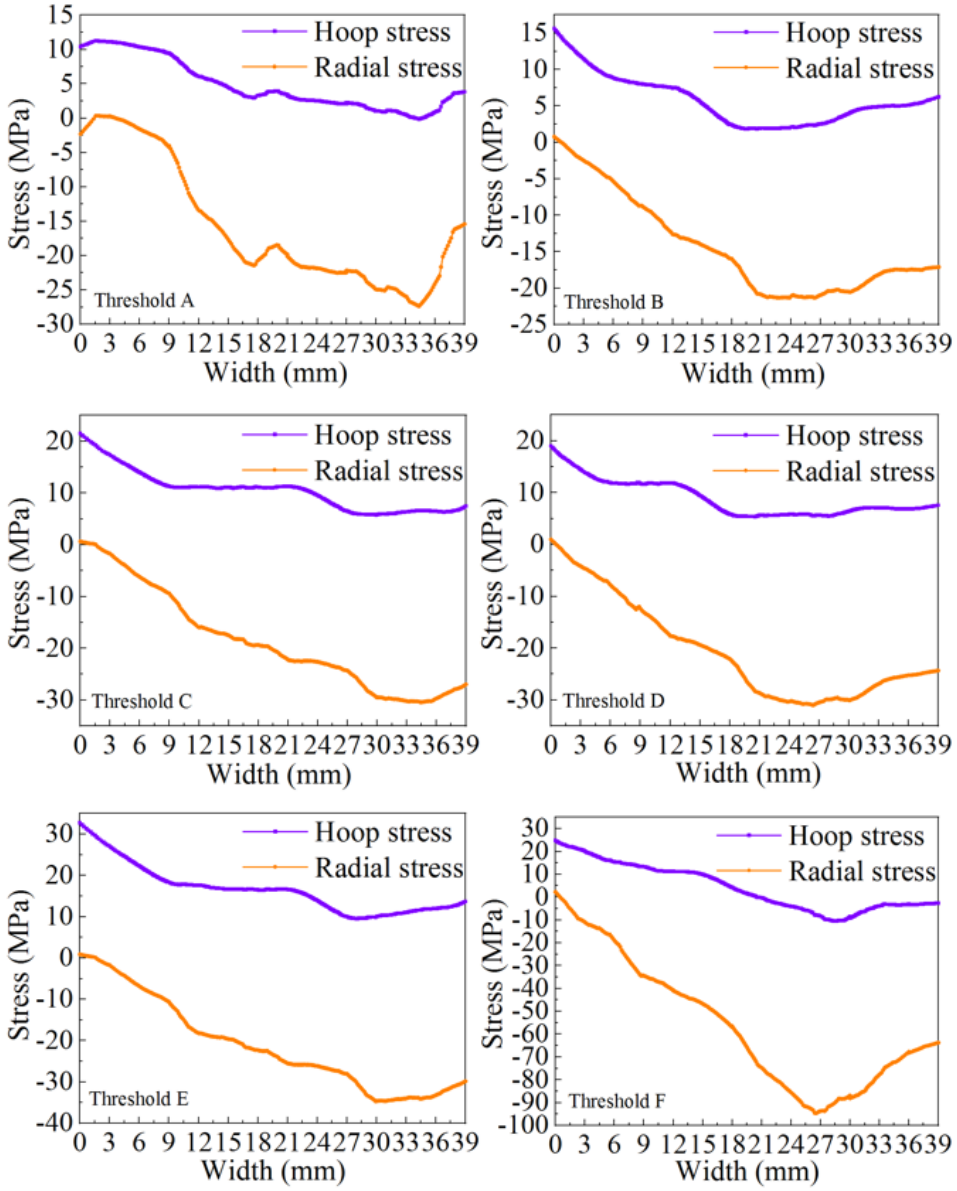

Fig.44. Hoop stress and radial stress in the thresholds of the star-link cabling units.

6.4.3.2 Mechanical stress in borders

The stress distribution along the borders might show a large degree of differences, which is caused by the high magnetic field gradient. In addition, it was found that the hoop stress along the borders was mainly a compressive stress, and the radial stress along borders was a tensile stress for the star-link cabling units. As shown in Fig.45, these borders were subjected to a higher impact from tensile stresses. Considering that REBCO coated conductors are more sensitive to tensile stresses, it is strongly recommended that reinforcement be provided on the top and bottom of the central solenoid coil. The

maximum stress occurs as the downward tensile stress that is distributed along border F, with a value of less than 100 MPa, which is within the stress tolerance of REBCO coated conductors as well. The present study demonstrates that the mechanical behavior of the star-link cabling system along REBCO coated conductors is operated in a safety mechanical margin that ensures the high performance of their current-carrying capacity.

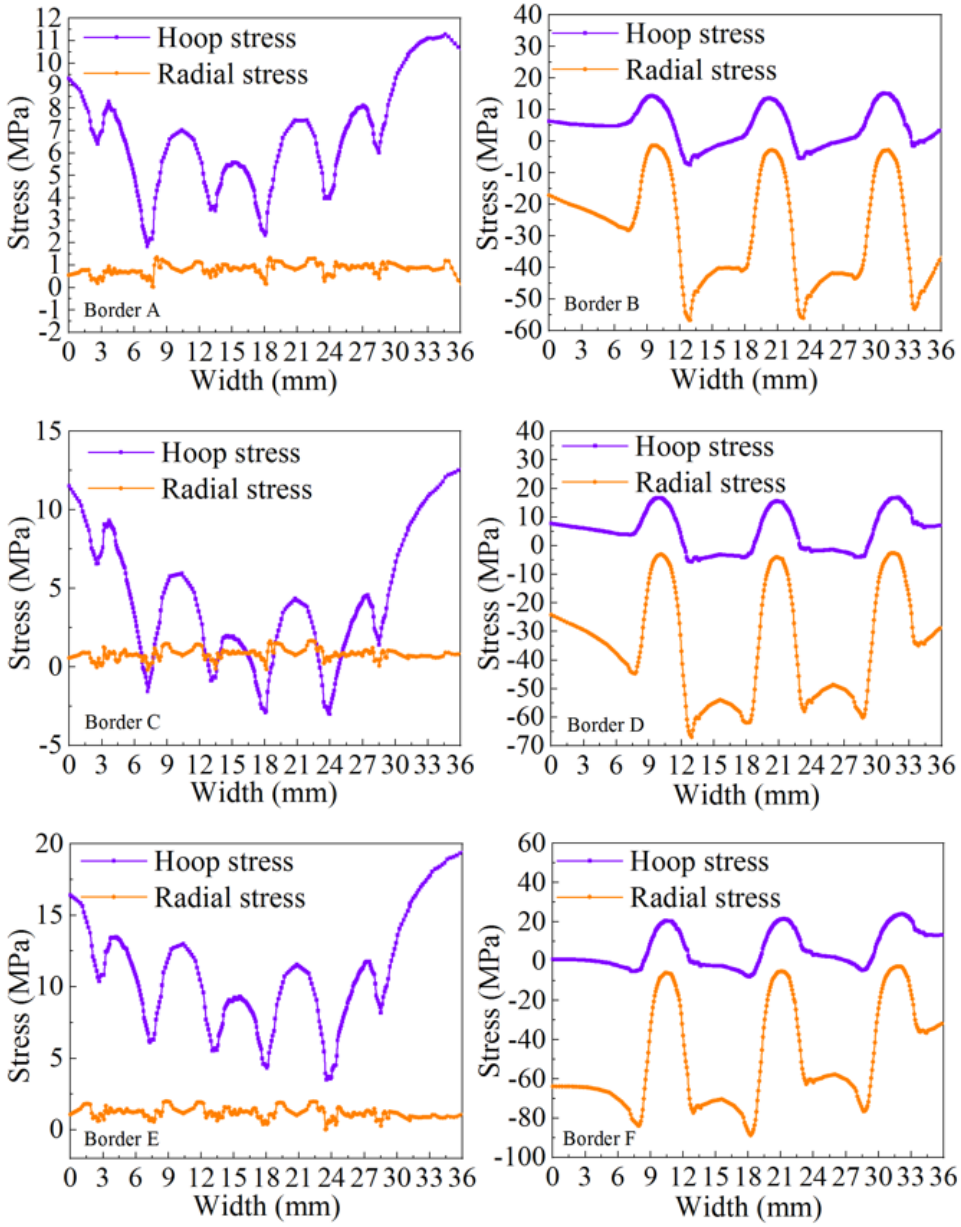

Fig.45. Hoop stress and radial stress in the borders of the star-link cabling units.

6.5 Summary

Concerned is the target of developing a feasible ultra-high-field REBCO coated conductor-based magnet system for the G-tune large-scale thermonuclear fusion reactor. This article explains the development of a star-link cabling method featuring outstanding current-carrying capacity and high-level inductance balance for the central solenoid coil system, which has the inherent feature of protecting the mechanical

behavior of REBCO coated conductors by virtue of, the entire winding process, when achieving inductance balance, having no torsion for the conductor and therefore avoids possible damage to the ceramic superconducting layers, thus enabling REBCO coated conductors to achieve very high engineering critical current density under ultra-high fields and a low-temperature operating environment. The operating current ramping rate of each REBCO coated conductor is 24 A/s, with a transient current duration of 5 seconds, which equals a field ramping rate of 4.814 T/s for the central solenoid coil system. This performance can meet the plasma charging requirement for fusion; while also allowing for enough current transmission margin for REBCO coated conductors to avoid quench in case the increasing external magnetic field and unstable operating temperature caused by power losses leads to an engineering critical current degradation in REBCO coated conductors. The power loss and mechanical stress of the star-link cabling units have presently been studied under real transient charging condition at an extremely high current ramping rate for the central solenoid coil system. It was found that more than 90% of losses came from hysteresis, but quenching in the context of superconductivity can be avoided by the addition of a high-power helium cooing system. In the analysis of mechanical stress in the star-link cabling units, it has been found that tensile stresses of approximately 100 MPa will be generated in the radial direction, which might affect the electromechanical behavior of REBCO coated conductors. Therefore, it is highly recommended to reinforce the top and bottom surfaces of the central solenoid coil. However, considering that the stress tolerance of REBCO coated conductor can be up to 500 MPa, the star-link cabling design ensures a reliable operating environment with the mechanical protection of the copper former. The star-link cabling system has been demonstrated to be electromagnetically and electromechanically feasible for the central solenoid coil systems of ultra-high-field large-scale thermonuclear fusion reactors. The work presented by this article should be of great significant and can provide a set of references for the research and development of the new generation ultra-high-field magnet system for compact and large-scale thermonuclear fusion reactors using the second-generation high temperature superconducting REBCO coated conductors.

7 Conclusion

This dissertation studied the electromagnetic behavior of REBCO coated conductors which were commercialized in 2006 by using experiments and finite element methods. Hereafter, five main REBCO cabling methods developed from 2008 have been investigated in detail with the manuscript entitled: High temperature superconducting REBCO coated conductors for ultra-high-field magnetic-confinement plasma devices. Afterwards, we studied the current-carrying capacity and magnetic behavior of the twisted-stacked tape-conductor cable which is currently employed as the feeder line for the toroidal field module coils of the SPARC compact fusion reactor that is operated in MIT. The study of REBCO cables developed during the past decades has laid a very good foundation for us to develop novel REBCO cables for ultra-high-field magnetic-confinement devices.

A non-twisted REBCO cable with outstanding current-carrying capacity has been proposed and developed for the toroidal field coil system of ultra-high-field magnetic-confinement devices. The electromechanical behavior of the independent toroidal field coil and the toroidal field coil modules has been studied. It is found that the toroidal field coil modules have the capacity to achieve an ultra-high-field of more than 20 Tesla with the assistance of the non-twisted cable. In addition, the maximum stress generated in the toroidal field coil modules is within the stress tolerance of REBCO coated conductors. However, it is highly suggest that the charging for the toroidal field coils with the non-twisted cable should be as slow as possible, due to the reason that the non-twisted cable has no capability in achieving inductance balance under high current ramping environment. Therefore, the non-twisted cable can be feasible for the stable toroidal field or poloidal field coils of ultra-high-field magnetic-confinement devices.

A star-link cabling method with extremely high inductance balance and high current-carry capacity has been developed for the central solenoid coils which are used for plasma charging under a high current ramping rate (4 T/s) environment. The demonstration of the cabling method has been carried out by the studying of AC losses in REBCO stacked tapes and eddy-current losses in the copper former. In addition, the electromechanical behavior of the star-link cabling method based central solenoid coil has been studied as well. The star-link cabling method should be of great significance in promoting the second generation high temperature superconducting REBCO coated conductors to ultra-high-field large-scale applications.

The research aims to provide theoretical and experimental basis for the research and development of using REBCO coated conductor for ultra-high-field magnet system in compact and large-scale fusion reactor. In addition, the developed non-twisted REBCO cable and the star-link cabling method have

great potential to be employed as the component of ultra-high-field magnet, which might be feasible for large-scale fusion, accelerators and MRI machines.

8 References

[1] Van Delft, Dirk. "History and significance of the discovery of superconductivity by Kamerlingh Onnes in 1911." *Physica C: Superconductivity* 479 (2012): 30-35.
[2] Meissner, W. and Ochsenfeld, R. (1933) Ein neuer Effekt bei eintritt der Supraleitfähigkeit. Naturwissenschaften, 21, 787-788.
[3] London F. and London H. 1935 The electromagnetic equations of the supraconductor *Proc. R. Soc. Lond*. A14971–88.
[4] Ginzburg, V.L., Landau, L.D. (2009). On the Theory of Superconductivity. *Superconductivity and Superfluidity*. Springer, Berlin, Heidelberg.
[5] Abrikosov, A. A. "On the magnetic properties of superconductors of the second type." *Zh. Eksperim. i Teor*. Fiz 32 (1957): 1442-1452.
[6] Molodyk, A., et al. "Development and large volume production of extremely high current density YBa2Cu3O7 superconducting wires for fusion." *Scientific reports* 11.1 (2021): 2084.
[7] Bardeen, John, Leon N. Cooper, and John Robert Schrieffer. "Theory of superconductivity." *Physical review* 108.5 (1957): 1175.
[8] Josephson, Brian David. "Possible new effects in superconductive tunnelling." *Physics letters* 1.7 (1962): 251-253.
[9] Ran, S. K. "Gravity probe B: Exploring Einstein's universe with gyroscopes." NASA. (2004): 26.
[10] Hashimoto T, Ota Y, Tsuzuki A, Nagashima T, Fukushima A, Kasahara S, Matsuda Y, Matsuura K, Mizukami Y, Shibauchi T, Shin S, Okazaki K. Bose-Einstein condensation superconductivity induced by disappearance of the nematic state. *Sci Adv*. 2020 Nov 6;6(45):eabb9052. doi: 10.1126/sciadv.abb9052. PMID: 33158862; PMCID: PMC7673702.
[11] O'Mahony, Shane M., et al. "On the electron pairing mechanism of copper-oxide high temperature superconductivity." *Proceedings of the National Academy of Sciences* 119.37 (2022): e2207449119.
[12] Bednorz, J.G., Müller, K.A. Possible highT c superconductivity in the Ba−La−Cu−O system. Z. *Physik B - Condensed Matter* 64, 189–193 (1986).
[13] Wu, Maw-Kuen, et al. "Superconductivity at 93 K in a new mixed-phase Y-Ba-Cu-O compound system at ambient pressure." *Physical review letters* 58.9 (1987): 908.
[14] https://fs.magnet.fsu.edu/~lee/plot/Je_vs_B-041118a_1280x929_PAL.png.
[15] Tsui, Yeekin, Elizabeth Surrey, and Damian Hampshire. "Soldered joints—an essential component of demountable high temperature superconducting fusion magnets." *Superconductor Science and Technology* 29.7 (2016): 075005.
[16] MacManus-Driscoll, Judith L., and Stuart C. Wimbush. "Processing and application of high-temperature superconducting coated conductors." *Nature Reviews Materials* 6.7 (2021): 587-604.
[17] Iwakuma, Masataka, et al. "Development of a 15 kW motor with a fixed YBCO superconducting field winding." *IEEE Transactions on Applied Superconductivity* 17.2 (2007): 1607-1610.
[18] Fair, Ruben, et al. "Development of an HTS hydroelectric power generator for the hirschaid power station." *Journal of Physics: Conference Series.* Vol. 234. No. 3. IOP Publishing, 2010.
[19] Hyun, Ok-Bae. "Brief review of the field test and application of a superconducting fault current limiter." *Progress in Superconductivity and Cryogenics* 19.4 (2017): 1-11.
[20] Glasson, Neil, et al. "Test results and conclusions from a 1 MVA superconducting transformer featuring 2G HTS Roebel cable." *IEEE Transactions on Applied Superconductivity* 27.4 (2016): 1-5.
[21] Kovalev, I. A., et al. "Test results of 12/18 kA ReBCO coated conductor current leads." *Cryogenics* 85 (2017): 71-77.
[22] Choi, Jongho, et al. "Commercial design and operating characteristics of a 300 kW superconducting induction heater (SIH) based on HTS magnets." *IEEE Transactions on Applied Superconductivity* 29.5 (2019): 1-5.
[23] Li, Xiaodong, et al. "Magneto-hydrodynamic characteristics of molten salts in a model-based high temperature superconducting conduction pump." *Physica C: Superconductivity and its Applications* 597 (2022): 1354061.
[24] X. Li, W. Yang, H. Zhang and R. Macian-Juan, "Numerical Study of AC Loss Characteristics in a Three-Phase Superconducting Induction Pump," in *IEEE Transactions on Applied Superconductivity*, vol. 31, no. 5, pp. 1-5, Aug. 2021, Art no. 5901005, doi: 10.1109/TASC.2021.3064787.

[25] Van der Laan, Daniel C. "YBa2Cu3O7− δ coated conductor cabling for low ac-loss and high-field magnet applications." *Superconductor Science and Technology* 22.6 (2009): 065013.
[26] Van der Laan, D. C., et al. “Engineering current density in excess of 200 A mm− 2 at 20 T in CORC® magnet cables containing RE-Ba2Cu3O7− δ tapes with 38 μm thick substrates.” *Superconductor Science and Technology* 28.12 (2015): 124001.
[27] Van der Laan, Daniel C., et al. “Characterization of a high-temperature superconducting conductor on round core cables in magnetic fields up to 20 T.” *Superconductor Science and Technology* 26.4 (2013): 045005.
[28] Van der Laan, D. C., et al. “Record current density of 344 A mm− 2 at 4.2 K and 17 T in CORC® accelerator magnet cables.” *Superconductor Science and Technology* 29.5 (2016): 055009.
[29] Barth, Christian, et al. “Temperature-and field-dependent characterization of a conductor on round core cable.” *Superconductor Science and Technology* 28.6 (2015): 065007.
[30] Michael, P. C., et al. “Behavior of a high-temperature superconducting conductor on a round core cable at current ramp rates as high as 67.8 kA s− 1 in background fields of up to 19 T.” *Superconductor Science and Technology* 29.4 (2016): 045003.
[31] Van der Laan, D. C., et al. “Engineering current density in excess of 200 A mm− 2 at 20 T in CORC® magnet cables containing RE-Ba2Cu3O7− δ tapes with 38 μm thick substrates.” *Superconductor Science and Technology* 28.12 (2015): 124001.
[32] Kar, Soumen, et al. “Symmetric tape round REBCO wire with Je (4.2 K, 15 T) beyond 450 A mm− 2 at 15 mm bend radius: a viable candidate for future compact accelerator magnet applications.” *Superconductor Science and Technology* 31.4 (2018): 04LT01.
[33] Kar, Soumen, et al. “Progress in scale-up of REBCO STAR™ wire for canted cosine theta coils and future strategies with enhanced flexibility.” *Superconductor Science and Technology* 33.9 (2020): 094001.
[34] Kar, Soumen, et al. “Next-generation highly flexible round REBCO STAR wires with over 580 A mm− 2 at 4.2 K, 20 T for future compact magnets.” *Superconductor Science and Technology* 32.10 (2019): 10LT01.
[35] Kar, Soumen, et al. “Progress in scale-up of REBCO STAR™ wire for canted cosine theta coils and future strategies with enhanced flexibility.” *Superconductor Science and Technology* 33.9 (2020): 094001.
[36] Rossi, Lucio. “IOP: Small REBCO isotropic round wire (STAR): an important step from performant material to practical conductor in high field HTS magnets.” *Supercond. Sci. Technol.* 32 (2019): 100501.
[37] Takayasu, Makoto, and Chiesa, Luisa. “Analytical investigation in bending characteristic of twisted stacked-tape cable conductor.” *IOP conference series: materials science and engineering.* Vol. 102. No. 1. IOP Publishing, 2015.
[38] Hartwig, Zachary S., et al. "VIPER: an industrially scalable high-current high-temperature superconductor cable." *Superconductor Science and Technology* 33.11 (2020): 11LT01.
[39] Takayasu, Makoto, Chiesa, Luisa, and Minervini. Joseph V. “Investigation of REBCO twisted stacked-tape cable conductor performance.” *Journal of Physics: Conference Series.* Vol. 507. No. 2. IOP Publishing, 2014.
[40] Takayasu, M. Mangiarotti, F.J. Chiesa, L. Bromberg, L. and Minervini, J. V. “Conductor Characterization of YBCO Twisted Stacked-Tape Cables,” in *IEEE Transactions on Applied Superconductivity*, vol. 23, no. 3, pp. 4800104-4800104, June 2013, art no. 4800104.
[41] Barth, Christian, et al. “Temperature-and field dependent characterization of a twisted stacked-tape cable.” *Superconductor Science and Technology* 28.4 (2015): 045015.
[42] Celentano, G., et al. “Design of an industrially feasible twisted-stack HTS cable-in-conduit conductor for fusion application.” *IEEE transactions on applied superconductivity* 24.3 (2013): 1-5.
[43] De Marzi, G., et al. “Bending tests of HTS cable-in-conduit conductors for high-field magnet applications.” *IEEE Transactions on Applied Superconductivity* 26.4 (2016): 1-7.
[44] De Marzi, Gianluca, et al. “Experimental and numerical studies on current distribution in stacks of HTS tapes for cable-in-conduit-conductors.” *Superconductor Science and Technology* 34.3 (2021): 035016.

[45] Li, X., Song, D., Y. Wu, Liu, Y., Yang, W and Macián-Juan, R "Current-Carrying Capability and Magnetic Behavior of the HTS Twisted Stacked-Tape Conductor Cable for the Compact Fusion Reactor," in *IEEE Transactions on Applied Superconductivity*, vol. 32, no. 4, pp. 1-5, June 2022, art no. 4200205.
[46] Otten S J. Characterisation of REBCO Roebel cables [M]. *KIT Scientific Publishing*, 2019.
[47] Goldacker. W, Frank, A, Kudymow A; et al. Status of high-transport current ROEBEL assembled coated conductor cables [J]. *Superconductor Science and Technology*, 2009, 22(3): 034003.
[48] Goldacker, Wilfried, et al. "Roebel cables from REBCO coated conductors: a one-century-old concept for the superconductivity of the future." *Superconductor Science and Technology* 27.9 (2014): 093001.
[49] Fleiter, Jérôme, et al. "Electrical characterization of REBCO Roebel cables." *Superconductor Science and Technology* 26.6 (2013): 065014.
[50] Pelegrin, J., Bailey, W. and Yang, Y. "Quench Characteristics of a 2G ReBCO Roebel Cable Pancake Coil in External Fields Up to 8T," in *IEEE Transactions on Applied Superconductivity*, vol. 31, no. 5, pp. 1-5, Aug. 2021, art no. 4802605.
[51] Fleiter, J., et al. "Characterization of Roebel cables for potential use in high-field magnets." *IEEE Transactions on Applied Superconductivity* 25.3 (2014): 1-4.
[52] Kragh, Helge (2011) Fermilab: Physics, the Frontier & Megascience, *Annals of Science*, 68:3, 437-440.
[53] Bykovsky, N., et al. "Performance evolution of 60 kA HTS cable prototypes in the EDIPO test facility." *Superconductor Science and Technology* 29.8 (2016): 084002.
[54] Kario, A., et al. "Investigation of a Rutherford cable using coated conductor Roebel cables as strands." *Superconductor Science and Technology* 26.8 (2013): 085019.
[55] Uglietti, D., et al. "Test of 60 kA coated conductor cable prototypes for fusion magnets." *Superconductor Science and Technology* 28.12 (2015): 124005.
[56] Takayasu, Makoto. "Width-bending characteristic of REBCO HTS tape and flat-tape Rutherford-type cabling." *Superconductor Science and Technology* 34.12 (2021): 125020.
[57] Zhang, Min, et al. "Total AC loss study of 2G HTS coils for fully HTS machine applications." *Superconductor Science and Technology* 28.11 (2015): 115011.
[58] Ma, Guangtong, et al. "Design, fabrication and testing of a coated conductor magnet for electrodynamic suspension." *Superconductor Science and Technology* 35.2 (2021): 025013.
[59] Lelekhov, Sergey A. "Analysis of a Possibility to Use Parallel Non-Twisted Stacks of HTS Tapes as Cable in High Current Conductor of Tokamak Toroidal Field Coils." *IEEE Transactions on Applied Superconductivity* 31.5 (2021): 1-5.
[60] Uglietti, Davide, et al. "Non-twisted stacks of coated conductors for magnets: Analysis of inductance and AC losses." *Cryogenics* 110 (2020): 103118.
[61] Brittles, Greg, "Development of the "Demo4" spherical tokamak HTS magnet demonstrator at Tokamak Energy" presented at the MT-27 conference. 2021.
[62] Z. S. Hartwig et al., "The SPARC Toroidal Field Model Coil Program," in *IEEE Transactions on Applied Superconductivity*, vol. 34, no. 2, pp. 1-16, March 2024, Art no. 0600316.
[63] Yanagi, Nagato, et al. "Design and development of a high-temperature superconducting magnet system with joint-winding for the helical fusion reactor." *Nuclear Fusion* 55.5 (2015): 053021.
[64] Brandt, Ernst Helmut. "Superconductors of finite thickness in a perpendicular magnetic field: Strips and slabs." *Physical review B* 54.6 (1996): 4246.
[65] Patel, A., and B. A. Glowacki. "Enhanced trapped field achieved in a superconducting bulk using high thermal conductivity structures following simulated pulsed field magnetization." *Superconductor Science and Technology* 25.12 (2012): 125015.
[66] Shen, Boyang, Francesco Grilli, and Tim Coombs. "Overview of H-formulation: A versatile tool for modeling electromagnetics in high-temperature superconductor applications." *IEEE access* 8 (2020): 100403-100414.
[67] Berrospe-Juarez, Edgar, et al. "Advanced electromagnetic modeling of large-scale high-temperature superconductor systems based on H and TA formulations." *Superconductor Science and Technology* 34.4 (2021): 044002.

[68] Zermeno, Victor MR, et al. "Calculation of alternating current losses in stacks and coils made of second-generation high temperature superconducting tapes for large scale applications." *Journal of Applied Physics* 114.17 (2013): 173901.
[69] Zhang, Huiming, Min Zhang, and Weijia Yuan. "An efficient 3D finite element method model based on the T–A formulation for superconducting coated conductors." *Superconductor Science and Technology* 30.2 (2016): 024005.
[70] Huber, Felix, et al. "The TA formulation: an efficient approach to model the macroscopic electromagnetic behaviour of HTS coated conductor applications." *Superconductor Science and Technology* 35.4 (2022): 043003.
[71] Liang, Fei, et al. "A finite element model for simulating second generation high temperature superconducting coils/stacks with large number of turns." *Journal of Applied Physics* 122.4 (2017): 043903.
[72] Campbell, A. M. "A new method of determining the critical state in superconductors." *Superconductor Science and Technology* 20.3 (2007): 292.
[73] Ruiz-Alonso, D., T. Coombs, and A. M. Campbell. "Computer modelling of high-temperature superconductors using an A–V formulation." *Superconductor Science and Technology* 17.5 (2004): S305.
[74] Mykola, Solovyov, and Gömöry Fedor. "A–V formulation for numerical modelling of superconductor magnetization in true 3D geometry." *Superconductor Science and Technology* 32.11 (2019): 115001.
[75] Busse, Christian, Andrew P. Kach, and Stephan M. Wagner. "Boundary conditions: What they are, how to explore them, why we need them, and when to consider them." *Organizational Research Methods* 20.4 (2017): 574-609.
[76] Moës, Nicolas, Eric Béchet, and Matthieu Tourbier. "Imposing Dirichlet boundary conditions in the extended finite element method." *International Journal for Numerical Methods in Engineering* 67.12 (2006): 1641-1669.
[77] Dipierro, Serena, Xavier Ros-Oton, and Enrico Valdinoci. "Nonlocal problems with Neumann boundary conditions." *Revista Matemática Iberoamericana* 33.2 (2017): 377-416.
[78] Alfonzetti, Salvatore, and Giuseppe Borzi. "Finite-element solution to electromagnetic scattering problems by means of the Robin boundary condition iteration method." *IEEE Transactions on Antennas and Propagation* 50.2 (2002): 132-140.
[79] A. Kishk and L. Shafai, "Different formulations for numerical solution of single or multibodies of revolution with mixed boundary conditions," in *IEEE Transactions on Antennas and Propagation*, vol. 34, no. 5, pp. 666-673, May 1986, doi: 10.1109/TAP.1986.1143875.
[80] Kolobov, A. G., T. V. Pak, and A. Yu Chebotarev. "Stationary problem of radiative heat transfer with Cauchy boundary conditions." *Computational Mathematics and Mathematical Physics* 59 (2019): 1199-1203.
[81] Chebotarev, Alexander Yu, Andrey E. Kovtanyuk, and Nikolai D. Botkin. "Problem of radiation heat exchange with boundary conditions of the Cauchy type." *Communications in Nonlinear Science and Numerical Simulation* 75 (2019): 262-269.
[82] Szilágyi, Bela, et al. "Cauchy boundaries in linearized gravitational theory." *Physical Review D* 62.10 (2000): 104006.
[83] Bruzzone, Pierluigi, et al. "High temperature superconductors for fusion magnets." *Nuclear Fusion* 58.10 (2018): 103001.
[84] Fietz, W. H., et al. "High temperature superconductor cables for EU-DEMO TF-magnets." *Fusion Engineering and Design* 125 (2017): 290-293.
[85] Jin, H., et al. "The performance of first CORC cable solenoid insert for development of CFETR high-field magnet." *Nuclear Fusion* 60.9 (2020): 096028.
[86] Creely, A. J., et al. "Overview of the SPARC tokamak." *Journal of Plasma Physics* 86.5 (2020): 865860502.
[87] Bayer, Christoph M. *Characterization of High Temperature Superconductor Cables for Magnet Toroidal Field Coils of the DEMO Fusion Power Plant*. Vol. 18. KIT Scientific Publishing, 2017.
[88] Costley, A. E. "Towards a compact spherical tokamak fusion pilot plant." *Philosophical Transactions of the Royal Society A* 377.2141 (2019): 20170439.

[89] Takayasu, Makoto, et al. "HTS twisted stacked-tape cable conductor." *Superconductor Science and Technology* 25.1 (2011): 014011.
[90] Takayasu, Makoto, et al. "Investigation of HTS twisted stacked-tape cable (TSTC) conductor for high-field, high-current fusion magnets." *IEEE Transactions on Applied Superconductivity* 27.4 (2017): 1-5.
[91] Benkel, Tara, et al. "T–A-formulation to model electrical machines with HTS coated conductor coils." *IEEE Transactions on Applied Superconductivity* 30.6 (2020): 1-7.
[92] Zermeño, Víctor MR, and Francesco Grilli. "3D modeling and simulation of 2G HTS stacks and coils." *Superconductor Science and Technology* 27.4 (2014): 044025.
[93] Ongena J, Koch R, Wolf R. et al. Magnetic-confinement fusion. *Nature Phys* 12, 398–410.
[94] Mitchell N, Breschi M, and Tronza V. "The use of Nb_3Sn in fusion: lessons learned from the ITER production including options for management of performance degradation." *Superconductor Science and Technology* 33.5 (2020): 054007.
[95] Strickland N M. "Qualifying high-temperature superconductors for fusion reactors." *Superconductor Science and Technology* 34.11 (2021): 110502.
[96] Dong Y, et al. "10 kV AC test verification of the high temperature superconducting fault current limiter with bias magnetic field." *Cryogenics* 112 (2020): 103195.
[97] Gupta R, et al. "Design, construction, and testing of a large-aperture high-field HTS SMES coil." *IEEE Transactions on Applied Superconductivity* 26.4 (2016): 5700208.
[98] Bergen A, et al. "Design and in-field testing of the world's first ReBCO rotor for a 3.6 MW wind generator." *Superconductor science and technology* 32.12 (2019): 125006.
[99] Parkinson B J, Bouloukakis K, and Slade R A. "A compact 3 T all HTS cryogen-free MRI system." *Superconductor Science and Technology* 30.12 (2017): 125009.
[100] Zani L, et al. "Overview of progress on the EU DEMO reactor magnet system design." *IEEE transactions on applied superconductivity* 26.4 (2016): 4204505.
[101] Zheng J, et al. "Overview of the design status of the superconducting magnet system of the CFETR." *IEEE Transactions on Applied Superconductivity* 28.3 (2018): 4204305.
[102] Zheng J, Kang R, and Song Y. "Electromagnetic and stability study on HTS/LTS hybrid superconducting central solenoid." *IEEE Transactions on Applied Superconductivity* 26.7 (2016): 4205505.
[103] Yanagi N, et al. "Progress in the conceptual design of the helical fusion reactor FFHR-d1." *Journal of Fusion Energy* 38.1 (2019): 147-161.
[104] Sagara A, et al. "Helical reactor design FFHR-d1 and c1 for steady-state DEMO." *Fusion Engineering and Design* 89.9-10 (2014): 2114-2120.
[105] Yanagi N, et al. "Design and development of high-temperature superconducting magnet system with joint-winding for the helical fusion reactor." *Nuclear Fusion* 55.5 (2015): 053021.
[106] Novikov M S, et al. "Current-carrying element based on second-generation high-temperature superconductor for the magnet system of a fusion neutron source." *Physics of Atomic Nuclei* 78.10 (2015): 1148-1154.
[107] Mulder T, et al. "Design and manufacturing of a 45 kA at 10 T REBCO-CORC cable-in-conduit conductor for large-scale magnets." *IEEE transactions on applied superconductivity* 26.4 (2016): 4803605.
[108] Terazaki Y, et al. "Current-carrying capability of the 100 kA-class HTS STARS conductor for the helical fusion reactor FFHR-d1." *Journal of Physics: Conference Series.* Vol. 871. No. 1. IOP Publishing, 2017.
[109] Mulder T, et al. "Recent progress in the development of CORC cable-in-conduit conductors." *IEEE Transactions on Applied Superconductivity* 30.4 (2020): 4800605.
[110] Plakida N. High-temperature cuprate superconductors: Experiment, theory, and applications. Vol. 166. *Springer Science & Business Media*, 2010.
[111] Lebrun P and Tavian L. "Cooling with superfluid helium." *CERN Yellow Report* 15.01 (2015):07156.
[112] Tsuchiya K, et al. "Critical current measurement of commercial REBCO conductors at 4.2 K." *Cryogenics* 85 (2017): 1-7.

[113] Keefe, Denis. "Inertial confinement fusion." *Annual Review of Nuclear and Particle Science* 32.1 (1982): 391-441.
[114] Mailloux, Joelle, et al. "Overview of JET results for optimizing ITER operation." *Nuclear Fusion* 62.4 (2022): 042026.
[115] Riccioli, R., et al. "Mechanical Analysis of Full-Scale Nb 3 Sn CICC Designs for Tokamaks." *IEEE Transactions on Applied Superconductivity* 32.6 (2022): 1-5.
[116] Li, Xiaodong, et al. "Electromechanical behaviour of REBCO coated conductor toroidal field coils for ultra-high-field magnetic-confinement plasma devices." *Journal of Physics D: Applied Physics* 56.4 (2022): 045001.
[117] Wang, Qiuliang, et al. "Progress of ultra-high-field superconducting magnets in China." *Superconductor Science and Technology* 35.2 (2021): 023001.
[118] Rodriguez-Fernandez, P., et al. "Overview of the SPARC physics basis towards the exploration of burning-plasma regimes in high-field, compact tokamaks." *Nuclear Fusion* 62.4 (2022): 042003.
[119] Bayer, C. M., et al. "Mechanical reinforcement for RACC cables in high magnetic background fields." *Superconductor Science and Technology* 29.2 (2015): 025007.
[120] Shen, Boyang, Francesco Grilli, and Tim Coombs. "Review of the AC loss computation for HTS using H formulation." *Superconductor Science and Technology* 33.3 (2020): 033002.
[121] Inanir, Fedai, and Rifki Terzioglu. "AC loss evaluation of a superconducting pancake coil with coated conductors using an extended AV formulation." *Physica C: Superconductivity and its Applications* 587 (2021): 1353910.
[122] Sass, F., et al. "Superconducting magnetic bearings with bulks and 2G HTS stacks: Comparison between simulations using H and AV formulations with measurements." *Superconductor Science and Technology* 31.2 (2018): 025006.
[123] Zhang, Kai, et al. "Fully-staggered-array bulk Re-Ba-Cu-O short-period undulator: large-scale 3D electromagnetic modelling and design optimization using AV and H-formulation methods." *Superconductor Science and Technology* 34.9 (2021): 094002.
[124] Arp, Vincent. "Stresses in superconducting solenoids." *Journal of Applied Physics* 48.5 (1977): 2026-2036.
[125] Xu, Xingchen. "A review and prospects for Nb_3Sn superconductor development." *Superconductor Science and Technology* 30.9 (2017): 093001.
[126] Anderson, Philip W. *The theory of superconductivity in the high-Tc cuprate superconductors*. 1997.
[127] Shen, Boyang, et al. "Power dissipation in HTS coated conductor coils under the simultaneous action of AC and DC currents and fields." *Superconductor Science and Technology* 31.7 (2018): 075005.
[128] Grilli, Francesco, et al. "Computation of losses in HTS under the action of varying magnetic fields and currents." *IEEE Transactions on Applied Superconductivity* 24.1 (2013): 78-110.
[129] Ma, Jun, et al. "A temperature-dependent multilayer model for direct current carrying HTS coated-conductors under perpendicular AC magnetic fields." *Superconductor Science and Technology* 33.4 (2020): 045007.